The Runny Gauge Plasma

Shear viscosity to entropy density for quarks and gluons

Greg Jackson

A thesis presented for the academic degree

Master of Science

in the Department of Physics

University of Cape Town

South Africa

2016

Submitted: 30 August 2016, Revised: 17 November 2016

Author: Greg Jackson[1]
Supervisor: André Peshier

[1]Electronic address: JCKGRE003@myuct.ac.za

Plagiarism Declaration

(i) I know that plagiarism is wrong. Plagiarism is to use anothers work and to pretend that it is ones own.

(ii) Each significant contribution to, and quotation in, this project from the work of other people has been been cited and referenced.

(iii) This report is my own work.

(iv) I have not allowed, and will not allow, anyone to copy my work with the intention of passing it off as his or her own work.

Name: Greg Jackson

Student number: JCKGRE003

Signature: Signed by candidate

Signature Removed

Date: 29 August 2016

Abstract

Heavy ion experiments at the LHC and RHIC have supported the existence of a quark-gluon plasma (QGP), which is strongly coupled and behaves as an almost ideal fluid. We shall discuss both bulk thermodynamic and off-equilibrium transport properties of the QGP, within the theory of quantum chromodynamics (QCD).

Meaningful approximations of most observables require quantum fluctuations to be taken into account. These arise in perturbation theory as loop corrections to tree level amplitudes, and describe both the scale-dependence of the coupling and charge screening in a many-body system. We emphasise that because the effective interaction strength, for a QGP, may vary considerably at the relevant scales, the running of the coupling cannot be ignored.

The goal of this thesis is to understand better a specific, long-standing question in the field of heavy ion physics: why the QGP has a remarkably small shear viscosity to entropy density ratio $\eta/s \lesssim 0.5$, near the confinement temperature. Our main argument hinges on combining both the thermal *and* vacuum fluctuations in resummation-improved perturbation theory. In this respect, we thoroughly analyse the range of applicability for perturbative approximations in which the coupling may be 'moderately' large.

Keywords: quark-gluon plasma, perturbation theory, viscosity

Contents

1. Introduction

Chemical elements are organised by the number of protons bound to their nuclear core. An equal number of electrons occupy quantised orbitals, thus forming the atomic charge density. Together with the neutron, these basic particles and their shell structure encompass all of the period table. Yet there is something unsettling about this picture; a nucleus *should* be unstable, due to mutual electric repulsion of protons in the core.

A first step to unravel this mystery, is that neutrons and protons are not fundamental particles. Their point-like substructure was revealed by Deep Inelastic Scattering (DIS), of highly virtual photons (short wavelengths) on target nucleons [1]. The quark model was put forward in the 1960s as an explanation, by Gell-Mann, Zweig and Ne'eman, which predicted a new particle, the Ω baryon, observed shortly thereafter [2]. But quarks have additional quantum numbers coming from the non-Abelian gauge symmetry (then unknown). Prototypes for exactly such theories, e. g. Ref. [3], had already been studied as generalisations of Quantum Electrodynamics (QED), the well-established theory of light and matter. These Yang-Mills theories re-emerged as a candidate for the strong nuclear force, possessing the sought after $SU(3)$ symmetry. In what is now called Quantum Chromodynamics (QCD), quarks interact via gluons, whose existence also solved a 'missing momentum' puzzle in DIS experiments. Ever since these theories were found to be renormalisable, they have underpinned the Standard Model [4].

Mobile quarks and gluons filled the entire universe up to $\sim 1\mu$s after the Big Bang, just before nucleosynthesis. Similar conditions are recreated by smashing nuclei into one-another; part of the nuclear programmes at the Large Hadron Collider (LHC) and Relativistic Heavy Ion Collider (RHIC). These accelerators can achieve energies up to 13 TeV per nucleon, but a single collision only lasts for about the time it takes light to cross a nuclear diameter. Hence typical temperatures and timespans are (respectively);

$$1\ \mathrm{GeV}/k_B \ \simeq\ 10^{13}\ \mathrm{K} \qquad \text{and} \qquad 1\ \mathrm{fm}/c \ \simeq\ \frac{1}{3}10^{-23}\ \mathrm{sec}\,.$$

Stretching two quarks beyond their 'natural' separation of about 10^{-15} m (nucleon scale) will be resisted by a constant string-like force, mediated by the gluons. It soon becomes energetically favourable to produce another quark-antiquark pair out of the vacuum, interrupting the string-like field configuration. The precursor is known as *confinement* and has been demonstrated in computer simulations based on lattice gauge theory, pioneered by Wilson [5]. Gluons play a crucial role in many-body chromodynamics; consider the neutron, a (udd) arrangement in the quark-model. Its mass ~ 1 GeV vastly exceeds the few MeV total from three light quarks. Thus constituent partons make a small contribution to the total energy – most comes from binding, i. e. the gluon field. Unlike their $U(1)$-partner, the photon, gluons carry 'charge' and thus interact not only with quarks and antiquarks, but also other gluons. This fact is also behind *asymptotic freedom*, which says that the effective colour charge diminishes at short distances [6]. The coupling α parametrises this interaction strength, which for QED is basically constant for many practical purposes and equal to $e^2/(4\pi\hbar)$. For QCD at low energies[2], α is non-perturbatively large. At high energies, α shrinks and tends to zero as the energy goes to infinity (see Fig. 1). There is no special value for the coupling, opposed to QED where for zero momentum-squared $\alpha_{\mathrm{em}}(0) \simeq 1/137$, conveniently nullifying many of the issues that hamper perturbation theory for QCD.

[2] Energies just above the QCD scale $\Lambda \sim 200$ MeV.

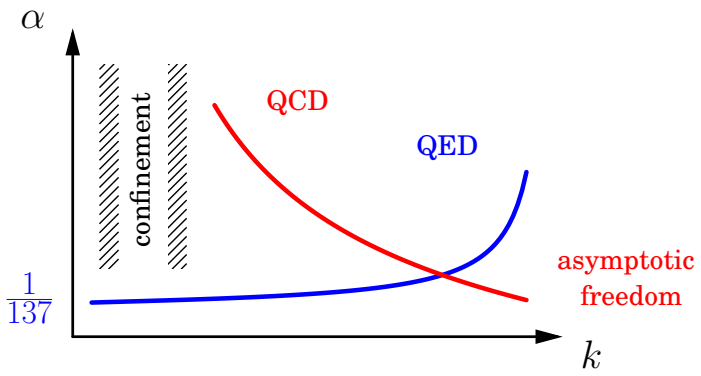

Figure 1: Energy dependence of the QED (blue) and QCD (red) effective coupling 'constants'. The electromagnetic coupling is exaggerated; for all practical purposes it is equal to 1/137. For QCD, little is known of the effective coupling at low energies. A pole at $k = \Lambda$ prohibits weak-coupling approaches below this point.

The $SU(3)$-symmetric theory, with minimal coupling to n_f fermions has the Lagrangian

$$\mathcal{L} \;=\; -\frac{1}{2}\,\mathrm{tr}\left(F^2\right) + \sum_f \bar{\psi}_f \left(i\not{D} - m_f\right)\psi_f \,, \tag{1.1}$$

where the trace is taken over colour degrees of freedom [7]. The 'chromo'-field tensor is F and quark 'flavour' species are labelled $f = \{\text{up, down, charm, strange, top, bottom}\}$. Studies of the reaction $e^-e^+ \to q\bar{q}$ and annihilation to hadrons, so far support $n_f = 6$ flavours (in total). The free parameters of this theory are the quark masses m_f and the charge g, which are *not* directly measured in experiment. Their numerical values are only 'determined' insofar as *observable* quantities may be derived (and compared with data, i. e. renormalised). As mentioned, the coupling $\alpha = g^2/4\pi$ is actually very sensitive to the energy scales involved.

In many-body systems, the coupling controls the mean potential energy between particles. At large energy densities, of about $\varepsilon \simeq 1$ GeV/fm^3, QCD predicts that ordinary nuclear matter melts into a deconfined *quark-gluon plasma* (QGP), where the average kinetic energy is sufficient to overcome the Coulomb-like binding energy (at short distances). The density of quanta is $n \sim (k_B T/\hbar)^3$, and gives $1/\sqrt[3]{n}$ to estimate their mean separation. Thus, for a thermal QGP phase, the mean potential energy

$$\frac{g^2}{4\pi}\,\sqrt[3]{n} \;\sim\; \alpha\hbar \cdot \left(\frac{\hbar}{k_B T}\right)^{-1} ,$$

should be less than $k_B T$ if $\alpha \lesssim 1$. No surprise then, that the transition from QGP to hadronic matter happens at a temperature T_c, close to the QCD scale $\Lambda \simeq 200$ MeV, characterising the coupling. The charm, top and bottom quarks are heavy compared with the energies of a few hundred MeV and are thus inert. The strange quark is intermediate, but up and down (light) quarks will be taken as massless. Thus deconfinement should be principally due to the gluons, and we study (1.1) with $n_f \leq 3$ massless flavours, to a good approximation of full QCD, leaving the only free parameter; $\Lambda \sim T_c$.

Heavy ion collisions (at RHIC, LHC) seem to be the only way of producing a QGP in the laboratory. The full space-time picture of a nucleus-nucleus collision, while intricate,

proceeds in basically three stages. An ultra-relativistic object is highly compressed in its direction of motion and consists of a 'wall' of highly virtual partons. This initial state has been dubbed a Colour Glass Condensate (CGC), distinguished by its over-occupation of gluons. Two impacting nuclei are mostly transparent to one another, but leave a stream of particles in their wake. This hot medium expands parallel to the beam direction and rapidly cools [8]. If the temperature allows for a CGC → off-equilibrium QGP stage, the subsequent thermalisation is rapid $\mathcal{O}(1\ \mathrm{fm}/c)$. After the thermal QGP has cooled further, i. e. $T \lesssim T_c$, the ensuing three-dimensional expansion expels colourless hadrons that are measured. Whether the QGP is strongly-coupled[3] supports either its interpretation as a gas or instead as a liquid.

Internal resistance of a fluid to flow is quantified by η, the shear viscosity. Particles interacting between layers tend to smoothen velocity gradients in a fluid. Lower interaction rates lead to larger values for η, because it takes more time to equilibrate when collisions are rare. But viscosity is an intensive quantity and it is useful to compare it with s – the entropy density. Marrying a transport coefficient, η, together with a static quantity, s, qualifies the applicability of hydrodynamics [9]. The ratio η/s plunges to a minimal value at a critical temperature, a universal feature of gas-liquid transitions [10]. In a quantum-dominated regime, the minimal value for $\eta/s \sim \hbar$ has been attributed to the uncertainty principle [11]. Remarkably, an ideal liquid approximation ($\eta = 0$) of the expanding medium agreed with many experiments. This surprised everyone and prompted RHIC to announce the creation of an (almost) perfect fluid with $\eta/s \leq \hbar$. It remains a theoretical task to understand *why* the QGP has such unique cohesive properties. A popular approach to this question is via the AdS/CFT correspondence [12], which has provided the limit $\eta/s \geq \hbar/(4\pi)$ for certain supersymmetric Yang-Mills theories. It may only be a coincidence that this compares favourably with the observations, since there is no connection to real-world QCD. On the other hand, there is a long-standing belief that QCD perturbation theory fails to explain the small viscosity, a view which we scrutinise here.

[3] The term 'strong coupling' is decidedly overused in Physics as it has no meaning out of context. We shall explore specific examples in the main text, and attempt to clarify the applicability of perturbation theory in these cases.

Outline

We will ultimately focus on the central quantity η/s. As a ratio of two observables, this report is similarly split into two main sections. The denominator is a bulk thermodynamic variable (static) and the numerator is a transport coefficient (dynamic).

§ 2 Static properties

We first calculate the non-interacting photon pressure in Coulomb gauge and explain how it generalises to QCD. The self-interaction of the gluon leads to substantial corrections to this free limit, which may be understood perturbatively. A truncated approximation for thermodynamic properties must first be regularised and then renormalised, which we propose to do by comparing with the *trace anomaly* from lattice calculations. Fixing the analytic results at a semi-perturbative temperature, we find that bulk properties tend to the free limit somewhat more gradually than expected.

Answering the question 'what is the force between two quarks?', we calculate the scattering amplitude for a heavy quark-antiquark pair in the colour singlet state. The result of a Born approximation is compared to the one-loop resummed expression (at $T = 0$) to re-derive the effective coupling constant for QCD. An equilibrated medium ($T > 0$) screens the potential at large distances, described by the boson self-energy in the static limit.

§ 3 Dynamical properties

The relativistic Boltzmann equation can describe how the distribution function evolves and may, in light of asymptotic freedom, aptly model the QGP. We review a general technique to linearise the Boltzmann equation for a slightly inhomogenous gas. This enables the calculation of transport coefficients, which are relevant for first order viscous hydrodynamics. Recasting the task as a variational problem has been used to determine the leading term in a fixed-α expansion for η. But the well-known formula is seemingly incompatible with the experimental findings, $\eta/s \lesssim 0.5$, for reasons we shall explain. To extrapolate to large coupling values, we find it necessary to take into account both screening and running coupling. In closing, we comment on the validity of a kinetic approach for 'strong coupling'.

Before beginning, let us make a general comment on the usefulness of perturbation theory for systems which may not be weakly coupled. Let us call a certain (approximate) calculational scheme a *model*, if it is based on a theory i. e. (1.1). A model, like a theory, has free parameters which need to be fixed by comparing against the measurements of some observable $\mathcal{R}(X)$. In quantum field theory, this process is called *renormalisation* and involves specifying, at a scale X, the value of α. We regard truncated expansions in α as a 'sequence of models', for which the formal issue of non-convergence is not an issue. With parameters fixed, we can use the model to make predictions; either for the same observable $\mathcal{R}$ at a modified scale X', or a related observable $\mathcal{R}'$. The main concern here, is the range of applicability (in X- and $\mathcal{R}$-space) for a given model with fixed parameters. For QCD, this is particularly important, as an ambiguity in the running coupling can sabotage the predictive power in any model.

Notation and conventions

We make use of the 'natural units' $1 := \hbar = c = k_B$ so that Planck's constant is $h = 2\pi$.

Euclidean (d-) vectors are flagged by Latin indices, like x_i. We write the boldface script,

$$\boldsymbol{x} = (x_1, x_2, \ldots, x_d)\,, \quad \text{where} \quad d = 3 \text{ (usually)}\,.$$

Summation convention will be used, and scalar products are denoted

$$\boldsymbol{x}\cdot\boldsymbol{y} \;=\; x_1y_1 + x_2y_2 + \ldots + x_dy_d \;=\; x_iy_i\,.$$

The magnitude of a vector is $x = |\boldsymbol{x}| = \sqrt{\boldsymbol{x}\cdot\boldsymbol{x}}$ and its direction $\hat{x} = \boldsymbol{x}/x$. We employ two abbreviations for spatial derivatives and momentum integrals, respectively;

$$\text{Coordinates:} \quad \nabla = \partial_i = \frac{\partial}{\partial x^i}\,, \qquad\qquad \text{Momentum:} \quad \int_{\boldsymbol{k}} = \int \frac{\mathrm{d}^d k}{h^d}\,.$$

For isotropic integrals, the measure in d-dimensions is

$$\mathrm{d}^d k \;=\; \frac{\pi^{d/2}}{\left[\frac{d}{2}-1\right]!}(k^2)^{\frac{d}{2}-1}\mathrm{d}(k^2)\,.$$

The components of $(d+1)$-spacetime vectors will be capitalised[4] and denoted by Greek indices $X_\alpha = (x_0, \boldsymbol{x})$. The covariant metric tensor in $d = 3$, Minkowski space

$$g_{\mu\nu} \;:=\; \mathrm{diag}\,(+,-,-,-)$$

and is self inverse: $g_{\mu\nu}g^{\mu}{}_{\rho} = g_{\nu\rho}$. Hence the 4-products are $X_\mu Y^\mu = x_0y_0 - \boldsymbol{x}\cdot\boldsymbol{y}$. We write the 4-momentum with components $K = (E, \boldsymbol{k})$. Fixed values (i. e. by energy conservation) will be denoted by $\underline{K}$.

The single particle distribution functions are

$$f(\epsilon) = \frac{1}{\exp(\epsilon/T) \mp 1} \quad \text{for} \quad \begin{cases} \text{Bosons} \\ \text{Fermions} \end{cases}\,, \tag{1.2}$$

which shall also be denoted f_{B} and f_{F} respectively. We denote $\bar{f} = 1 \pm f$ (the + sign reflects Pauli-blocked states and the − signals the Bose enhancement).

Functionals shall be denoted with rectangular brackets for arguments, i. e. $\mathcal{F}[\phi]$. Derivatives and integrals over the operator-space are

$$\frac{\delta\mathcal{F}}{\delta\phi} \qquad \text{and} \qquad \int \mathcal{D}\phi\,\mathcal{F}\,.$$

The energy-momentum tensor shall be denoted

$$\Theta^{\mu\nu}[f] \;=\; \int \frac{1}{k^0} K^\mu K^\nu f\left(k^0\right)\,.$$

The Hamiltonian and Lagrangian densities shall be written $\mathcal{H}$ and $\mathcal{L}$ respectively. For quantities depending only on position: $\mathcal{U}$ is the external potential energy, and $\mathcal{V}$ for a two body (central) potential.

Extensive quantities are given roman capitals $E, V, N, \ldots$. While the intensive variables will be lower case: $\varepsilon = E/V$ for the energy density and p for the pressure. Mean values for distributed quantities are represented with an over-bar $\bar{O}$.

[4] With the exception of $u_\mu = \gamma(1, \boldsymbol{u})$, the four-velocity.

2. Static Properties

A key quantity in thermodynamics is the partition function, from which relevant observables can be calculated. For an equilibrated system at temperature T, the partition function Z is obtained as a sum over all degrees of freedom

$$Z(\beta) = \mathrm{tr}\left[e^{-\beta\mathcal{H}}\right] \quad \text{with} \quad \beta = 1/T\,.$$

The bulk properties of a gas in equilibrium may be derived from the closely related free energy $\Omega = -T\log(Z)$, also known as the *Grand potential*. Such a function of state variables (here V, T and μ) quantities how the energy content responds to thermal, chemical, or mechanical work.

In the thermodynamic limit, a rescaling of the volume $V \to \kappa V$ increases the number of microstates by the same factor κ. Because of this, extensive quantities grow linearly with volume [13]. In this case it is favourable to start with $\Omega(V,T,\mu)$, where

$$\mathrm{d}\Omega \;=\; -p\mathrm{d}V - S\mathrm{d}T - N\mathrm{d}\mu\,.$$

This Grand potential is natural when treating systems at a given temperature, for which the particle number may change. The pressure measures how internal energy responds to changes in volume, i. e.in the thermodynamic limit

$$p(T,\mu) \;=\; -\left.\frac{\partial\Omega(V,T,\mu)}{\partial V}\right|_{T,\mu} \;=\; T\frac{1}{V}\log\left(Z\right)\,. \tag{2.1}$$

Hence p is directly related to the partition sum Z, and independent of V.

The entropy is the negative temperature derivative of Ω, at constant chemical potential, and therefore the entropy density $s = S/V$ may be derived from the pressure;

$$s(T,\mu) \;=\; \left.\frac{\partial p(T,\mu)}{\partial T}\right|_{\mu}\,. \tag{2.2}$$

Note that positivity of the entropy implies p is an *increasing* function of T.

Taking, rather, the derivative of Ω with respect to μ, at constant temperature, gives the total particle number N, so that particle density reads

$$n(T,\mu) \;=\; \frac{N}{V} \;=\; \left.\frac{\partial p(T,\mu)}{\partial\mu}\right|_{T}\,. \tag{2.3}$$

Eqs. (2.2) (2.3) are often combined into the Gibbs-Duhem relation, viz. $\mathrm{d}p = s\mathrm{d}T + n\mathrm{d}\mu$. Thus, by its relation to the total energy, $E = \Omega + ST + N\mu$, the energy density ε satisfies

$$\varepsilon(T,\mu) \;=\; -p(T,\mu) + s(T,\mu)T + n(T,\mu)\mu\,. \tag{2.4}$$

If the particle number N is not conserved, then the dual variable μ must be zero, (otherwise the entropy could be increased by adding or removing a particle). This is the case for gluons, where number-changing process can occur (in a colour-neutral system), but not for quarks due to Baryon number conservation. Hence in our case studies of $n_f = 0$ we shall assume $\mu = 0$.

2.1 Partition function in Coulomb gauge

Here we evaluate the partition function for the $U(1)$-symmetric theory in Coulomb gauge. Covariant gauges are more popular for this derivation, e. g. Ref. [14], because of Lorentz invariance. However, the presence of a thermal heat bath distinguishes a frame, breaking Lorentz symmetry in any case. We repeat the calculation in Coulomb gauge and thus generate the Feynman rules (Appendix A), where the benefit will become more apparent for QCD and shall be used in subsequent perturbative calculations.

The fields are $\{\varphi, \boldsymbol{A}\}$ where φ is the electrostatic potential, and $\boldsymbol{A}$ is the d-component vector potential. The Hamiltonian density is, in terms of the fields, $\mathcal{H} = \frac{1}{2}(E^2 + B^2)$ which can be used to calculate the partition function for pure 'Quantum Photodynamics'. After Wick rotating $t \to i\tau$, one may express Z by functional-integration over the field configuration, (see Ref. [15]) with the gauge condition $\nabla \cdot \boldsymbol{A} = 0$,

$$Z = \int \mathcal{D}\varphi\, \mathcal{D}\boldsymbol{A}\, \delta(\nabla \cdot \boldsymbol{A}) \det\left(-\nabla^2\right) \exp\Big[- \int_0^\beta \mathrm{d}\tau \int_V \mathrm{d}^d x\, \mathcal{L} \Big]. \tag{2.5}$$

For Bosons, the temporal direction is compactified around a circle in imaginary time $\tau \in [0, \beta]$, and thus the fields satisfies periodic boundary conditions $A_\mu(0, \boldsymbol{x}) = A_\mu(\beta, \boldsymbol{x})$. The integration over $(d+1)$ field components in (2.5) is restricted by the gauge condition and the functional determinant. We express the Lagrangian, related to $\mathcal{H}$ by a Legendre transform, in terms of the potentials

$$\begin{aligned} \mathcal{L} &= \frac{1}{2}\Big[\left(\nabla\varphi + \dot{\boldsymbol{A}}\right)^2 - (\nabla \times \boldsymbol{A})^2\Big] \\ &= \frac{1}{2}\left[(\nabla\varphi)^2 - (\partial_\tau \boldsymbol{A})^2 - (\nabla \times \boldsymbol{A})^2\right] + \underline{\left(\nabla\varphi \cdot \dot{\boldsymbol{A}}\right)}. \end{aligned}$$

The dot denotes a (real) time derivative $\partial/\partial t$. Once expanded, and integrated by parts, the underlined term may be replaced by $\varphi \nabla \cdot \dot{\boldsymbol{A}}$ which is zero in Coulomb gauge. Hence the partition function decouples into longitudinal and transverse modes (φ and $\boldsymbol{A}$ respectively). The d components of $\boldsymbol{A}$ are not independent, owing to the gauge condition $\nabla \cdot \boldsymbol{A} = 0$. We wish to diagonalise the quadratic forms for each of the fields in $\{\varphi, \boldsymbol{A}\}$, which should reveal the independent contributions. Because the kernels are Gaussian, we may do this by a Fourier mode expansion, viz.

$$\varphi(\boldsymbol{x}) = \sum_{\boldsymbol{k}} \varphi_{\boldsymbol{k}} \frac{e^{i\boldsymbol{x}\cdot\boldsymbol{k}}}{V} \quad \text{and} \quad \varphi(\tau) = T \sum_{\omega} \varphi(\omega) e^{i\tau\omega},$$

and similarly for the $\boldsymbol{A}$-fields. Note that the periodicity in τ means that the frequency can only take values $\omega = 2\pi T n$, $n \in \mathbb{Z}$, the so-called *Matsubara frequencies*. If the spatial volume is finite, the momentum modes are also discrete.

Although $\boldsymbol{A} \in \mathbb{R}^d$, in the Coulomb gauge one of the directions is redundant since $\boldsymbol{k} \perp \boldsymbol{A}$. Therefore we shall split $\boldsymbol{A} = (A^\parallel, A^\perp)$ into a component $A^\parallel$, which is parallel to $\boldsymbol{k}$, and a transverse projection $A^\perp$. Note that $A^\perp$ has $(d-1)$ components and satisfies $[\boldsymbol{k} \times \boldsymbol{A}]^2 = k^2 \left|A^\perp_{\boldsymbol{k}}\right|^2$. Returning to (2.5), the δ-functional sets the parallel component to zero:

$$\int \mathcal{D}A^\parallel\, \delta\big(|k|\, A^\parallel\big)\, f(A^\parallel) = \frac{1}{\sqrt{\det \boldsymbol{k}^2}} f(0).$$

After this simplification the partition function, now in a diagonal basis, is

$$Z = \int \mathcal{D}\varphi \mathcal{D}A^{\perp} \sqrt{\det \boldsymbol{k}^2} \exp\Big[-\frac{1}{2}\sum_{\boldsymbol{k}} \boldsymbol{k}^2 |\varphi_{\boldsymbol{k}}|^2 \Big] \cdot \exp\Big[\frac{1}{2}\sum_{\boldsymbol{k},\omega} \left(\omega^2 + \boldsymbol{k}^2\right) \left|A^{\perp}_{\boldsymbol{k}}\right|^2 \Big] . \tag{2.6}$$

The φ-field can be integrated out, using standard techniques [16], and cancels the $\sqrt{\det}$ term. All that remains, therefore, is the functional integration over the $A^{\perp}$-fields. These $d_{\perp} = (d-1)$ degrees of freedom are what correspond, in $d = 3$ dimensions, to the two polarisations of light. One benefit to calculating Z in Coulomb gauge is that there is no necessity to introduce ghost fields via the functional determinants (2.6). Albeit of little consequence for QED, ghosts play a ubiquitous role in non-Abelian theories in many favoured gauges.

The resulting determinant is a product of its eigenvalues, this time for the $A^{\perp}$ fields. We find in Z, for each component of $A^{\perp}$ in the exponent (2.6), a factor

$$\sqrt{\det\left(\partial_{\tau}^2 + \nabla^2\right)} = \Big[\prod_{\boldsymbol{k},\omega} \beta^2 \left(\omega^2 + \boldsymbol{k}^2\right) \Big]^{1/2} .$$

Hence taking the logarithm of Z will unzip the product to a sum over $\boldsymbol{k}$ and ω , which we combine into a *Euclidean* 4-momentum $K = (i\omega, \boldsymbol{k})$ for each oscillator. In the infinite volume limit $\sum_{\boldsymbol{k}} = V \int \mathrm{d}^d\boldsymbol{k}/h^d$, and the pressure (2.1) is

$$\beta p = \frac{\log Z}{V} = -\frac{d_{\perp}}{2} \oint\!\!\!\!\!\!\sum_{K} \log\left(-\Delta_K^{-1}\right) , \tag{2.7}$$

where $\Delta_K = -\left(\omega^2 + \boldsymbol{k}^2\right)^{-1}$. The sum over discrete Matsubara ω-modes can be taken (see Appendix B, where we also define in general the notation $\oint\!\!\!\!\!\!\sum_K = T\sum_{\omega}\int_{\boldsymbol{k}}$), and the result is

$$p(T) = -d_{\perp} \int_{\boldsymbol{k}} \Big[\frac{k}{2} + T \log\left(1 - e^{-\beta k}\right) \Big] . \tag{2.8}$$

In physical terms, Eq. (2.6) represents the photon field as a set of (infinitely many) harmonic oscillators, all independent. By this approach, we see how the static fields manage to 'cancel' the contribution from the unphysical $A^{\parallel}$. Only the $d_{\perp} = d-1$ transverse fields contribute the pressure, the longitudinal polarisations are 'inert'. The first term in square brackets of (2.8) is the divergent vacuum part of the pressure. It originates from the zero Matsubara mode and may[5], e. g. by dimensional regularisation, be formally dropped [17].

QCD pressure

Generalising to QCD with $n_f = 0$ is rather straightforward. The Lagrangian (1.1) has a *local* $SU(N_c)$ symmetry with the covariant derivative $D_{\mu}[A] = \partial_{\mu} + igA_{\mu}$, meaning that the 4-vector potential $A_{\mu} = (\varphi, \vec{A})$ takes values in the Lie algebra,

$$A_{\mu} := A^a_{\mu} t^a \in \mathbb{R}^{d+1} \otimes \mathfrak{su}(N_c) .$$

Thus the functional derivative now carries an extra colour label $a = 1, 2, \ldots N_c^2 - 1$. The field strength tensor $F_{\mu\nu} = \frac{1}{ig}[D_{\mu}, D_{\nu}]$ has the correct transformation properties for gauge

[5] It is equally valid to argue from the fact that only differences in pressure are measurable. Thus an absolute (constant) infinity will always cancel in observations, unless $V < \infty$, as for the Casimir effect.

invariance. The kinetic term thus reads,

$$\begin{aligned} F^2 \;=\; & (\partial_\mu A_\nu - \partial_\nu A_\mu)\,(\partial^\mu A^\nu - \partial^\nu A^\mu) \\ & +(-ig)\;(\partial_\mu A_\nu - \partial_\nu A_\mu)\,[A^\mu,\, A^\nu] \\ & +(-ig)^2\,[A_\mu,\, A_\nu]\,[A^\mu,\, A^\nu]\;. \end{aligned} \tag{2.9}$$

Only the first line above appears in QED, where the gauge fields commute. But for non-Abelian theories $[A_\mu,\, A_\nu] = iA^a_\mu A^b_\nu f^{abc} t^c \neq 0$ and the last two terms in (2.9) lead to the three- and four-gluon vertices.

The non-interacting gluon gas $g \to 0$ returns (2.9) to the QED-like Lagrangian (furnished with extra colour quantum numbers). Hence the Stefan-Boltzmann pressure is, after dropping the vacuum part,

$$\begin{aligned} p(T) \;&=\; -d_g T \int_{\boldsymbol{k}} \log\left(1 - e^{-\beta k}\right) \\ &=\; -d_g T \int_{\boldsymbol{k}} \frac{k}{d}\;\left(e^{\beta k} - 1\right)^{-1} \;=\; d_g \frac{T^{d+1}}{(4\pi)^{d/2}} \frac{d!}{(d/2)!}\zeta(d+1)\,, \end{aligned}$$

after integrating by parts. Here $d_g = d_\perp(N_c^2 - 1)$ is the gluon degeneracy. Thus the entropy follows from (2.2), $s = \partial p/\partial T = (d+1)p/T$. The energy density is therefore [by (2.4)] equal to $\varepsilon = d \cdot p$, reflecting that the pressure acts on the d-faces of a infinitesimal (hyper-)cube.

Taking into account (massless) quarks is simple; in the non-interacting case Z decouples into a boson and a fermion partition function, and these two species of particle give independent contributions to the pressure. All that changes in (2.7), assuming $\mu = 0$, is that the Matsubara frequencies occur at odd integer multiples of $i\pi T$ (see Appendix B), and a degeneracy $d_q = 4N_c n_f$. For $d = 3$, the result is

$$p_0(T) = \underline{d}\frac{\pi^2}{90}T^4\;, \qquad s_0(T) = \underline{d}\frac{2\pi^2}{45}T^3\;, \qquad \varepsilon_0(T) = \underline{d}\frac{\pi^2}{30}T^4\,; \tag{2.10}$$

$\underline{d} = d_g + (7/8)d_q$. These formulae are the QCD Stefan-Boltzmann laws, and, although Eqs. (2.2) (2.4) are general, were derived for a non-interacting gas. However, for $g > 0$, (2.5) can be expanded according to perturbation theory [18]. But before considering interaction effects, we shall discuss some aspects of the relativistic formulation of these bulk properties.

Relativistic stress-tensor

In an ideal fluid the total entropy and particle number are conserved. However, the respective densities for these bulk quantities may change if the volume changes;

$$\frac{\mathrm{d}\varepsilon}{\varepsilon + p} \;=\; \frac{\mathrm{d}s}{s} \;=\; \frac{\mathrm{d}n}{n} \;=\; \frac{\mathrm{d}V}{V}\,.$$

Relativistic systems are conveniently characterised by the energy-momentum tensor $\Theta_{\mu\nu}$, which summarises both the energy content and momentum flux, and a particle current j_μ. For an ideal fluid in equilibrium, moving with four-velocity $u_\mu = \gamma(1, \boldsymbol{u})$ in the 'laboratory' frame, the energy-momentum tensor reads

$$\Theta_{\mu\nu} \;=\; (\varepsilon + p)u_\mu u_\nu - p g_{\mu\nu} \quad \xrightarrow{u_\mu = (1,\boldsymbol{0})} \quad \mathrm{diag}\,(\varepsilon, p, p, p)\,. \tag{2.11}$$

The four-velocity u_μ is another equilibrium parameter, which has time-like normalisation $u_\mu u^\mu = +1$. The Landau-Lifshitz definition for the local rest frame is as the solution to the eigenvalue problem [19]

$$u_\mu \Theta^\mu{}_\nu \;=\; \varepsilon u_\nu \;; \qquad (\nu = 0, 1, 2, \ldots, d)\,. \tag{2.12}$$

Notice that the trace of Θ vanishes, i. e. $\Theta^\mu{}_\mu = 0$, for a non-interacting system of massless particles [such as that described by (2.10)]. In general, $\Theta^\mu{}_\mu$ is some positive factor multiplied by the on-shell mass ($K^\mu K_\mu = m^2$) and therefore, as a robust inequality [13],

$$\operatorname{tr}\Theta \;=\; \varepsilon - d\cdot p \;\geq\; 0\,. \tag{2.13}$$

To understand the system of $(d+1)$ equations in (2.12), we shall describe the process to change between the independent quantities $\varepsilon \in \mathbb{R}$ and $\boldsymbol{u}$, and the components of the energy momentum tensor (this is a bijection between the $d+1$ independent quantities). Define

$$a \;\coloneqq\; \Theta_{00}\,, \quad b_i \;\coloneqq\; \Theta_{0i}\,; \qquad (i = 1, 2, \ldots, d)\,.$$

The pressure is an additional thermodynamic quantity, which is fixed by the equation of state, i. e. $p = p(\varepsilon)$, which we assume to be $\varepsilon = d\cdot p$ for an ideal gas. In that case, by definition,

$$a = \left[(d+1)\gamma^2 - 1\right] p\,, \qquad \boldsymbol{b} = (1+d)\gamma^2 p\;\boldsymbol{u}\,. \tag{2.14}$$

Hence, the spatial components sum to

$$\begin{aligned} \boldsymbol{b}^2 = \sum_{i=1}^{d} b_i^2 \;&=\; \left[(d+1)\gamma p\right]^2 (1-\gamma^2)\,, \\ \Rightarrow\quad a^2(d+1)^2 - 4d\boldsymbol{b}^2 \;&=\; (d+1)^2\left[(d-1)\gamma^2 + 1\right]^2 p^2\,, \end{aligned}$$

using the fact that $1-\gamma^2 = u^2$. Hence one finds

$$\varepsilon \;=\; \frac{1}{2}\sqrt{a^2(d+1)^2 - 4d\,\boldsymbol{b}^2} \;-\; \frac{1}{2}a(d-1)\,. \tag{2.15}$$

To calculate the components of the velocities, simply note that $a - \varepsilon = (d+1)(\gamma^2-1)p$ which allows the simplification

$$\boldsymbol{u} = \boldsymbol{b}\cdot\left(\frac{a-\varepsilon}{\boldsymbol{b}^2}\right). \tag{2.16}$$

Summarising, Eq. (2.14) determines (a, b_i) from ε and $\boldsymbol{u}$. Eqs. (2.15) and (2.16) inverts the whole process. Thus the equilibrium parameters are in a bijection with the energy momentum tensor $\Theta_{\mu\nu}$, with a trace that characterises the equation of state (we shall return to this point shortly).

2.2 Weak coupling; $p(\alpha)$

Interactions, built into QCD via the coupling parameter α, cause the pressure to deviate from its free value. Knowing the temperature dependence of the pressure, i. e. $p(T)$, is enough to obtain other thermodynamic quantities of interest through Eqs. (2.2)-(2.4). Because $\alpha(k)$ becomes smaller for large arguments ($k \gg \Lambda$, which we define later), perturbation theory can be used. This is the case in particular at high temperatures, where the

average momentum $\bar{k}$ is similar to the temperature, $\bar{k} \sim T$ (in equilibrium). Let the pressure be represented (naïvely) as an expansion in powers of α, with

$$p(T;\alpha) \;=\; p_0(T) + p_1(T) + p_2(T) + \dots\,, \tag{2.17}$$

where $p_n(T) \sim \mathcal{O}(\alpha^n)$. The normalisation is set by $p_0(T) = p(T;0)$ given in Eq. (2.10) and yields an upper bound $p_0(T) \geq p(T;\alpha)$. For T sufficiently below the transition temperature T_c, the massive confinement degrees of freedom give a drastically smaller value of p.

The lowest order $\mathcal{O}(\alpha)$ diagrams give a negative correction to the pressure, which may also be related to an 'excluded volume'. The relevant loop diagrams are

$p_1(T) \;=\; \frac{1}{8}$ 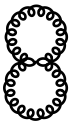 $+\; \frac{1}{12}$  $-\; \frac{1}{2}\, n_f$  . (2.18)

In QED, the last term above is the only contribution, which makes the pressure no longer independent for quark and gluon fields. Even if $n_f = 0$, the first two terms in (2.18) give a correction to the pressure due to the self interaction of the gluons.

Cross-coupling of quarks and gluons

To illustrate the leading order contribution to the pressure, we evaluate the last term in (2.18). This diagram is also important because it indicates that corrections to the free pressure do not decouple for bosonic and fermionic species. For simplicity, we present the calculation in a covariant gauge. The fermionic propagator is $\not{Q}\,\Delta_Q$ and the gauge boson is $g_{\mu\nu}\Delta_Q$ so that the diagram reads

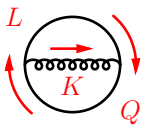

$$= \; g^2 \oint\!\!\!\!\!\!\sum_{L,Q,K} (2\pi)^4 \delta^4(K - L + Q)\;\; \mathrm{tr}\left[\gamma^\mu \not{L} \gamma_\mu \not{Q}\right] \Delta_L\, \Delta_Q\, \Delta_K\,. \tag{2.19}$$

The gluon momentum is fixed by the 4-momentum conserving Δ0function, i. e. $\underline{K} = L - Q$. The trace simplifies $\mathrm{tr}\,[\cdots] = -8L.Q$ the fermion numerators, and with $\underline{K}^2 = L^2 - 2L.Q + Q^2$ (the underline flags the *fixed* value) one finds

$$= \; -8g^2 \oint\!\!\!\!\!\!\sum_{L,Q} \underbrace{\frac{L.Q}{L^2 Q^2}\, \underline{K}^{-2}} \tag{2.20}$$

$$= \left[\Delta_L \Delta_{\underline{K}} + \Delta_Q \Delta_{\underline{K}} - \Delta_L \Delta_Q\right]$$

after a rewriting of the 4-product $L.Q = \frac{1}{2}\left(L^2 + Q^2 - \underline{K}^2\right)$. The result is proportional to a combination of elementary tadpole diagrams (see Appendix B)

$$\oint\!\!\!\!\!\!\sum_{L,K} \frac{1}{L^2\, K^2} + \oint\!\!\!\!\!\!\sum_{Q,K} \frac{1}{Q^2\, K^2} - \oint\!\!\!\!\!\!\sum_{L,Q} \frac{1}{L^2\, Q^2} \;=\; -\frac{T^4}{4} \cdot \frac{5}{144}\,.$$

Altogether, this diagram gives a 2-loop contribution to the pressure,

$$\log(Z)\big|_{2\text{–loop}} \;=\; -\frac{1}{2}$$  $$\;=\; -\alpha T^4 \cdot \frac{5\pi}{72}\,. \tag{2.21}$$

We conclude that this interaction *reduces* the pressure from the free limit, to first order.

Screening

For certain graphs of order $\mathcal{O}(\alpha^n)$, $n \geq 2$, the direct evaluation gives $p_n = \infty$. Such a *non-analytic* property (for p as an function of α) stems from the long ranged nature of the (gauge) force, and is well known from the classical Coulomb gas [20]. The remedy is to resum infinitely many diagrams, of the ring-type topology, which actually give a *fractional* power of α in (2), namely $\alpha^{3/2}$,

$$p_{3/2}(T) \;=\; \sum_{\ell\geq 2} \frac{(-)^\ell}{\ell} \Bigg(\quad \vdots \quad \Bigg) \,; \qquad \ell = \text{number of blobs} \,.$$

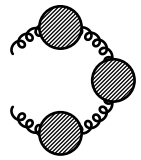

Each shaded blob represents the gluon self energy and $p_{3/2}(T)$ is finite, even though each term in the sum is infinite. To first order, without ghosts in Coulomb gauge, the self energy is

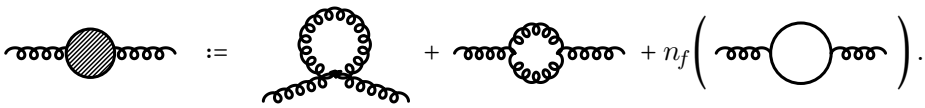

$$:= \quad + \quad + n_f \Bigg(\quad \Bigg) \,. \qquad (2.22)$$

As a side remark, the 2-point functions above may be obtained by 'cutting' one of the gluon lines in (2.18). This is a general topological relation between the 2-particle irreducible diagrams for the pressure and the self energy to a corresponding order [21].

Once this resummation has been made, the $\mathcal{O}(\alpha^2)$ is finite but its 'coefficient' depends on α through a new term $\alpha^2 \log(\alpha)$. Its evaluation requires 3-loop diagrams to be properly screened [22]. Furthermore, the $\mathcal{O}(\alpha^2)$ formula compels the use of the scale dependent coupling $\alpha(\mu)$, where μ is a renormalisation scale appearing in a manner such that $\partial p\left(T;\, \alpha(\mu)\right)/\partial\mu = 0$ up to higher order terms than the approximation used.

The perturbative expansion for $p(T;\, \alpha)$ is known analytically through order $\mathcal{O}(\alpha^{5/2})$, beyond which the serious infrared difficulties of QCD hamper further progress [23]. To be precise; the coefficient of $\alpha^3 \log \alpha$ is known, but the coefficient of α^3 is not accessible by perturbative means. Nevertheless, asymptotic formulae[6] can be useful when truncated to a finite number of terms. A *fixed order* calculation becomes precise in the limit $\alpha \to 0$, for which purpose we shall study (as a *model*)

$$p\Big(T;\, \alpha(2\pi T)\Big) \;=\; p_0(T) \left\{ 1 + c_1\alpha + c_{3/2}\alpha^{3/2} + \alpha^2(c_2 + c_2' \log(\alpha)) + c_{5/2}\alpha^{5/2} + \mathcal{O}(\alpha^3) \right\} . \qquad (2.23)$$

The term $\mathcal{O}(\alpha^3)$ has the coefficient $c_3 + c_3' \log(\alpha)$, where c_3' is the final perturbative piece, see [24], and c_3 must be calculated by non-perturbative means.

Complementing the weak-coupling approach, numerical results based on lattice QCD (lQCD) have revealed much about the equation of state (Fig. 2). Such non-perturbative studies, which basically Monte Carlo sample discrete versions of (1.1), have become remarkably accurate in the vicinity of the critical temperature, due to modern hardware and

[6] Perturbative QCD gives, at best, something similar to an asymptotic series. Thus suggests that the absolute error tends to zero, although the sign may (and does in this case) depend on the level of truncation.

improved actions [25]. There is no longer any doubt that the transition from a hadronic to partonic system happens smoothly at the confinement temperature $T \sim T_c$. Moreover, the asymptotic approach to the Stefan-Boltzmann limit (2.10) is very gradual, which has been understood in terms of the underlying quasiparticle degrees of freedom [26]. For the quenched case, recent calculations have been able to cover a huge temperature range from slightly below T_c up to $10^3 T_c$ [27]. Since the asymptotic expansion $p(T;\alpha)$ does not converge, it is particularly sensitive to c_3 – which has been 'fit' (for $n_f = 0$) by the authors of [27]. They also concluded that Eq. (2.23), including the now established term $p_3(T)$, was applicable all the way down to about $10T_c$. Let us point out that although $p(T)$ *can* be calculated on the lattice [28], it is more convenient to start from the *interaction measure* [also called trace anomaly by its connection with (2.13)],

$$w(T) \;:=\; \varepsilon(T) - 3p(T) \;=\; \mathrm{tr}\;\Theta\;, \tag{2.24}$$

where $\Theta_{\mu\nu}(T)$ is the energy momentum tensor (2.11).

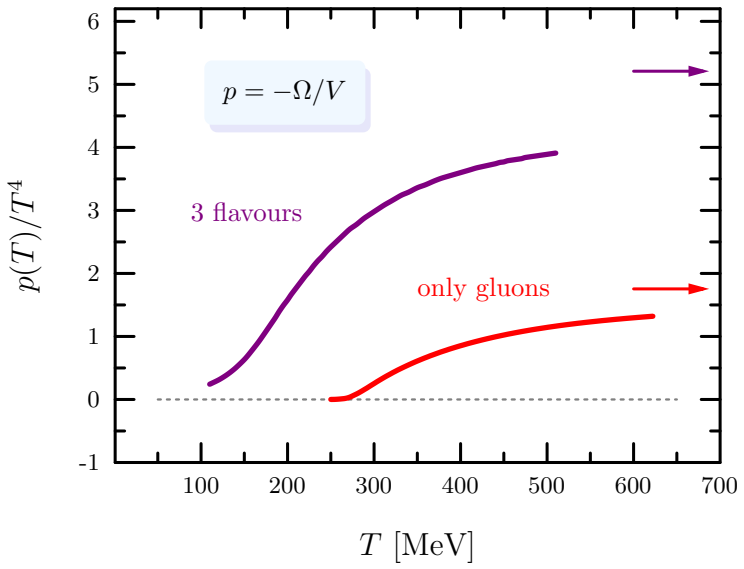

Figure 2: Here we show the continuum extrapolated lattice data, $n_f = 0$ [29, 27] and $n_f = 2+1$ [30, 31], for the scaled pressure $p(T)/T^4$. The increase at $T \sim T_c$ is due to a larger number of partonic degrees of freedom which become available at higher temperatures. The arrows mark the Stefan-Boltzmann limit, (2.10), which is approached in the perturbative limit.

We briefly comment on $w(T)$ in the context of perturbation theory, before moving on to discuss its usefulness in lattice QCD. For a conformal theory, the equation of state $\varepsilon(T) = 3p(T)$ is true even for fully interacting systems (due the fact that the partition function Z is a function of T and V in the combination T^3V). Therefore, $w(T) \neq 0$ can only arise for a system with an additional scale, other than T and V. This is indeed the case for QCD, where the energy scale Λ enters by dimensional transmutation and replaces α as the free parameter in the model (in the sense defined in the outline). In the perturbative expression for the scale-dependent ('running') coupling, Λ is a pole, for example the 2-loop

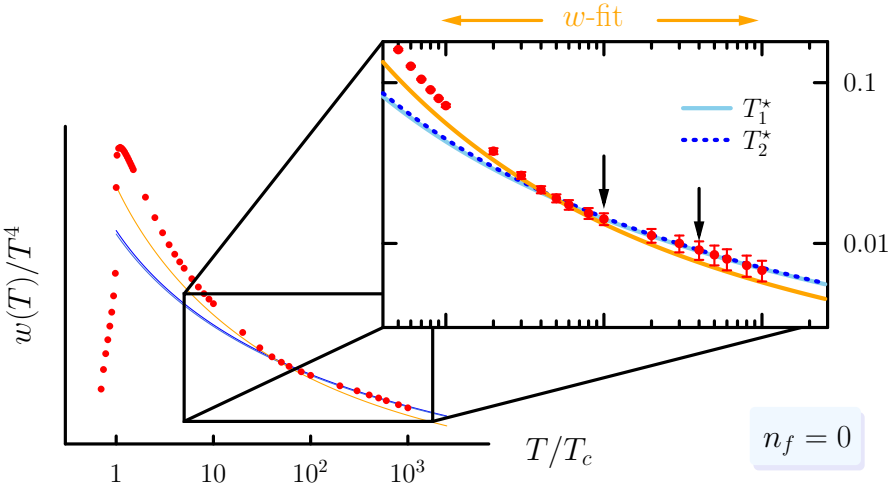

Figure 3: The interaction measure as a function of temperature ($n_f = 0$) as calculated on the lattice [27]. The inset zooms in on $T \gtrsim 5T_c$, and shows the perturbative result for $w(T)$ with the renormalisation points (indicated by arrows) at $T_\star = \{100, 400\}T_c$. For $T \gtrsim 30T_c$, the perturbative model is valid and the two (blue) lines basically overlap. Shown in orange is the $\mathcal{O}(\alpha^3)$ result, with c_3 fitted for $10T_c < T < 10^3 T_c$ [27] (the uncertainty band is as thick as the line).

formula

$$\alpha(\mu) \;\simeq\; \frac{4\pi}{11t}\Big\{1 - \frac{102\log t}{121t}\Big\}\,; \qquad t = \log(\mu^2/\Lambda^2)\,.$$

The auxiliary scale μ emerges from the regularised calculation [22], for the first time at the order $\mathcal{O}(\alpha^2)$ (as mentioned), $p(T;\alpha(\mu))$ has only higher order dependence on μ. To clarify this point, suppose that $\mu \sim T$ (as it should be for a useful perturbative expansion). Then the definition for $w(T)$ along with thermodynamic identities allow us to relate it to the slope of the scaled pressure in Fig. 2, viz.

$$w(T) \;=\; T^5 \frac{\mathrm{d}}{\mathrm{d}T}\Big(\frac{p(T)}{T^4}\Big)\,. \tag{2.25}$$

Note that positivity $w(T) \geq 0$ [originating from (2.13)], implies that $p(T)/p_0(T)$ is a smoothly *increasing* function of T and thus $p_0(T)$ is an upper bound for the pressure. For a 'fixed' coupling, $p(T;\alpha)/T^4$ is constant and thus $w(T) = 0$. A non-zero $w(T)$ is a direct consequence of the renormalisation scale μ, which emerges at the three loop level[7] and determines a manner in which α depends on T. For a direct comparison with [27], we also specify $\mu = 2\pi T$ and use the 2-loop formula for the coupling, so that

$$t \;=\; \log\Big(\frac{2\pi}{l}\frac{T}{T_c}\Big)^2\,,$$

with the dimensionless parameter $l = \Lambda/T_c$ to be adjusted.

Applying (2.25) to Eq.(2.23) yields a model for $w(T)$ and, if we elect to use the $p_{5/2}$ truncation[8], the only free paramter is l. Our idea is then to fix the residual scale Λ, by

[7] It can also be obtained 'by hand' from using a running coupling in lower order result.

[8] Only $p(T;\alpha)$ up to $\mathcal{O}(\alpha^n)$ for $n = 1, 5/2$ and 3 (depending on c_3) are monotonously decreasing functions of α. However in the LO result, α is strictly a fixed coupling, with no T dependence.

directly matching the perturbative formula to the lattice value, viz. $w(T_\star) = w_\star$. In order to test *stability* of a truncated perturbative model, we may choose different 'renormalisation points' $T_i^\star$, which are large but still smaller than the maximal simulated temperature in [27], so that the asymptotic agreement is verified. Fig. 3 shows the results for $w(T)$, using a semi-perturbative $T_\star$ to fix the value of l. Testing the scheme at $T_i^\star = \{10^2, \dots 10^3\}T_c$ produces the array

$T_i^\star/T_c$	100	200	300	400	500	600	800	1000
Λ/T_c	0.5477	0.5601	0.5917	0.5795	0.5737	0.5555	0.5280	0.5015

,

which are fairly consistent and yield visually indistinguishable curves (see Fig. 3). Since $\alpha(T_\star)$ is sufficiently small[9] for larger T, perturbation theory is expected to improve for $T \gg T_\star$. Our matching scheme indeed approximates $w(T)$ well for $T > T_\star$, corroborating the lattice values and ruling out the possibility of an misinterpreted fit.

Actually 'measured' in lattice simulations is $w(T)$, which avoids having to subtract the zero point contribution, as would be necessary for $p(T)$ or $\varepsilon(T)$ [see the '$\frac{1}{2}$' in (2.8)]. On the other hand, from (2.25), it is possible to obtain the pressure via the so-called integral method [32],

$$\frac{p(T)}{T^4} \;=\; \frac{p(T_0)}{T_0^4} + \int_{T_0}^{T} \frac{d\tau}{\tau}\,\frac{w(\tau)}{\tau^4}\,. \tag{2.26}$$

From the interaction measure (2.25), given as a function of T, the pressure can be reconstructed, up to an integration constant which ought to be declared at the reference temperature. In particular, the area bounded by the interaction measure over all temperatures gives the normalisation of $p(T)$ [presuming that $p(T) \to 0$ at zero temperature]. However, integrating up from $T_0 = 0$ introduces another source of uncertainty: increasing correlation lengths near T_c lead to finite-size effects which can at best be estimated by a scaling analysis. But for $T > T_c$, the integral in (2.26) receives a large numerical contribution from the peak in w/T^4 at $T \sim 1.1T_c$ (see Fig. 3) and this may lead to uncertainties in p for $T \to \infty$. Choosing to integrate *down* from T_0 circumvents this issue, since the constant of integration in (2.26) is the familiar Stefan-Boltzmann constant (2.10). With information on $w(T)$ only at a finite set of values for T, Eq.(2.26) requires extrapolating $w(T)$ beyond the endpoint of simulation. The perturbative expression (2.23), used with (2.25) is convenient for that purpose, provided the matching scheme is applied for suitably large temperatures. In [27] this was done by fitting the non-perturbative coefficient c_3 in the temperature range $[10, 10^3]T_c$, giving $c_3 \approx -71.8$ (with an uncertainty of about 1% from varying the endpoints of the fit interval), and $l = 1/1.26$. The fact that perturbation theory apparently works down to $T \sim 10T_c$ seems quite remarkable, and warrants confirmation.

Given the precision of pure gauge lQCD data, we now point out a discrepancy that has so far escaped notice. Shown in Fig. 4 is $p(T)$ at large temperatures $T > 10T_c$ according to our approach, in which the perturbative series is *matched* at some single temperature value $T_i^\star$ and then verified by confirming *local* agreement. The pressure $p(T)$ obtained from the pQCD result (2.23), which is made to reproduce $w(T_\star)$ and *does* agree with $w(T)$ in a fairly wide T-range (down to about $T \sim 40T_c$), is incompatible with [27] using (2.26). Disagreement between the latter and our adjusted perturbative result does not become smaller for larger T, where perturbation theory is expected to work better. The perturbative analysis of the QCD trace anomaly indicates a slower approach of the $p(T)$ to the free limit [and similarly

[9] Characterising α as 'small' can be justified *a posteriori* by testing stability of the fitting scheme.

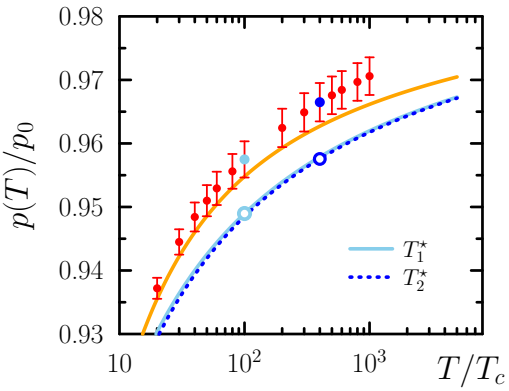

Figure 4: The pressure as a function of temperature (in units of the free value) for $n_f = 0$. Shown as (red) points are the lattice data [27]. The 'renormalisation' points $T_i^\star = \{100, 400\}T_c$ are shown, and are systematically lower than the data proposed by [27]. Evidently there is a discrepancy of $\sim 1\%$ in p with the lattice data, which is also suspicious given that the (orange) curve using the fitted c_3 value lies at the lower limit of the error bars.

for $e(T)$ and $s(T)$]. In the physical case, such a discrepancy would probably be too small to have phenomenological implications. However, an uncertainty of one percent in $p(T)/p_0$ can translate into half an order of magnitude in the temperature T/T_c (see Fig. 4). It may therefore be worthwhile to reconsider, given that the failure emerges in a well-defined limit, which should provide firm baseline for analytical techniques, such as improved resummation frameworks [33].

Polarisation tensor

We found in (2.7), that without interactions only the transverse degrees of freedom contributed to the pressure. A consequence thereof, the gluon propagator in Coulomb gauge separated into the two polarisation states, elaborated in Appendix B. This decomposition is also possible in general (with interactions), and we now discuss the structure of the gluon self-energy [cf. (2.22)], where the medium 'couples' these orthogonal degrees of freedom. The polarisation tensor is a 2-point function, denoted $\Pi_{\mu\nu}$, which is not measurable itself (except in certain limits) and depends on the choice of gauge. Nonetheless, it is a necessary to include screening effects in the calculation of observables[10].

It is important to distinguish the corrections at $T = 0$, from those which arise due to the presence of a thermal medium;

$$\Pi_{\mu\nu}(Q) \;=\; \Pi_{\mu\nu}\Big|_{T=0} \;+\; \widetilde{\Pi}_{\mu\nu}\,. \tag{2.27}$$

Firm statements about the Lorentz components of $\Pi_{\mu\nu}$ can be guided by the Ward identity, viz. $Q^\mu \Pi_{\mu\nu}(Q) = 0$, which also holds at finite temperature [34]. In vacuum there is only one possible combination of the two available symmetric tensors $\{g_{\mu\nu}, Q_\mu Q_\nu\}$, namely

$$\mathbb{P}_{\mu\nu} \;=\; \Big(g_{\mu\nu} - \frac{Q_\mu Q_\nu}{Q^2}\Big)\,,$$

that is orthogonal to Q^μ and idempotent. Furthermore, at zero temperature $\Pi_{\mu\nu}$ depends on ω and $\boldsymbol{q}$ only in the covariant combination $Q^2 = \omega^2 - \boldsymbol{q}^2$. These considerations mean that we need only focus on one dimensionless function of Q^2, denoted $\bar{\pi}$, which satisfies

$$\Pi_{\mu\nu}\Big|_{T=0} \;=\; \alpha\; Q^2 \cdot \bar{\pi}(Q^2)\mathbb{P}_{\mu\nu}\,. \tag{2.28}$$

[10] Many observables actually require screening to render finite the (otherwise occurring) divergences.

Note that $\bar{\pi}$ is of order $\mathcal{O}(1)$ in the coupling, since we have factored out α in the definition as well as Q^2 to give the correct dimension.

The Lorentz structure at $T > 0$ is more complicated by the addition of $\{u_\mu u_\nu,\, u_\mu K_\nu + K_\mu u_\nu\}$ to the symmetric tensor basis for $\Pi_{\mu\nu}$, where u_μ is the four-velocity of the fluid's rest frame [defined in (2.12)]. Two additional scalar functions, longitudinal (L) and transverse (T), can describe $\widetilde{\Pi}_{\mu\nu}$. Corresponding projectors

$$\begin{aligned} \mathbb{P}^L_{\mu\nu} &= -\frac{\widetilde{Q}_\mu \widetilde{Q}_\nu}{Q^2}\,, \quad \text{where} \qquad \widetilde{Q}_\mu := \frac{(Q_\nu u^\nu) Q_\mu - Q^2 u_\mu}{\sqrt{(Q_\nu u^\nu)^2 - Q^2}}\,, \\ \mathbb{P}^T_{\mu\nu} &= \mathbb{P}_{\mu\nu} - \mathbb{P}^L_{\mu\nu}\,, \end{aligned} \tag{2.29}$$

form one such basis [35]. In the local rest frame (i. e. $\boldsymbol{u} = 0$), the tensors read explicitly

$$\mathbb{P}^L_{\mu\nu} = -\frac{1}{Q^2}\begin{pmatrix} \boldsymbol{q}^2 & \omega \boldsymbol{q} \\ \omega \boldsymbol{q} & \omega^2 \hat{q}_i \hat{q}_j \end{pmatrix}, \qquad \mathbb{P}^T_{\mu\nu} = -\begin{pmatrix} 0 & 0 \\ 0 & (\delta_{ij} - \hat{q}_i \hat{q}_j) \end{pmatrix}.$$

Scalar functions, $\widetilde{\Pi}_i = \alpha T^2 \cdot \widetilde{\pi}_i(\omega, \boldsymbol{q})$, for the two polarisations $i = (T, L)$ depend on ω and $\boldsymbol{q}$ separately so that

$$\widetilde{\Pi}_{\mu\nu} = \widetilde{\Pi}_L \mathbb{P}^L_{\mu\nu} + \widetilde{\Pi}_T \mathbb{P}^T_{\mu\nu} = \alpha\, T^2 \cdot \sum_i \widetilde{\pi}_i(\omega, \boldsymbol{q}) \mathbb{P}^i_{\mu\nu}\,.$$

As in Eq. (2.28), we have factored out α and the overall dimension (now set by the temperature). From the projections operators (2.29), the scalar functions may be obtained from the general tensor by

$$\Pi_L = -\frac{Q^2}{\boldsymbol{q}^2}\Pi_{00}\,, \qquad \Pi_T = -\frac{1}{2}\left(\delta_{ij} - \hat{q}_i \hat{q}_j\right)\Pi_{ij}\,. \tag{2.30}$$

We may write the combined self energy as

$$\Pi_{\mu\nu} = \alpha \sum_i \left[\; Q^2 \cdot \bar{\pi}\left(Q^2\right) + T^2 \cdot \widetilde{\pi}_i(\omega, \boldsymbol{q}) \;\right] \mathbb{P}^i_{\mu\nu}\,. \tag{2.31}$$

Despite appearances, there is still only one vacuum term since $\mathbb{P}^T + \mathbb{P}^L = \mathbb{P}$. It is tempting to argue that the vacuum corrections may be 'dropped' (after renormalisation), e. g. because $T^2 \gg Q^2$ in Eq. (2.31). On the contrary, they are infinite before being regularised and then renormalised. Absorbing the (divergent) vacuum contribution into a *running* coupling is actually necessary in order to be able to calculate quantitatively the thermal corrections. Before elaborating this, we shall calculate Π_L in the Coulomb gauge to see both the vacuum and thermal fluctuations on an equal footing.

2.3 Evaluation of Π_L for $T \geq 0$

In Coulomb gauge, the Coulomb field is not dynamical, it is just an instantaneous potential. This makes it rather peculiar and we therefore consider its self-energy. The longitudinal polarisations are given when $\mu = \nu = 0$; from (2.30). We study this entry, using the diagrammatic rules laid out in Appendix A. To leading order $\mathcal{O}(\alpha)$, Π_{00} is the sum[11] of the four diagrams (a)-(d) in Fig. 5. A physical interpretation of the result is left for the next section, and here we calculate the contributions (a)-(d). The reader may skip this section,

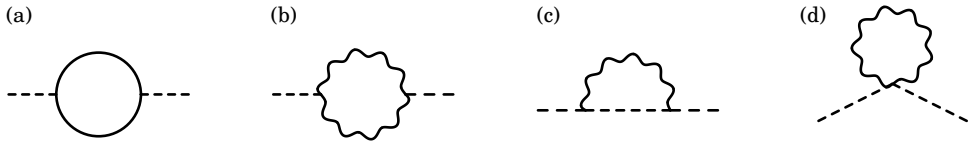

Figure 5: The first corrections to the longitudinal gluon self-energy; the fermion loop (a) and transverse gluon loop (b) give rise to screening effects (both in vacuum and in medium). The Coulomb gluon (c) is the sole cause for anti-screening at $T = 0$ which ultimately leads to asymptotic freedom. Diagram (d) is the tadpole, zero in vacuum but a mass term at $T > 0$.

accepting the result for Π_{00} at the end, and proceed to § 2.4 where we consider the static quark potential.

We shall calculate the diagrams in Fig. 5, loop by loop. For notational convenience, the colour factors are not made explicit; the $SU(3)$ and Lorentz components of diagrams can be separated. Each case will start with the evaluation of the Matsubara sum (see Appendix B), which will help to separate the vacuum from the thermal contribution. The latter shall be reduced to a one dimensional integration without further simplification (yet dependent on choice of gauge).

Analytic expressions for the finite thermal self-energy may be derived in an important limit, namely where the outer momenta $\omega, q \ll T$. In this limit, the behaviour of the Bose function for small arguments $f_{\mathrm{B}}(q) \simeq T/q$ may change the naïve order in α of a diagram if $q \sim \sqrt{\alpha}T$. Perturbation theory must be reorganised in this limit, the so called *hard thermal loop* (HTL) approximation [36]. A general $\Pi_{\mu\nu}$ can be efficiently recast in terms of certain 'master integrals' [36] and simplify to gauge invariant (analytic) functions.

The imaginary part of the vacuum diagrams is easily evaluated by means of the Cutkotsky rules [37], and is sufficient to identify the UV divergence at $T = 0$. Based on analytic properties in the complex plane of the outer momentum variable Q, the imaginary part only has support for $Q^2 > 0$, the threshold for massless pair production. Internal lines are put on shell by taking the imaginary part of

$$\Delta_K = \mathcal{P}\frac{1}{K^2} - i\pi\delta(K^2)\,,$$

and, as explained in Appendix C, may be used to calculate $\bar{\pi}$ in dimensional regularisation. For reasons given below, this strategy fails for (c) and (d), in which the $T = 0$ case is special.

Loop kinematics

Of the loops in Fig. 5, (a)-(c) are topologically the same. Tadpole diagrams, like (d), are local in momentum space and thus Q-independent. The prototype for a 1-loop diagram is shown in Fig. 6, where we specify the relevant momenta. Since $\Pi_{\mu\nu}$ is integrated over all intermediate states, it will be useful to pause and discuss the relevant phase space.

Let the four-momentum running in the loop be $L = (\ell_0, \boldsymbol{\ell})$ and, for outer momentum Q, abbreviate $\underline{K} = Q + L$. The external 3-momentum $\boldsymbol{q}$ distinguishes a preferred direction to organise the $\mathrm{d}^3\boldsymbol{\ell}$-integration. We choose to align the ℓ_z axis with $\boldsymbol{q}$, so that the azimuthal integration is trivial. Instead of a polar integration over $\theta = \cos^{-1}(\hat{\ell}\cdot\hat{q})$, we integrate over the magnitude of $\boldsymbol{k}$, which is $k = \sqrt{\ell^2 + q^2 + 2\boldsymbol{\ell}\cdot\boldsymbol{q}}$. The angular θ-integration translates

[11] The exclusion of certain singly-linked diagrams is permitted by Furry's theorem.

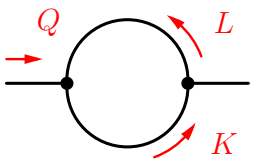

Figure 6: Our convention for labelling of the momentum variables in 1-loop self energies. The external momentum is $Q = (\omega, \boldsymbol{q})$, and the loop integration is taken over $L = (\ell_0, \boldsymbol{\ell})$. Energy and momentum conservation at the vertex fixed $K = (k_0, \boldsymbol{k}) = Q + L$.

into a kinematic restriction; $|\ell - q| < k < |\ell + q|$ (see Fig. 7). Hence it is more convenient to perform the remaining 2-dimensional integral in the quantities k and ℓ. In particular, one has

$$\int_{-1}^{+1} \mathrm{d}(\cos\theta) \;=\; \int_{|\ell-q|}^{|\ell+q|} \mathrm{d}k\, \frac{k}{q\ell}\;. \tag{2.32}$$

These variables are convenient for (ℓ, k)-symmetric integrals, see Fig. 7. All the relevant dot products may be formed in terms of these variables, using

$$\begin{aligned} \boldsymbol{k}\cdot\boldsymbol{\ell} &= \frac{1}{2}\left(k^2 + \ell^2 - q^2\right), \\ \boldsymbol{k}\cdot\boldsymbol{q} &= \frac{1}{2}\left(k^2 + q^2 - \ell^2\right), \\ \boldsymbol{\ell}\cdot\boldsymbol{q} &= \frac{1}{2}\left(k^2 - \ell^2 - q^2\right). \end{aligned} \tag{2.33}$$

When internal lines are on shell, the phase space is restricted to a single dimension and (2.32) may be evaluated in general [see Eq. (C.7)].

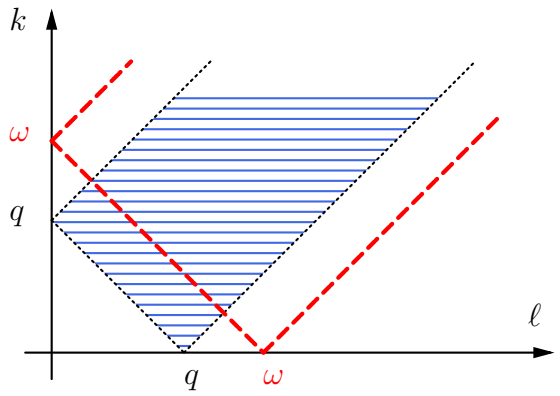

Figure 7: Region of integration over the loop momenta ℓ and k permissible by kinematics. The area hatched (blue) is allowed by energy and momentum conservation. Note the salient points where $\ell = |k \pm \omega|$, give rise to the red line (shown for $Q^2 = \omega^2 - q^2 > 0$). The red line corresponds to small-angle splittings, either forward or backward, which is where the spectral strength will be peaked for masslesss particles.

(a) – Fermion loop

The first diagram is identical to the one-loop photon self energy (since we omit colour factors). Working in Coulomb gauge, we directly calculate the diagram for a (virtual)

longitudinal gluon to transition into itself by splitting into a quark-antiquark pair and recombining (omitting for now the colour indices)

$$\Pi_{00}^{(\mathrm{a})} \;=\; \text{ 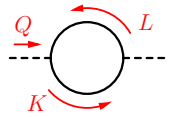 } \;=\; +g^2 \oint_L \boxed{\mathrm{tr}\left[\gamma_0 \underline{\not{K}} \gamma_0 \not{L}\right]} \;\Delta_L \Delta_{\underline{K}} \,. \tag{2.34}$$

$$= 4(k_0\ell_0 + \boldsymbol{k}\cdot\boldsymbol{\ell})$$

Elementary properties of the γ-matrices have been used to simplify the trace for fixed $\underline{K} = Q + L$. The Matusbara ℓ_0-sum can be carried out using Eqs. (B.5) and (B.7). After using the (ℓ, k)-integration variables [see (2.32)] and re-expressing the distribution function $f_{\mathrm{F}}(k)$ by $f_{\mathrm{F}}(\ell)$ thanks to symmetry of the integrand (which gives a factor 2),

$$\begin{aligned}\widetilde{\Pi}_{00}^{(\mathrm{a})} \;=\; -2g^2 \int_{\boldsymbol{\ell}} f_{\mathrm{F}}(\ell) \Big\{ & -\left[\frac{1}{\omega+\ell+k} - \frac{1}{\omega-\ell-k} - \frac{1}{\omega-\ell+k} + \frac{1}{\omega+\ell-k}\right] \\ & + (\hat{\ell}\cdot\hat{k})\left[\frac{1}{\omega+\ell+k} - \frac{1}{\omega-\ell-k} + \frac{1}{\omega-\ell+k} - \frac{1}{\omega+\ell-k}\right] \Big\} \,.\end{aligned} \tag{2.35}$$

Using (2.32), the k-integration may be performed analytically, with the help of (2.33) (although the expressions are lengthly). All that is left is a one dimensional integration over ℓ [which is cut off by the distribution function $f_{\mathrm{F}}(\ell)$ at $\ell \sim T$].

For soft outer momenta, $\omega, q \ll T$, and since the typical loop momentum is hard, $k \sim T$, the cosine term $\hat{\ell}\cdot\hat{k} \approx 1$. Thus Eq. (2.39) simplifies drastically[12], and the k-integration can be done. The result in this HTL approximation, usually calculated slightly differently [15], is

$$\Pi_{\mathrm{HTL}}^{(\mathrm{a})}(\omega, \boldsymbol{q}) \;=\; g^2 \frac{T^2}{6}\left(2 - \frac{\omega}{q}\log\left[\frac{\omega+q}{\omega-q}\right]\right) . \tag{2.36}$$

Instead of calculating $\Pi_{00}^{(\mathrm{a})}$ at zero temperature, we calculate only its (finite) imaginary part by using the Cutkotsky rules [38]. The remaining loop-integral can be reduced, as derived in Appendix C, to

$$\mathrm{Im}\left[\Pi_{00}^{(\mathrm{a})}\right]_{T=0} \;=\; -\frac{g^2}{2\pi q}\theta(Q^2) \int_{\frac{1}{2}(\omega-q)}^{\frac{1}{2}(\omega+q)} \mathrm{d}\ell\,[(-\ell)\underline{k}_0 + \boldsymbol{\ell}\cdot\boldsymbol{k}] \;=\; -\frac{\alpha}{4\pi}\boldsymbol{q}^2\theta(Q^2)\frac{4\pi}{3} \,,$$

where the θ-function reflects that the spectral function only has support for $Q^2 > 0$. Returning to the form Eq. (2.28), we can easily infer the divergent part of the loop, viz.

$$\bar{\pi}^{(\mathrm{a})}(Q^2) \;=\; -\frac{4/3}{4\pi}\frac{1}{\varepsilon}\left(\frac{Q^2}{\mu^2}\right)^{-\varepsilon} \,. \tag{2.37}$$

(b) – Transverse loop

In principle, loop (b) is calculated in just the same way as (a); with bosons replaced by fermions. Note that although loops (b) and (c) are together proportional to $\mathbb{P}_{00}^{L}$, they do

[12] It is actually possible to derive the same result assuming only $-Q^2 \ll T^2$ with the help of (2.33).

not do so separately. The self-energy (b) is given by (the symmetry factor $\frac{1}{2}$ is included)

$$\Pi_{00}^{(\mathrm{b})} \;=\; \tag{2.38}$$

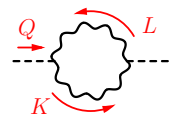

$$= \; -g^2 \frac{1}{2} \oint_L \boxed{\Big(\delta^{ij} - \hat{k}^i\hat{k}^j\Big)\Big(\delta^{ij} - \hat{\ell}^i\hat{\ell}^j\Big)} \; (\underline{k}_0 + \ell_0)^2 \;\; \Delta_L \Delta_{\underline{K}} \,.$$

$$= \big[(d-2) + (\hat{\ell}\cdot\hat{k})^2\big]$$

Here $\underline{K} = Q + L$ is fixed and thus

$$(k_0+\ell_0)^2 \;=\; (2\ell_0+\omega)(2k_0-\omega) \;=\; 4\ell_0 k_0 + 2\omega(k_0-\ell_0) - \omega^2 \;=\; 4\ell_0 k_0 + \omega^2 \,.$$

Again Eqs. (B.5) and (B.7) may be used to carry out the ℓ_0-sum. By the inherent symmetry $\ell \leftrightarrow k$ in (2.32), we may again change variables so that the distribution function appears with only one argument; say ℓ.

The $T > 0$ self-energy reads (setting $d = 3$, since the result is finite),

$$\begin{aligned}\widetilde{\Pi}_{00}^{(\mathrm{b})} \;=\; & -\frac{g^2}{4}\int_{\boldsymbol{\ell}} \big[1 + (\hat{\ell}\cdot\hat{k})^2\big]\, f_{\mathrm{B}}(\ell) \Big\{ \\ & -4\left[\frac{1}{\omega+\ell+k} - \frac{1}{\omega-\ell-k} + \frac{1}{\omega-\ell+k} - \frac{1}{\omega+\ell-k}\right] \\ & + \frac{\omega^2}{\ell k}\left[\frac{1}{\omega+\ell+k} - \frac{1}{\omega-\ell-k} - \frac{1}{\omega-\ell+k} + \frac{1}{\omega+\ell-k}\right] \Big\} \,.\end{aligned} \tag{2.39}$$

The dot product can be rewritten in terms of ℓ and k [see (2.33)], which allows for the k-integration to be completed analytically using (2.32) .

The HTL contribution may be derived as for (a), taking $\hat{\ell}\cdot\hat{k} \approx 1$. Furthermore, since $\omega \ll \ell$, the third line in Eq. (2.39) may be dropped. The result is

$$\Pi_{\mathrm{HTL}}^{(\mathrm{b})}(\omega, \boldsymbol{q}) \;=\; g^2 \frac{T^2}{6}\Big(3 - \frac{\omega}{q}\log\Big[\frac{\omega+q}{\omega-q}\Big]\Big) \,. \tag{2.40}$$

As for the $T = 0$ contribution, we again opt to calculate the imaginary part, using (C.8) for the cut diagram. It is somewhat more complicated than the fermion loop, and yields

$$\mathrm{Im}\Big[\Pi_{00}^{(\mathrm{b})}\Big]_{T=0} \;=\; \frac{g^2}{4\pi}\frac{\theta(Q^2)}{8q}\int_{\frac{1}{2}(\omega-q)}^{\frac{1}{2}(\omega+q)} \mathrm{d}\ell \Big[1 + (\hat{\ell}\cdot\hat{k})^2\Big]\Big(4\ell[\ell-\omega] - \omega^2\Big) \,.$$

Note that this function depends on ω and $\boldsymbol{q}$ separately, because $\Pi_{00}^{(\mathrm{b})}$ is by itself not Lorentz invariant. All that is needed to extract the UV divergence, is the large-Q^2 behaviour [38] (i. e. $\omega \gg q$),

$$\bar{\pi}^{(\mathrm{b})}(Q^2) \;=\; -\frac{1/3}{4\pi}\frac{1}{\varepsilon}\left(\frac{Q^2}{\mu^2}\right)^{-\varepsilon} + \mathcal{O}\big(q/\omega\big) \,. \tag{2.41}$$

(c) – Coulomb loop

The loop with a Coulomb gluon and a transverse one depends only on $\boldsymbol{q}$ and not ω, since the external energy may be directed through the static Coulomb gluon propagator. Thus

$$\Pi^{(\mathrm{c})}_{00} \;=\;$$

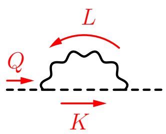

$$= \; g^2 \sum\!\!\!\!\!\!\int_L \underbrace{\boxed{(q+k)_i\Big(\delta_{ij} - \hat{\ell}_i\hat{\ell}_j\Big)(q+k)_j}}_{=\,4\boldsymbol{k}^2\left[1-(\hat{\ell}\cdot\hat{k})^2\right]} \; \frac{\Delta_L}{\boldsymbol{k}^2}\,. \tag{2.42}$$

The boxed term was simplified by $\boldsymbol{q} = \boldsymbol{k} - \boldsymbol{\ell}$ and noticing that all terms parallel with $\boldsymbol{\ell}$ are projected out. By choosing to route the loop momentum L through the transverse gluon, the frequency sum becomes trivial. The only ℓ_0-dependent part is the propagator Δ_L, therefore (see Appendix B),

$$\Pi^{(\mathrm{c})}_{00} \;=\; 4g^2 \int_{\boldsymbol{\ell}} \left[1-(\hat{\ell}\cdot\hat{k})^2\right]\left[\frac{1}{2} + f_{\mathrm{B}}(\ell)\right]\frac{1}{\ell}\,. \tag{2.43}$$

The $T > 0$ contribution comes from the term involving the Bose-distribution function f_{B}. Since it is finite we may set $d = 3$ and use (2.32) to formulate the integration. Simplifying the dot products with the help of (2.33) gives

$$\begin{aligned}\widetilde{\Pi}^{(\mathrm{c})}_{00} &= \frac{g^2}{\pi^2}\int \mathrm{d}\ell\mathrm{d}k\frac{k}{q}\left[1-(\hat{\ell}\cdot\hat{k})^2\right] f_{\mathrm{B}}(\ell) \\ &= \frac{g^2}{4\pi^2}\int \mathrm{d}\ell\,\frac{1}{\ell^2 q}\left\{\,2\ell q(\ell^2+q^2) + (\ell^2-q^2)^2\log\left|\frac{\ell-q}{\ell+q}\right|\,\right\} f_{\mathrm{B}}(\ell)\,.\end{aligned} \tag{2.44}$$

Eq. (2.44) is manifestly positive, monotonically increasing with q (see Fig. 8) and, as anticipated, independent of ω. For large or small three momentum, i. e. $q \lessgtr T$, the term in braces may be expanded and we find the limiting values

$$\widetilde{\Pi}^{(\mathrm{c})}_{00} \;=\; \left\{\begin{array}{c} 0 \\ \frac{2}{9}g^2T^2 \end{array}\right. \quad \text{for} \quad \begin{array}{c} q \ll T \\ q \gg T \end{array}\,.$$

Therefore (c) is zero in HTL approximation.

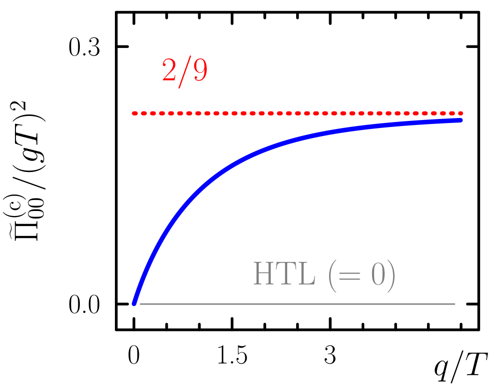

Figure 8: The $T > 0$ part of diagram (c), which is independent of ω, Eq. (2.44).

For the vacuum contribution, the imaginary part is zero [since there is no ω dependence, see Appendix C], a remarkable feature of QCD[13]. Therefore we cannot conveniently infer the divergence from the imaginary part, but the self energy can be calculated directly in d-dimensions using textbook techniques. Starting from (2.43), but focussing on the vacuum contribution, we make use of the Feynman-parameter trick, introducing χ as an extra integration variable to rewrite the denominators;

$$\begin{aligned}\Pi_{00}^{(\mathrm{c})} &= 2g^2 \int_{\boldsymbol{\ell}} \underbrace{\frac{1}{\left(\boldsymbol{\ell}^2\right)^{3/2} \boldsymbol{k}^2}} \left[\boldsymbol{\ell}^2\boldsymbol{k}^2 - (\boldsymbol{\ell}\cdot\boldsymbol{k})^2\right] . \\ &= \frac{3}{2}\int_0^1 \mathrm{d}\chi \, \frac{\sqrt{\chi}}{\left\{\chi\boldsymbol{\ell}^2 + (1-\chi)\boldsymbol{k}^2\right\}^{5/2}} \end{aligned} \tag{2.45}$$

We shift the integration variable to $\boldsymbol{p} := \boldsymbol{\ell} + (1-\chi)\boldsymbol{q}$ and call $\boldsymbol{\Delta}^2 := \chi(1-\chi)\boldsymbol{q}^2$. Doing this simplifies the denominator of Eq. (2.45), after completing the square it turns into $\{\ldots\} = \boldsymbol{p}^2 + \boldsymbol{\Delta}^2$, where $\boldsymbol{\Delta}$ depends on χ.

The order of integration over $\boldsymbol{p}$ may be swapped with χ and performed in d-spatial dimensions to regulate the divergence. In the end, writing $d = 3 - 2\varepsilon$.and expanding in ε, on may isolate the UV log-divergence. The result is [38],

$$\bar{\pi}^{(\mathrm{c})}(Q^2) = \frac{4}{4\pi}\frac{1}{\varepsilon}\left(\frac{Q^2}{\mu^2}\right)^{-\varepsilon} . \tag{2.46}$$

Unlike the corresponding function for diagrams (a) and (b), cf. (2.37) and (2.41), the sign in (2.46) is positive. Because $\Pi_{00}^{(\mathrm{c})}$ is independent of ω, it has no cut in the complex ω plane and therefore no spectral density. A spectral representation can *only* cause screening, as exlained in Eq. (C.5), while (2.46) gives 'anti-screening'.

(d) – Tadpole

The simplest diagram comes last. As mentioned, it is local in momentum-space and is thus independent of Q, (note the symmetry factor)

$\Pi_{00}^{(\mathrm{d})}$ = 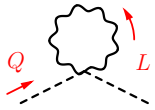

$= -g^2\frac{1}{2}\oint_L \underbrace{\left(\delta^{ij} - \hat{\ell}^i\hat{\ell}^j\right)\delta^{ij}}_{=(d-1)} \Delta_L .$ (2.47)

The frequency sum is easily read off from Eq. (B.4). In vacuum, the massless loop is divergent for $d \geq 2$ and is zero in dimensional regularisation;

$$\Pi_{00}^{(\mathrm{d})}\Big|_{T=0} = -g^2\frac{1}{2}(d-1)\int_{\boldsymbol{\ell}}\frac{1}{\ell} \xrightarrow{d=3} 0 .$$

On the other hand, the finite thermal piece is (in $d = 3$)

$$\widetilde{\Pi}_{00}^{(\mathrm{d})} = -\frac{g^2}{\pi^2}\int_0^\infty \mathrm{d}\ell\,\ell f_{\mathrm{B}}(\ell) = -g^2\frac{T^2}{12} = -\alpha\frac{\pi}{3}T^2 . \tag{2.48}$$

Because (2.48) is constant in Q, it acts just like a thermal mass.

[13] Consider the transverse field mediating the interaction between the (static) quark pair. At 0th order they do not interact. The first correction is second order, loop (c), which lowers the ground state of the transverse field, see Ref. [7]. This causes the Coulomb attraction between the two quarks to become stronger, which is 'antiscreening'.

Altogether

Having discussed the Lorentz structure of the four loop diagrams in Fig. 5, we now restore the colour factors. The fermion loop, (a), is multiplied by $\mathrm{tr}[t^a t^b] = T_F \delta^{ab}$ and the three gluon loops, (b)-(c), come with a $f^{acd} f^{cdb} = C_A \delta^{ab}$ [mind the factor 2 for (d)],

$$\Pi_{\mu\nu} \;=\; n_f T_F \Pi^{(\mathrm{a})}_{\mu\nu} + C_A \left(\Pi^{(\mathrm{b})}_{\mu\nu} + \Pi^{(\mathrm{c})}_{\mu\nu} + 2\Pi^{(\mathrm{d})}_{\mu\nu} \right) . \tag{2.49}$$

Let us consider the separate expressions for the vacuum and thermal contributions to Π_{00}, as we have just derived them in Coulomb gauge.

For $T = 0$, we assemble Eqs. (2.37), (2.41) and (2.46) to give the dimensionless scalar functions in (2.31), [recall (d) is zero in vacuum],

$$\bar{\pi}(Q^2) \;=\; \frac{-1}{4\pi} \left[\frac{4}{3} n_f T_F - C_A \Big(4 - \frac{1}{3} \Big) \right] \frac{1}{\varepsilon} \left(\frac{Q^2}{\mu^2} \right)^{-\varepsilon} .$$

At the one loop level, this is the UV divergent contribution to the longitudinal gluon self-energy. The significance of the formula shall be discussed in the next section, although we may already compare the $U(1)$ and non-Abelian theories. For QED, $C_A = 0$ and $n_f T_F = 1$ so that the overall coefficient is negative. In QCD, $C_A = 3$ and $T_F = \frac{1}{2}$ so that for relevant possibilities for n_f, the coefficient is *positive* [due to the '4' which came from diagram (c)].

The finite temperature part of (2.49), namely $\widetilde{\Pi}_{00}(\omega, \boldsymbol{q})$, must, for general outer momenta, be evaluated numerically. In the HTL limit, we confirm a familiar result in Coulomb gauge [36], the expression is

$$\widetilde{\Pi}^{\mathrm{HTL}}_{00}(\omega, \boldsymbol{q}) \;=\; g^2 \frac{T^2}{3} \left[C_A + n_f T_F \right] \left(1 - \frac{\omega}{2q} \log \left[\frac{\omega + q}{\omega - q} \right] \right) . \tag{2.50}$$

By gauge invariance, the dimensionless function of $(\omega, \boldsymbol{q})$ is the same for both the fermion loop, and the gluon loop. We compare this to the full combination of Eqs. (2.34), (2.38), (2.42) and (2.47) without approximation, as shown in Fig. 9. A previous study into the quality of HTL self-energies has been made in Feynman gauge [39] (which apparently has little effect on the numerical results). The HTL limit is approached for soft momenta Q, as well as near the light cone $\omega \sim q$. Note that $\mathrm{Im}(\Pi_L) \neq 0$ above the lightcone, for $\omega > q$, which is an indication of residual attenuation for hard external momenta.

2.4 Heavy quark potential

Before presenting the QCD calculation, we shall give context from classical electromagnetism, by investigating the lengths over which charge neutrality may be violated [13]. If all charges in a 'slice of plasma' of thickness l were displaced by a distance l, a local electric field $\boldsymbol{E}$ would be generated. The field strength is $E = enl$, whence the potential energy increases by an amount

$$\Delta \mathcal{U} \;=\; eE \cdot l \;=\; ne^2 l^2 .$$

The inequality $\Delta \mathcal{U} < T$ provides the maximum distance over which the medium shields itself from local fluctuations in charge. This happens because each charge creates around itself a non-uniform cloud of charges. Suppose we place a test charge Q in the plasma, which induces a charge density $n_{\mathrm{ind}}(\boldsymbol{r})$ about itself, where $\boldsymbol{r}$ is the displacement from the

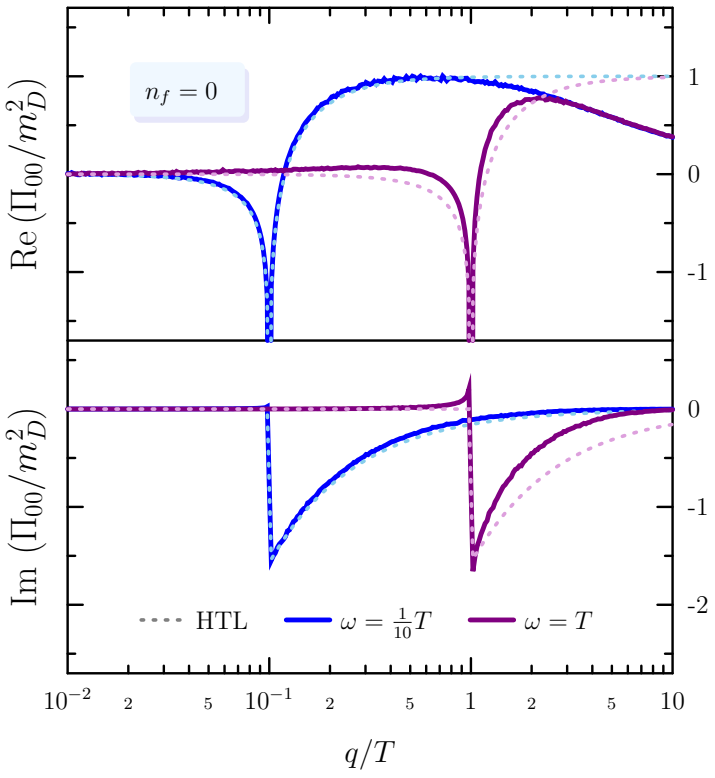

Figure 9: Real (upper panel) and imaginary (lower panel) parts of the longitudinal gluon self energy (for $n_f = 0$), in units of the Debye mass $m_D^2 = C_A g^2 T^2/3$. The solid lines show the full one-loop approximation and the dashed lines represent the HTL limit, which is valid near the lightcone $q \sim \omega$ (even for larger ω). We display the 3-momentum dependence at two representative values of the energy, $\omega = \{\frac{1}{10}, 1\}T$.

coordinate of the charge[14]. To a fair approximation, (in equilibrium) the induced *effective* electrostatic potential $\Phi(\boldsymbol{r})$, multiplied by e, gives the mean potential energy for an electron at $\boldsymbol{r}$. Then the induced particle density is (presuming Boltzmann statistics for simplicity)

$$n_{\rm ind}\,(\boldsymbol{r}) \;=\; n\cdot e^{-e\Phi(\boldsymbol{r})/T}\,. \tag{2.51}$$

The constant prefactor ensures that far away (where $\Phi \to 0$), the mean density of the ion cloud is equal to the average density, n. The potential Φ satisfies Poisson's equation,

$$\nabla^2\Phi(\boldsymbol{r}) \;=\; \varrho - e\; n_{\rm ind}(\boldsymbol{r})\,, \tag{2.52}$$

where $\varrho = en$ is the (constant) uniform charge background. Eqs. (2.51) and (2.52) determine self-consistently Φ. Expanding the exponent, (if T is large or e is small),

$$\left(\nabla^2 - m_D^2\right)\Phi \;\approx\; 0\,,$$

where we have introduced the *Debye mass* for electrical screening

$$m_D^2 \;=\; \frac{ne^2}{T}\,. \tag{2.53}$$

[14]The density $n_{\rm ind}(\boldsymbol{r})$ will be on average spherically symmetric.

In a relativistic plasma, $n \sim T^3$ so that $m_D \sim eT$. The spherically symmetric solution for Φ is the screened Coulomb potential,

$$\Phi(r) = \frac{e}{4\pi}\frac{1}{r}\exp\left(-r m_D\right) .$$

The exponential factor suppresses the potential at large distances, compared to the radial length m_D^{-1}. Here, a screening mechanism leads to the modification of the potential energy due to a point charge.

QCD Potential

The same physics is at work in quantum field theory, which formally emerges from the self energy modifications to the free particle propagator. Let us consider as one of the most elementary observable for QCD; the force between two infinitely heavy quarks. In this static limit, there is no frequency dependence and we shall only need to use the longitudinal gluon self energy calculated in the previous section [see (2.49)]. We shall explore the (chromo-)electric field exerted by an infinite mass quark, which shall be used to illustrate the nature of both vacuum and thermal fluctuations.

The qualitative behaviour has been well established; for large distances a constant 'string' force prohibits arbitrary separation of bound quarks and at short distances the potential is similar to QED (see Fig. 11). The former case is intrinsically non-perturbative, but has been accurately determined on the lattice [40]. For the latter, small-r, regime we may use the tree level cross section as a starting point for a perturbative calculation. Perturbation theory is justified at the short distance scales, compared to about 1 fm, but larger separations warrant non-perturbative approaches. The situation is very similar to our discussion of the pressure $p(T)$, where perturbation theory seems justified only for very large temperatures, for the pressure it seemed to work down to $T \gtrsim 40 T_c$.

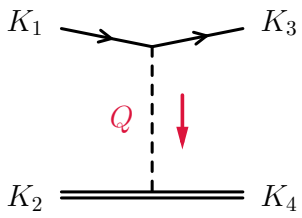

Figure 10: Parton scattering off a heavy quark (double line) via the exchange of a longitudinal gluon. Even though the test particle may couple to the transverse gluon, its tree level interaction with a static source is mediated by a Coulomb gluon.

Consider a very heavy quark (mass M) at rest and measure the force it exerts by scattering another (light) parton off it, Fig. 10. If we parametrise the effect of the heavy quark at rest by an 'external' potential Φ, the amplitude is (cf. Ref. [41])

$$i\mathcal{M} \;=\; \left[ig\;\bar{u}_3\gamma_\mu t^a u_1\right]\Phi^a_\mu(\omega,\boldsymbol{q}) \qquad \text{with} \qquad \Phi^a_\mu \;:=\; \left[ig\;\bar{u}_4\gamma^\nu t^b u_2\right]\delta^{ab}D_{\mu\nu}(\omega,\boldsymbol{q})\,. \tag{2.54}$$

The fermion spinors $u_i = u(K_i)$ are labelled according to Fig. 10. $D_{\mu\nu}$ is the gluon propagator and $Q = (\omega, \boldsymbol{q})$ is fixed by the momentum exchange; viz. $Q = K_1 - K_3$. In the $M \to \infty$ limit, the heavy quark is static with on-shell *kinetic* energy $E = 0$ and the propagator is $\boldsymbol{k}$-independent;

$$\frac{i}{\not{K} - M} \;=\; i\gamma_0\left(E - \frac{\boldsymbol{k}^2}{2M} + \ldots\right)^{-1} \quad \xrightarrow{M\to\infty} \quad \frac{i\gamma_0}{E}\,.$$

It follows that the heavy quark is 'anchored' in coordinate space, and propagates forward in time. There can be no energy transfer, i. e. $\omega = 0$, which follows by requiring $(K_2{+}Q)^2 = M^2$. In Coulomb gauge, the heavy quark vertex does not couple to the transverse gluon, only to the longitudinal gluon; $\nu = 0$ in (2.54).

The above yields a chromo-*static* source, $\Phi^a(Q) \simeq \big(\delta(\omega)\Phi_0^a, \mathbf{0}\big)$ where

$$\Phi_0^a(\boldsymbol{q}) \;=\; igt^a \left[\frac{\bar{u}_4 u_2}{2M}\right] D_{00}\,(\omega,\boldsymbol{q})\Big|_{\omega=0} \;=\; igt^a D_{00}\,(0,\boldsymbol{q})\;.$$

The test charge feels an effective potential $\mathcal{V}_{\boldsymbol{q}} = -\mathcal{M} = \mathrm{tr}\,[igt^a\Phi_0^a]$, where the minus sign is important because it indicates whether the static field (assumed to be in a colour singlet state) is attractive or repulsive. In coordinate space, (taking the Fourier transform) the potential as a function of distance from the source is [41],

$$\begin{aligned}\mathcal{V}(\boldsymbol{r}) \;&=\; \sum_{\boldsymbol{q}} \mathcal{V}_{\boldsymbol{q}} \frac{e^{i\boldsymbol{r}\cdot\boldsymbol{q}}}{V} \\ &=\; g\,\mathrm{tr}\Big[\; t^a \int_{\boldsymbol{q}} \Phi_0^a(\boldsymbol{q})\; e^{i\boldsymbol{r}\cdot\boldsymbol{q}}\;\Big] \;=\; C_F g^2 \int_{\boldsymbol{q}} D_{00}\,(0,\boldsymbol{q})\;\; e^{i\boldsymbol{r}\cdot\boldsymbol{q}}\,,\end{aligned} \tag{2.55}$$

where $C_F = \mathrm{tr}[t^a t^a]$ is the Casimir operator in the fundamental representation, equal to $(N_c^2-1)/(2N_c)$ for $SU(N_c)$ symmetric theories. Eq. (2.55) relates a specific limit for the gluon propagator, with the potential which is (in principle) an observable, up to a constant.

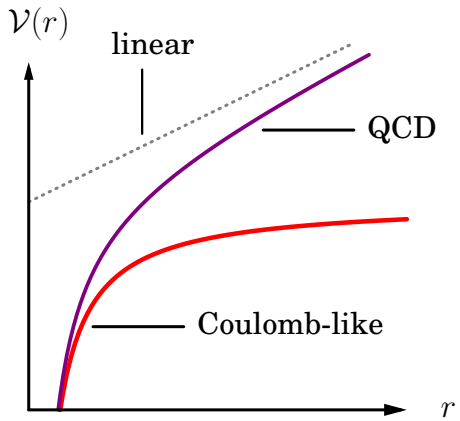

Figure 11: Coordinate space potential (at $T = 0$) for two infinitely heavy quarks, a distance r apart. At short distances, perturbation theory is applicable; the potential is Coulomb-like, see Eq. (2.55), with a running coupling. But beyond about $r \sim 1$ fm, to which physical partons are confined, a linear potential gives a constant force.

At tree level, i. e. using the bare propagator in Appendix A, we replace $D_{00} \to -1/\boldsymbol{q}^2$ in (2.55). This zeroth order approximation gives the attractive potential for the $Q\bar{Q}$ singlet channel

$$\mathcal{V}_0(\boldsymbol{r}) \;=\; -C_F g^2 \int_{\boldsymbol{q}} \frac{e^{i\boldsymbol{q}\cdot\boldsymbol{r}}}{\boldsymbol{q}^2} \;=\; -C_F \frac{\alpha}{|\boldsymbol{r}|}\,; \qquad \alpha = \frac{g^2}{4\pi}\,. \tag{2.56}$$

Together with the replacement $\alpha_{\mathrm{em}} \to C_F\alpha$, the expression matches the classical potential between two opposite charges in electrostatics, where α is the *bare* coupling appearing in the Lagrangian (1.1). Sadly, Eq. (2.56) captures neither of the key features of QCD; confinement and asymptotic freedom. When confronted with lQCD results for the potential at $T = 0$,

one finds that the Coulomb-like behaviour only dominates at short separations $r \lesssim 1$ fm. As a 'mended' approximation, we may take the Cornell parametrisation

$$\mathcal{V}_{\rm cp}(r) \;=\; -C_F \frac{a}{r} + \sigma r\,,$$

which is (2.56), plus a linear term whose coefficient σ gives the string tension and parametrises confinement. Let us stress that a here is only a fit parameter which gives some indication as to the average charge of the Coulomb-like term in $\mathcal{V}_{\rm cp}$. In [40] its value, fitted to short distances, was found to be $a \approx 0.2$.

It is convenient to consider the QCD force, given by $\mathrm{d}\mathcal{V}(r)/\mathrm{d}r$, to define the coupling as a function of r, namely

$$\alpha_{qq}(r) \;=\; -C_F^{-1} r^2 \frac{\mathrm{d}}{\mathrm{d}r}\mathcal{V}(\boldsymbol{r})\,. \tag{2.57}$$

In this formula any additive constant to the potential drops out, making it a promising means to *define* an effective coupling (in coordinate space) by its natural comparison with Eq. (2.56). As determined on the lattice, $\alpha_{qq}(r)$ is defined in both perturbative and non-perturbative regimes. The Cornell parametrisation gives $\alpha_{qq} = C_F^{-1}\sigma r^2$ for large r, i. e. a quadratic increase, with a strength given by the string tension $\sqrt{\sigma} \approx 420$ GeV.

While $\mathcal{V}_{\rm cp}$ does phenomenologically take into account confinement, its lack of a running coupling renders it unable to describe asymptotic freedom. Lattice based approaches, to calculate $\mathcal{V}(r)$, may only sample gridsites that are as close as the lattice spacing itself. Since the lattice spacing cannot be made arbitrarily small, current limitations are about 0.1 fm, which is still far from the perturbative limit but small enough to see indications of a running coupling. Because α varies considerably for $r \to 0$, QCD quantum corrections to the tree level amplitude are important, and shall be discusses shortly. After that, we can use (2.57) to study the semi-perturbative crossover and speculate on the validity of the perturbative approximation for 'large' values of α.

Loop corrections

The tree-level interaction pictured in Fig. 10 yields the cross-section of a fixed point charge. But, as with bulk thermal properties, fluctuations lead to corrections for Eq. (2.56). We shall draw out the leading order corrections to $\mathcal{M}$ in Coulomb gauge (omitting for instance, ladder diagrams, etc.), at both $T = 0$ (vacuum) and $T > 0$ (heat bath). The former shall derive the running coupling to one-loop order leading to a re-interpretation of the interaction vertex. The latter produce the effects of thermal screening.

A prevalent reason for our choice of gauge comes from the Ward identities, which in QED lead to a cancellation of the external leg renormalisation and the vertex correction. Indeed Coulomb gauge QCD has a similar feature, (see Ref. [7]), which we spell out at first order. Because the infinitely heavy quark propagator does not depend on $\boldsymbol{k}$, its self energy

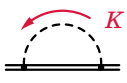

$$\sim \int \mathrm{d}^d\boldsymbol{k}\; \frac{e^{i\boldsymbol{k}\cdot\boldsymbol{r}}}{\boldsymbol{k}^2}\bigg|_{\boldsymbol{r}=0}\,. \tag{2.58}$$

The Coulomb gluon propagates *only* in space and the heavy quark propagates *only* in time. Hence the two vertices in (2.58) are at the same space-time location. It gives a linear divergence which is zero in dimensional regularisation. For similar reasons, the vertex corrections are also zero.

That leaves the polarisation corrections to the 'bare' propagator. Dressed lines can be resummed;

$D_{00}(\omega, \boldsymbol{q})$ =  + ... ,

(2.59)

in terms of 1-particle irreducible (1PI) components. Summing up the geometric series gives

$$D_{00}(\omega, \boldsymbol{q}) \;=\; -\big(\boldsymbol{q}^2 + \Pi_{00}\big)^{-1} \qquad \text{with} \qquad \Pi_{00} \;=\; \Big(\; -- \text{} -- \;\Big)\,. \tag{2.60}$$

In fact this Dyson equation is generic. Using the projection operators in (2.29), to invert (2.59) for the remaining components of $\Pi_{\mu\nu}$ leads to the 1-loop resummed (or dressed) propagators

$$\begin{aligned} D_{00} \;&=\; \frac{-Q^2}{\boldsymbol{q}^2(Q^2 - \Pi_L)}\,, \qquad D_{ij} \;=\; \frac{-(\delta_{ij} - \hat{q}_i\hat{q}_j)}{Q^2 - \Pi_T}\,, \\ D_{i0} \;&=\; D_{0i} \;=\; 0\,. \end{aligned} \tag{2.61}$$

The propagators themselves are in general gauge dependent but the poles, which give the dispersion relation, should be invariant [42]. Because the potential directly samples the 2-point function (2.55), a modified propagator leads to a dressed amplitude which also changes the potential $\mathcal{V}(r)$.

Running coupling

Let us now consider how the running coupling originates by loop corrections, as opposed to the *phenomenological* definition (2.57). The bare coupling α may be related to physical observables by a scattering experiment at $T = 0$. For this purpose, take the static quark potential $\mathcal{V}_{\boldsymbol{q}}$, considering that it may be measured relative to another momentum scale $\boldsymbol{q} \to \boldsymbol{q}_\star$. Let us take into account these variations by a function $\alpha(\boldsymbol{q}^2)$, whose value is defined by an experiment at $\boldsymbol{q}$, such that

$$-C_F \frac{\alpha(\boldsymbol{q}^2)}{\boldsymbol{q}^2} \;:=\; \mathcal{V}_{\boldsymbol{q}}\,. \tag{2.62}$$

If we base our model for $\mathcal{V}_{\boldsymbol{q}}$ using (2.60) for D_{00}, this definition may be seen as replacing the bare coupling $\alpha \to \alpha(\boldsymbol{q}^2)$ in the tree level approximation, Fig. 12. Dimensional regularisation was used to calculate $\bar{\pi}$, and introduced the auxiliary scale μ, which is related to α by the renormalisation group equation. In particular, for μ to have no effect on the potential, $\mathcal{V}_{\boldsymbol{q}}$ must satisfy a Callan-Symanzik equation [41],

$$\Big[\,\mu\frac{\partial}{\partial\mu} + \beta(g)\frac{\partial}{\partial g}\,\Big]\mathcal{V}_{\boldsymbol{q}}(g,\mu) \;=\; 0\,, \tag{2.63}$$

where $g = \sqrt{4\pi\alpha(\mu^2)}$ is the renormalised charge. This flow equation is solved by the implicit function $\mathcal{V}_{\boldsymbol{q}}\big(\alpha(\mu^2)\big)$, whose argument α satisfies a characteristic equation with the β-function, namely

$$\mu\frac{\mathrm{d}\alpha}{\mathrm{d}\mu} \;=\; -2\beta(\alpha)\alpha\,.$$

Based on our model for $\mathcal{V}_{\boldsymbol{q}}$, the 'experimental' definition (2.62) for $\alpha(\boldsymbol{q}^2)$ is equivalent to

$$\alpha^{-1}(\boldsymbol{q}^2) \;:=\; \alpha^{-1} + \bar{\pi}(-\boldsymbol{q}^2)\,, \tag{2.64}$$

which, when inserted into the characteristic equation gives

$$\beta(\alpha) \;=\; \beta_0 \frac{\alpha}{4\pi} + \mathcal{O}(\alpha^2) \qquad \text{with} \qquad \beta_0 \;=\; \frac{11}{3} C_A - \frac{4}{3} n_f T_F\,.$$

The sign of β_0 qualifies the stability of the $\alpha = 0$ fixed point, which is crucial to understand the μ-dependence. When $\beta_0 < 0$, larger distances (smaller μ) give a decreasing $\alpha(\mu^2)$ and thus corresponds to the usual picture of charge screening. This is so for QED, where $\beta_0 = -4/3$ and the stable fixed point is $\alpha_{\text{em}}(0) \simeq 1/137$. For QCD, provided $n_f < 17$ (which is physical), the coupling is infrared-stable (i. e. asymptotically free).

The sign of β_0 in non-Abelian gauge theories was historically a surprising discovery in quantum field theories. It was calculated several times independently by different researchers, and we have followed the first correct derivation by Khriplovich [43], in a more modern language [38]. He used Coulomb gauge to calculate Π_{00} in vacuum, since the Ward identities are simple and there are no ghost fields, this is all that is necessary to renormalise the charge. When QCD became a candidate theory for the strong force, β_0 was reobtained by Gross, Wilczek [6] and Politzer [44]. Let us follow this line of reasoning to its conclusion, by solving Eq. (2.63) and arriving at an expression for $\alpha(\boldsymbol{q}^2)$.

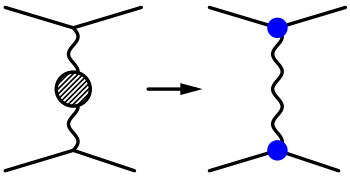

Figure 12: The *renormalised* coupling can be seen as a simple substitution of the bare vertices in a Born cross section by a running coupling. In the t-channel shown, the relevant scale in $\alpha(Q^2)$ is the exchanged four-momentum squared of the exchanged boson.

Instead of solving the characteristic equation for $\alpha(\mu^2)$, let us give an elementary argument for the same function. Suppose that our experiment fixed the value $\alpha_\star = \alpha(\boldsymbol{q}_\star^2)$; and subtract from it the definition (2.64) at some arbitrary scale,

$$\alpha_\star^{-1} - \alpha^{-1}(\boldsymbol{q}^2) \;=\; \bar{\pi}(\boldsymbol{q}_\star^2) - \bar{\pi}(\boldsymbol{q}^2) \;=\; \frac{\beta_0}{4\pi} \log\left(\boldsymbol{q}^2/\boldsymbol{q}_\star^2\right).$$

Or in the more common, but equivalent, form in terms of the QCD scale Λ,

$$\alpha(\boldsymbol{q}^2) \;=\; \frac{\beta_0/(4\pi)}{\log(\boldsymbol{q}^2/\Lambda^2)}\;; \qquad \Lambda = q_\star \cdot \exp\left[\frac{-2\pi}{\alpha_\star \beta_0}\right]. \tag{2.65}$$

To underline the main idea (in light of what we regard as a 'model'), note that by construction $\alpha_\star = \alpha(\boldsymbol{q}_\star)$ and therefore $\mathcal{V}_\star$ agrees with its value at $\boldsymbol{q}_\star$. This seemingly trivial point signifies that the absolute magnitude of $\alpha_\star$ is not relevant in the step of adjusting parameters[15]. Once model parameters for $\mathcal{V}_{\boldsymbol{q}}$ are fixed (say by comparing with lQCD at $T = 0$), we may use the model to make a prediction for the potential at an adjusted scale (i. e. $T > 0$), or for related observables. What does matter, is by how much $\mathcal{V}_{\boldsymbol{q}}$ changes, as we move away from the renormalisation point $\boldsymbol{q}_\star$ to $\boldsymbol{q}$. It is thus natural to explore the scope of Eq. (2.65), by confronting it with non-perturbative lQCD results as obtained in [45]. The

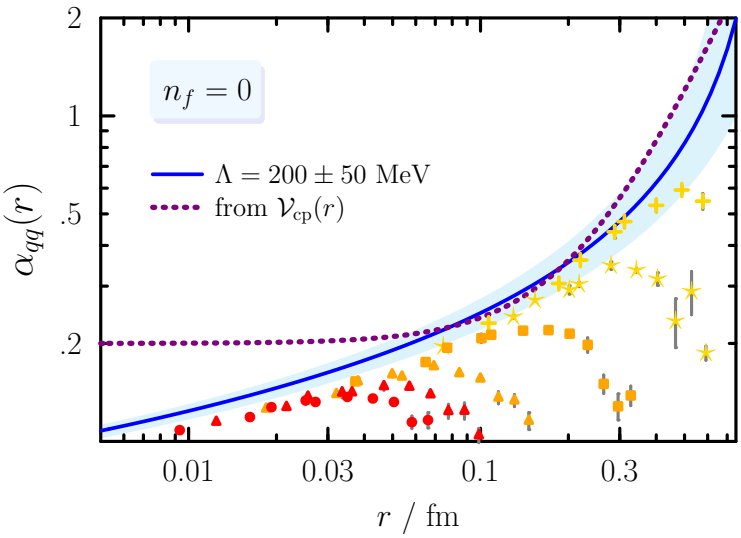

Figure 13: Coordinate space running coupling for $n_f = 0$, as obtained from the static quark potential for various $T > 0$ [46] (the red markers correspond to higher temperatures, and the yellow to lower). Debye screening for large-r reduces the effective coupling obtained via (2.57). For comparison, we take Eq. (2.65) with $\boldsymbol{q}^2 \to \boldsymbol{r}^{-2}$ as an *ansatz* to be judged against the non-perturbative definition (2.57). The (fitted) Cornell potential $\mathcal{V}_{\rm cp}$ overestimates the strength of the coupling for $r \lesssim 0.1$ fm, while the 1-loop perturbative coupling extrapolates well for 'moderately large' vlues $\alpha \simeq 1$.

static quark potential is perfect for this comparison, as Eq. (2.57) provides a convenient definition of the coordinate space coupling in lattice [40].

To compare with the extracted Cornell potential, we shall evaluate (2.65) at the inverse separation $\boldsymbol{q} \to \boldsymbol{r}^{-1}$. Strictly speaking, it should be obtained by a Fourier transform [Eq. (2.55) with a running coupling], but the final (numerical) result is not much different. Shown in Fig. 13 is the effective $Q\bar{Q}$ coupling defined via (2.57) from lQCD at various temperatures (so that we may see the onset of asymptotic freedom). Although it may be surprising that a LO formula is able to describe a non-perturbative result, in Fig. 13 the Cornell potential almost coincides with the 1-loop running coupling for $r \gtrsim 0.1$ fm (up to $r = \Lambda^{-1}$), the chosen value for $\Lambda = 200 \pm 50$ MeV is in the expected vicinity of the critical temperature $T_c \sim 300$ MeV (for the quenched case). The only free parameter in our perturbative model is $l = \Lambda/T_c$, which should be $l = \mathcal{O}(1)$ (independent of the number of active flavours, n_f). In our earlier analysis of the pressure, we were very careful to use a high order formula for $\alpha(Q)$ which was prudent to test the stability of a truncated series in α for a bulk property. Here we are concerned with a simpler resummation scheme which is apparently capable of giving fairly robust estimates at lower temperatures.

Thermal modifications

If the heavy quark system is placed in a heat bath, the exchanged boson acquires a self energy $\widetilde{\Pi} \sim \alpha T^2$, cf. (2.31). A canonical procedure for fixed-α calculations in thermal field

[15] Certainly the physicists of the 19th century would not have had any anxiety over whether the electric charge was 'small', i. e. $e^2/(4\pi) \simeq 1/137$. In QCD, quantum corrections are more prevalent, as the coupling varies substantially over scales of interest.

theory is to 'drop' the vacuum contribution $\bar{\pi}$ to the self energy, so that $\Pi_{00} = \alpha T^2 \cdot \widetilde{\pi}(\omega, \boldsymbol{q})$. Chromoelectric screening [QCD equivalent to (2.53)] may be derived in the static limit, i. e. $\omega = 0$, from the gauge boson propagator

$$m_D^2 \;:=\; \lim_{\boldsymbol{q}\to 0} \Pi_{00}(\omega = 0, \boldsymbol{q}) \;=\; \alpha T^2 \cdot \frac{4\pi}{3}\big[C_F + n_f T_F\big] .$$

The longitudinal propagator in this limit has a poles at $|\boldsymbol{q}| = \pm i m_D$, and consequently leads to an exponential screening in the potential,

$$\mathcal{V}(r) \;=\; g^2 \int_{\boldsymbol{q}} \frac{e^{i\boldsymbol{q}\cdot\boldsymbol{r}}}{\boldsymbol{q}^2 + \Pi_{00}(0, \boldsymbol{q})} \;=\; \frac{\alpha}{r} \exp\big[- r \cdot m_D \big] . \tag{2.66}$$

As an approximation, this result is on the same footing as (2.56) because α is left unspecified. In this regard, it may be appropriate to describe large distances, where a Debye screening overrides the linear string tension. However, note that m_D in (2.66) is not a free paramter – its value is fully specified by α and T. It is commonly reckoned that the fixed coupling may be substituted by a running coupling at a thermal scale, $\alpha_{\rm fix} \to \alpha(Q_T^2)$, usually chosen to be $Q_T = \nu \cdot 2\pi T$, i. e. the lowest Matsubara frequency up to a rescaling $\nu \in [\frac{1}{2}, 2]$. This approach systematically underestimates m_D/T by a factor 1.5, see Fig. 14 (even with the generous uncertainty band coming from ν).

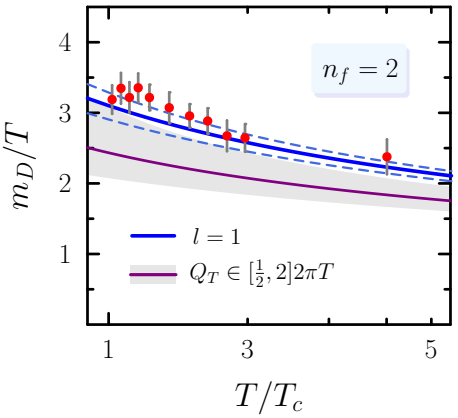

Figure 14: The $SU(3)$ Debye mass ($n_f = 2$), just above the critical temperature with the lattice results calculated from the singlet free energy [47] (i. e. $\mathcal{V}(r)$ at $T > 0$). Shown as a solid (purple) line in a gray band is the perturbative Debye mass, with the coupling evaluated at the naïve scale $Q_T = 2\pi T$ (varied by a factor of two). Eq. (2.67) leads to the solid (blue curve) with $l = \Lambda/T_c = 1$, and the two dashed curves estimate the uncertainty by adjusting $l \in [0.8, 1.2]$.

We shall argue on general terms how to remedy (2.66) so that *both* vacuum and thermal fluctuations are taken into account. The dressed propagators in (2.30) have poles determined by $Q^2 - \Pi_i = 0$ where $i = (L, T)$, which may be written [via (2.31)]

$$Q^2 \cdot \big(\alpha^{-1} - \bar{\pi}(Q^2)\big) \;=\; T^2 \cdot \widetilde{\pi}_i(\omega, \boldsymbol{q}) .$$

The renormalisation group equation (2.63) remains true for $T > 0$, and we shall keep definition (2.64) for $\alpha(\boldsymbol{q}^2)$, which we recognise in the parentheses. Hence the location of the pole in D_{00} satisties a self-consistent relation,

$$Q^2 \;=\; \alpha(Q^2) T^2 \cdot \widetilde{\pi}_i(\omega, \boldsymbol{q}) . \tag{2.67}$$

Without any amendments, the equation is finite and the renormalisation scale μ has dropped out. This feature is intuitive, since the bare coupling in the termal self energy has been replaced by the running coupling, evaluated at the external 4-momentum squared.

As a special case, we return to the static quark potential. Evidently for the Debye mass to satisfy (2.67) in the static limit, it must be that [45]

$$m_D^2 \;=\; \alpha\big(m_D^2\big)T^2 \cdot \frac{4\pi}{3}\big[C_A + n_f T_F\big]\,. \tag{2.68}$$

This implicit equation, with (2.65), can be solved using Lambert's W-function [45]. Instead of the coupling being evaluated at a 'hard' thermal scale $\sim T$, it seems that the relevant scale is the 'soft' electric scale $\sim \sqrt{\alpha}T \ll T$ for $\alpha \ll 1$. If $m_D < Q_T$, it is easy to see that the self-consistent solution will yield a stronger screening than the 'conventional' estimate. Let us make a *prediction* for the thermal Debye mass, based on the potential at $T = 0$. We choose, from Fig. 13 and based on expectation, a value $l = \Lambda/T_c = 1$ in the conventional form of $\alpha(Q^2)$. Then (2.68) is fully specified and shown as a function of temperature in Fig. 14.

The running of the coupling is determined by the vacuum parts of the very same loop corrections whose thermal contributions are mandatory for screening, for which there is no 'fixed coupling'. Rather, α must always be related to a particular scale which should be an outcome of the physical process. Of course, for renormalization-group invariant approximations, the choice of 'the' argument of the running coupling $\alpha(Q)$ is arbitrary: rescaling $Q \to \tilde{Q}$ is compensated by emerging $\alpha(\tilde{Q})\log(\tilde{Q}/Q)$ correction terms. These terms should either be included, or be minimized by a canonical choice of scale for the relevant processes, e. g. $Q^2 \sim t$ for the t-channel process considered in the heavy quark potential, (2.54). Otherwise, *ad hoc* choices like $Q = Q_T$ may result in considerable inaccuracies when extrapolated to larger α, in particular for quantities which depends on higher powers of the coupling.

Based on the provocative observation in the previous subsection, namely that the perturbative $\alpha(r^{-1})$ matches with the non-perturbative definition (2.57) even for *large distances*, corresponding to $\alpha \simeq 1$. As a central quantity in thermal physics, we examine the self-consistent Deybe mass given in (2.68) with free parameter $l = 1$ by comparison with the $T = 0$ potential. This *prediction* is shown in Fig. 14 an agrees with the lattice data values down to about $1.2T_c$. To summarise; we renormalise the model at $T = 0$ [i. e. determine $l = \Lambda/T_c$ from $\mathcal{V}(r)$], and then verify the approach for larger couplings by calculating the Debye mass near T_c. In fact, these two observables are closely related by the scattering process in Eq. (2.54), for which $m_D(T)$ features in (2.66) as a special limit of the self-energy.

3. Dynamical Properties

Consider a test particle, which moves with velocity $\boldsymbol{v}$ through a static medium as depicted in Fig. 15. As it travels unimpeded through the cubic unit, it encounters nv other particles per unit of time. The total area comprised by obstacles to this motion is thus $\sigma \cdot nv$, where σ is the cross section. The ratio of this area to one square fermi is the probability that it will collide with another particle, per second. The *mean free time* between collisions is denoted τ, so that the probability of scattering per unit of time is

$$1/\tau \;=\; \sigma \cdot nv \,. \tag{3.1}$$

This formula relates the mean velocity and density to the interaction rate. The *mean free path* is another quantity which can be defined by $\lambda := v\tau = 1/n\sigma$. One can interpret $\lambda\sigma$ as the volume of a cylinder, in which there will be on average one other particle hence being equal to $1/n$.

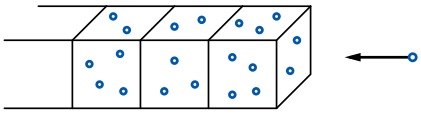

Figure 15: A given particle sweeps through a cloud of similar particles (at rest) with a speed v. In one unit of time, it traverses a distance v, containing σn particles per unit length.

Strictly speaking it is incorrect to refer to $1/\tau$ as a *probability*, since it then appears that the total probability for having a collision in a time interval $t > \tau$ can be larger than unity! The formula (3.1) ought only be related to probability for short times $\mathrm{d}t$ and many trials. We could imagine a monoenergetic beam of $\mathcal{N}$ particles incident on the medium in Fig. 15, $\mathrm{d}\mathcal{N}$ of which undergo scattering. The fraction of these scattered particles would be proportional to the time interval considered,

$$\mathrm{d}\mathcal{N}/\mathcal{N} \;=\; -\mathrm{d}t/\tau \qquad \Rightarrow \qquad \mathcal{N}(t) \;=\; \mathcal{N}_0 \;\exp\left(-t/\tau\right) \,.$$

The integration constant $\mathcal{N}_0$ represents the initially incident number. Whence the fraction that *has* collided is $1 - \exp\left(-t/\tau\right)$. This is the quantity which ought to be taken as a probability, which approaches 1 for $t \gg \tau$.

There are several issues which complicated the details above, but not the idea. Firstly, the target particles in a thermal medium are not stationary, they are themselves moving around. Not only this, but the particles do not all have the same speed – they are in some way distributed in phase space. Also, the individual particles may be indistinguishable from the test particle which was singled out.

3.1 The Boltzmann Equation

Physical quantities, such as momentum and heat energy, are continuously 're-organised' in coordinate space through particle interactions which drive the system to equilibrium. We characterise the system with the *one-particle* phase space density $f(t, \boldsymbol{x}, \boldsymbol{k})$, which counts the parton number per volume element $\mathrm{d}^3\boldsymbol{x}\mathrm{d}^3\boldsymbol{k}/h^3$ at a time t. Implicit in the definition,

of course, is some sort of averaging process; taken over several ensembles, or "short" time intervals. For the moment, we keep this notion imprecise. Because N, the total number of particles, is the same in all frames (as is the phase space measure $\mathrm{d}^3\boldsymbol{x}\mathrm{d}^3\boldsymbol{k}$), f is also a Lorentz invariant. However the particle density, $n(\boldsymbol{x},t) = \int_{\boldsymbol{k}} f(\boldsymbol{k})$ is not.

Although the Boltzmann equation can be rigorously derived from the Bogoliubov-Born-Green-Kirkwood-Yvon (BBKGY) hierarchy, elementary ideas may be used to arrive at the correct form [48]. It is easy to point out the shortcomings of the Boltzmann equation, but it is another matter entirely to improve upon them. Even in describing transport phenomena for heavy-ion collisions, it remains one of the most promising tools. Few-body densities from the BBKGY equations are time reversal invariant, a quality which is lost after the assumption of *molecular chaos* for the joint particle distribution functions [20]. Thus it is suitable to describe the single-particle density – namely f – as it approaches a 'steady-state' solution.

Consider a number of particles δN in the volume $\mathrm{d}^3\boldsymbol{x}\mathrm{d}^3\boldsymbol{k}/h^3$, which is equal to $\delta N' = f(t+\delta t, \boldsymbol{x}', \boldsymbol{k}')\mathrm{d}^3\boldsymbol{x}'\mathrm{d}^3\boldsymbol{k}'/h^3$ at a later time. In the absence of particle collisions, the phase space coordinates of one particle change as

$$\boldsymbol{x}' \;=\; \boldsymbol{x} + \boldsymbol{v}\;\delta t\,, \qquad \boldsymbol{k}' \;=\; \boldsymbol{k} + \boldsymbol{F}\;\delta t\,,$$

where $\boldsymbol{F}$ is an external force. As long as this force is conservative, Liouville's theorem gives $\mathrm{d}^3\boldsymbol{x}\mathrm{d}^3\boldsymbol{k} = \mathrm{d}^3\boldsymbol{x}'\mathrm{d}^3\boldsymbol{k}'$. Therefore, the rate at which collisions change f is given by

$$\frac{\delta N' - \delta N}{\delta t \cdot \mathrm{d}^3\boldsymbol{x}\mathrm{d}^3\boldsymbol{k}/h^3} \;\approx\; \Big[\partial_t + \boldsymbol{v}\cdot\nabla + \boldsymbol{F}\cdot\frac{\partial}{\partial\boldsymbol{k}}\Big]f \;=\; \mathcal{D}f\,. \tag{3.2}$$

If interactions between particles are entirely negligible, individual particles would each constitute a closed subsystem and $\mathcal{D}f = 0$. The convective term $\boldsymbol{v}\cdot\nabla f$ is the decrease per unit time per phase space element because of the free motion of the molecules.

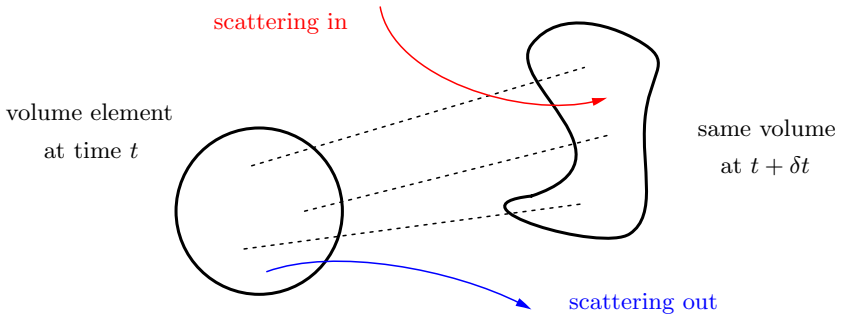

Figure 16: Cartoon depiction of the phase space motion for an infinitesimal volume element. This rearrangement happens when two 'molecules' collide resulting in particles entering or leaving $\mathrm{d}^3\boldsymbol{k}$.

When two particles collide, their momenta are changed (and also possibly other internal properties, i. e. spin), thus $\mathcal{D}f \neq 0$. The phase space volume element may either gain or lose particles in collisions (see Fig. 16), and the rate is given by a *collisional operator*, denoted $\mathcal{C}[f]$, which is a functional of the current distribution. At this point, one needs to be careful about the different timescales in the problem. The quantity we called δt is really an *extrinsic* time, coming from the external potential via $\boldsymbol{F} = -\partial_{\boldsymbol{x}}\mathcal{U}$. As a function of position only, $\mathcal{U}(\boldsymbol{x})$ reflects the macroscopic variations (for instance a container of size L)

and $\delta t \simeq L/v$. Interactions manifest themselves by $\mathcal{V}$, depending on the relative coordinates of all particles in the system. This *intrinsic* timescale is of the order of the molecular size d (or the range of the force), $\tau_c \simeq d/v$. Finally, there is the mean time between collisions, $\tau = 1/(d^2 \cdot nv)$ as encountered in (3.1).

Assuming that δt is larger than the duration of a collision and that no more than two particles collide within this 'window', several collisions may occur in δt, some scattering into the momentum interval $\mathrm{d}^3\boldsymbol{k}$ and some out of it. A dilute gas provides a physical example from everyday life. For molecules at room temperature, $v \approx \mathcal{O}(100\ \mathrm{m/s})$. So for a small box $L \approx .1$ m, $\delta t \simeq 1$ ms. While the atomic diameter $d \simeq 10^{-10}$ m, so that $\tau_c \approx 10^{-12}$ s.

Of course, equilibration is impossible in a system without particle interactions. The first approximation we can make is based on the ordering of timescales above. To be specific, we regard only two-particle interactions so that $\tau \gg \tau_c$. For binary scatterings (see Fig. 17) the collisional operator reads

$$\mathcal{D}f \;=\; \mathcal{C}[f](\boldsymbol{k}) \;:=\; \frac{1}{2E}\int \mathrm{d}\Gamma\ |\mathcal{M}|^2 \cdot \mathcal{F}[f]\,. \tag{3.3}$$

Without resolving the space-time structure of the collision, we assume that all distribution functions are evaluated at the same coordinate $\boldsymbol{x}$. The operator $\mathcal{C}$ is the number of *effective* collisions per time (i. e.those that actually redistribute momenta). It is a compensation of the gain and loss processes;

$$\mathcal{F}[f_1] \;=\; \bar{f}_1\bar{f}_2 f_3 f_4 - f_1 f_2 \bar{f}_3 \bar{f}_4\ ,$$

where the subscript refers to the momentum argument, $f_i = f(\boldsymbol{k}_i)$.

Eq. (3.3) is known as the *Boltzmann equation*, it describes the differential rate by a difference of gain and loss. Quantum effects[16] are included by the bracketed term (3.3); we use the notation $\bar{f} = 1 \pm f$, with the upper sign for Bosons and the lower for Fermions. The collisional operator, local in space-time, vanishes for equilibrium particle distributions because $\mathcal{F}[f_{\mathrm{eq}}] = 0$. Two-body phase space is abbreviated

$$\int \mathrm{d}\Gamma \;:=\; d_1 \int_{234} \frac{(2\pi)^4}{8E_2E_3E_4}\delta^{(4)}\left(K_1 + K_2 - K_3 - K_4\right)\,,$$

with the shorthand $\int_i = \int \mathrm{d}^3k_i/h^3$ for phase space integrals and the i-th parton degeneracy denoted d_i (for gluons $d_g = 16$ and for quarks $d_q = 12n_f$). Note that although the functional $\mathcal{F}[f]$ appears quartic in the f's, it is actually only cubic due to a cancellation of the leading powers.

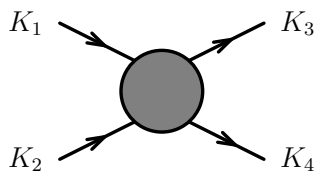

Figure 17: Convention for the labeling of external momenta $\{K_1, K_2\} \to \{K_3, K_4\}$.

[16]The probability for bosons to scatter into the same final state is enhanced, whereas fermions are less likely to do so because of Pauli blocking.

For a relativistic system, several subtleties are worth mentioning. Firstly, the streamline derivative becomes (3.2) (for massless particles) has $\boldsymbol{v} = \hat{k}$, and a thermal mass, i. e. (2.31), brings only $\mathcal{O}(\alpha)$ corrections which we drop. Secondly, there is no agreement on the *order* of individual collisions in the many-body system (it depends on the frame) and thus it might seem that the *approach* to equilibrium happens differently in different frames. But because f itself is invariant, as is $\int \mathrm{d}\Gamma$ defined above, the Boltzmann equation (3.3) is indeed relativistically invariant. In (3.3), the matrix element $|\mathcal{M}|^2$ is summed over spin and colour of particles 2, 3 and 4 (taking into account double counting of final states), but averaged over the spin and colour of particle 1. In vacuum at Born level, $|\mathcal{M}|^2$ is dependent only on the Mandelstam invariants

$$s = (K_1 + K_2)^2\,, \quad t = (K_1 - K_3)^2\,, \quad u = (K_1 - K_4)^2\,.$$

Equilibrium (i. e. stationary and uniform in $\boldsymbol{x}$) of a heat bath with collective flow is characterised[17] by a temperature T and velocity $\boldsymbol{u}$. The Jüttner distribution function

$$f_{\mathrm{eq}}(\boldsymbol{k}\,;T,\boldsymbol{u}) \;=\; \Big(\,\exp\big[\gamma(k-\boldsymbol{k}\cdot\boldsymbol{u})/T\big]\mp 1\,\Big)^{-1}\,, \tag{3.4}$$

where $\gamma = \big(1-u^2\big)^{-1/2}$, solves (3.3) trivially since $\mathcal{F}\,[f_{\mathrm{eq}}] = 0$ irrespective of spatial variations in equilibrium paramters. Eq. (3.4) is both necessary and sufficient for equilibrium; i. e. requiring $\mathcal{F}[f] = 0$ leads to $\log(f/\bar{f})$ being additive in conserved quantities [20].

When the energy momentum tensor

$$\Theta_{\mu\nu}[f] \;=\; \int_{\boldsymbol{k}} K_\mu K_\nu \frac{1}{k} f(\boldsymbol{k})\,,$$

is evaluated at f_{eq}, it gives Eq. (2.11).

A useful, albeit crude, basis for the collision term in (3.3) is by the relaxation time approximation. Since $\mathcal{C}[f]$ is related to the average time elapsed between successive collisions, we may replace (with the intention of a simple approximation) the full collisional integral with

$$\mathcal{C}[f] \;\approx\; -\big(f - f_{\mathrm{eq}}\big)/\tau\,, \tag{3.5}$$

where τ is the so-called *relaxation time*, the typical timescale characterising the approach to equilibrium. This equation simply drives $f \to f_{\mathrm{eq}}$ exponentially at each point in phase space. We shall refine (3.5) later, as relevant for QCD, but for now let us explore the consequences of such a simple model for collisions.

Toy example

To (over) simplify the evolution of a heavy-ion collision, consider massless gluons in $d = 1$. Such a scenario is already peculiar, in that particles may only travel in one directions, and they do so at the speed of light. Thus if the distribution function is spatially localised, it will immediately separate into particles travelling, say, left and those going right. From the shortcomings of such an oversimplification, we gain some insights into $d = 3$ physics.

Perhaps a relevant scenario to study is the following. Two spatially separated distribution functions travel towards one another in the z-direction, see Fig. 18. Suppose that each 'wave packet' is thermal, so that we may express the two momentum distributions as

$$f_\pm(k_z) \;=\; \theta(\pm k_z)\,\big[\,\exp\left(\pm k_z/T_\pm\right) - 1\,\big]^{-1}\,,$$

[17] We consider only zero chemical potential.

where the θ-function ensures that the particles all travel in the same direction. Although $f_\pm$ are not equilibrium distribution functions, they are stable solutions. The only opportunity for collisions will be when $f_\pm$ overlap near $z = 0$ (see state 2 in Fig. 18). Evidently, if $T_+ = T_-$, then $f_+ + f_-$ is just a regular Bose function in the argument k_z, thus, according to (3.5), the 'pancakes' will pass through one another unimpeded. Otherwise, if the two temperatures are different, we calculated the energy momentum tensor and match it to the equilibrium. By splitting the integration over positive and negative k_z, one finds for the two non-trivial components of the energy momentum tensor,

$$a = \Theta_{00} = \frac{\pi}{12}\left(T_+^2 + T_-^2\right), \quad \text{and} \quad b_1 = \Theta_{01} = \frac{\pi}{12}\left(T_+^2 - T_-^2\right). \tag{3.6}$$

Thus the energy density is $\varepsilon = \sqrt{a^2 - b_1^2}$ by Eq. (2.15), and this should to be equal to $\pi T^2/6$, the equilibrium energy density of massless bosons in $d = 1$. Therefore the equilibrium temperature for the right hand side of the relaxation-time collision term, in (3.5), turns out to be the geometric mean of T_- and T_+, viz.

$$T = \sqrt{T_+ T_-}\,.$$

Using (2.16), the flow velocity is readily found to be

$$u = \frac{T_+ - T_-}{T_- + T_+}\,.$$

This expression intuitively gives the 'net' velocity, since u points in the direction of the $f_\pm$ with the larger temperature.

Let us denote $f_{(1)} = f_+ + f_-$ to be the off-equilibrium distribution *immediately* after they overlap, and $f_{(2)}$ to be the new isotropic distribution with T and u above. For the argument's sake, suppose that the pancakes overlap for a time Δt, smaller than the relaxation timescale (so that the system is not able to fully equilibrate). The convective derivative is approximately $\mathcal{D}f \approx \Delta f/\Delta t$, where $\Delta f = f_{(3)} - f_{(1)}$ and $f_{(3)}$ being the final distribution function in Fig. 18, frame (3). Under these assumptions, (3.5) used to update $f_{(1)}$ gives

$$f_{(3)} \;=\; (1-\nu) f_{(1)} + \nu f_{(2)}\,; \qquad \nu = \frac{\Delta t}{\tau}\,.$$

The quantity Δt represents the timescale over which the interactions take place, which is related to the longitudinal extent of the wavepackets[18].

It is amusing to note that $f_{(1)}$ and $f_{(2)}$ are one and the same functions. To confirm this, notice that the argument of the equilibrium $f_{(2)}$ may be simplified (since u and k_z are of course parallel)

$$\gamma(k - \boldsymbol{k}\cdot\boldsymbol{u})/T \;=\; |k_z|\frac{1 \pm u}{T\sqrt{1-u^2}} \;=\; |k_z|/T_\pm \qquad \text{for} \quad k_z \lessgtr 0\,.$$

And hence $f_{(1)}$ and $f_{(2)}$ are both equal to $f_{(3)}$, i. e. the distribution remains unchanged during the overlap, no matter what the value of ν is! Hence the two pancakes are transparent to one another, even though interactions *do* happen, they just cannot be distinguished from no interactions at all (since there is no dispersion in velocity in the single propagation direction).

The space-time evolution for an ultrarelativistic heavy-ion collision is far more complicated, yet it remains true that the projectiles to some extent pass through one another.

[18] A value $\nu = 1$ corresponds to instantaneous relaxation, and $\nu = 0$ means no interactions at all.

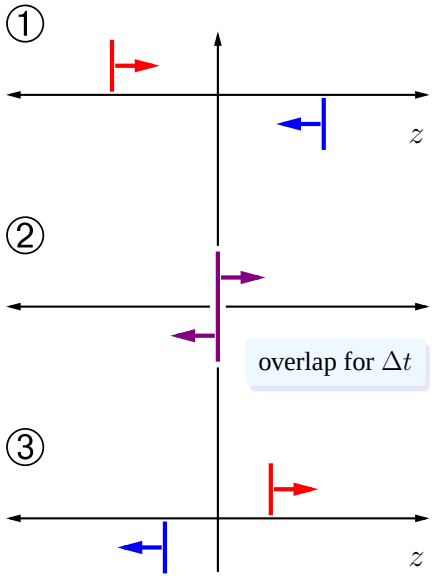

Figure 18: The vertical axes represent momentum in the z-direction, with the coloured bands indicating the presence of particles of a particular momentum. Consider two spatially separated (equilibrium)distributions, which travel towards one-another, shown at stage (1). At the point $z = 0$, these two 'packets' overlap and therefore interact in some manner, which we presume to take place for a time Δt. Subsequently, the particles with $k_z > 0$ continue to the right, and the particles with $k_z < 0$ pass left.

Shortly after the nuclei interpenetrate, the distribution function is peaked about $k_z = 0$ and particles may scatter into the transverse direction ($d > 1$), bringing the distribution towards an isotropic one. According to Bjorken's simple model [8], particles emanate from the collision point $z = 0$ at $t = 0$ and reach equilibrium very soon after the 'pancakes' recede. For large nuclei, the central region is approximately homogeneous and expands longitudinally so that a fluid at z from the midpoint moves with velocity z/t. This 'boost invariant' approximation is supported by a plateau at central rapidities in the measured particle spectra. A relaxation time study (in $d = 3$) for the onset of equilibrium, shows that collisions build up a longitudinal pressure, as work is done to 'cool' the central region [49]. Heavy-ion collisions entail a competition between the fluid-like expansion and particle collisional rate. This brings us to our next and main topic: the shear viscosity η, a central quantity of interest for QGP physics, as discussed in the introduction.

3.2 General relations for η

Consider a simple experiment: (cf. Fig. 19) two solid panels containing a fluid, with a fluid velocity only in the x-direction, the magnitude being a function of y, i. e. $u_x = u_x(y)$. At the surface of a solid the relative velocity of the fluid is zero[19]. Fluid layers, parallel to the plates, *must* be moving at different velocities and thus exert tangential forces above and below. The idea that forces can act in the plane of the interface separating layers, leads us

[19]For example: the blades of a fan will collect a very thin layer of dust that remains after blowing air.

to describe the situation by the Maxwell stress tensor Θ_{ij} (also the spatial sub-block of the full energy momentum tensor), where the index i designates the orientation of the plane, and j the component of force across this plane. When $i = j$, we recover the usual isotropic pressure in the d orthogonal directions. Let us, for clarity, specify $d = 3$ in this section.

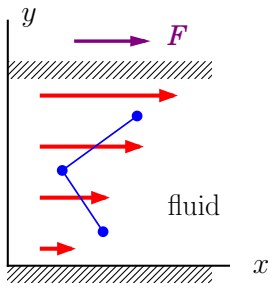

Figure 19: Viscous drag between two parallel plates; the top plate is maintained at a constant velocity, and the lower plate is held fixed. A force $\boldsymbol{F}$ on the top plate is required to maintain a steady velocity gradient $\boldsymbol{u} = (u_x(y), 0, 0)$. The relative fluid velocity must be zero at the point of contacts with the plates and the gradient leads to an apparent 'internal friction'.

Equilibrium is disturbed by the fact that $\partial u_x/\partial y \neq 0$, implying that Θ_{12} must depend on this gradient. If the gradient is small, we expect a linear relation,

$$\Theta_{12} = -\eta \frac{\partial u_x}{\partial y}\,; \tag{3.7}$$

η is called the coefficient of shear viscosity. If u_x increases with y, the fluid below the $y = \text{const}$ plane tends to slow the fluid above, meaning that $\Theta_{12} < 0$ (i. e. $\eta > 0$). Further, the linear form (3.7) also satisfies the symmetry requirement that Θ_{12} changes sign when the motion is reversed.

In kinetic theory [50], one may estimate the viscosity (here ι is a numerical factor)

$$\eta \simeq \iota \cdot n\bar{p}\lambda \tag{3.8}$$

from n, the density of particles, which can transport a typical momentum $\bar{p}$ over a path length λ specified by the corresponding cross section [$\lambda = v\tau$, as given (3.1)]. Eq. (3.8) is simple to derive for a non-relativistic gas, consisting of particles of mass m and average velocity $\bar{v}$. The off-diagonal Θ_{12} is the mean increase (or decrease) of the x-component of momentum due to partons crossing the plane normal to y, per unit time and per area. Of n particle per volume, about $1/3$ will have largest velocity component in the y-direction (half moving up, half moving down). We suppose that only these particles carry their momentum across layers. Therefore, per unit time, approximately $\frac{1}{6}n\bar{v}$ cross a given unit area from below (and similarly from below). Presuming particles to originate from layers a distance of about one mean free path (which is why we required them to be mostly moving in the y-direction). In the lower layer, the mean x-velocity is $u_x(y - \lambda)$, and above it is $u_x(y + \lambda)$. The *net* transfer is given be the difference, and on average

$$\Theta_{12} \;=\; \frac{1}{6}n\bar{v}\big(mu_x(y+\lambda) - mu_x(y-\lambda)\big) \;\approx\; \frac{1}{3}n(m\bar{v})\lambda\frac{\partial u_x}{\partial y}\,,$$

after a Taylor expansion in the $u_x(y \pm \lambda)$, assuming small gradients. Matching this against (3.7), we arrive at Eq. (3.8) with $\iota \simeq 1/3$.

Convection of particles across layers is necessary to obtain a shear force. In Fig. 19, particles at the bottom layer (at rest) have no directional preference; as many go left as right. Not so at the (overlying) top layer, where the bulk flow is to the right. But then a few particles from the lower group will move up, and a few from the top will move down,

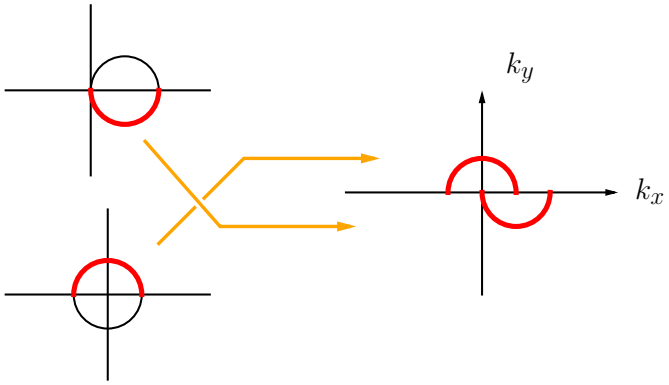

Figure 20: Particles entering a layer from above tend to be moving towards the right, while those from beneath have no bias. Convection thus sets up a skew momentum distribution $f(p_x, p_y)$, i. e. there is a net transfer of momentum in the x-direction and $\Theta_{12} \neq 0$. Figure inspired by [51].

while motion in the y direction is isotropic. At an interface the momentum distribution will be asymmetric, (see Fig. 20).

Spatial symmetry imposes constraints on the form of the stress energy tensor Θ_{ij} for a viscous fluid [52]. We generalise Eq. (3.7) from the simple laminar flow in Fig. 19, where the fluid moves not only along $\hat{x}$, but also along $\hat{y}$. In the absence of rotational flow, $\Theta_{12} = \Theta_{21}$ and hence we require that the two non-zero gradients $\partial u_x/\partial y$ and $\partial u_y/\partial x$ combine in a symmetric fashion,

$$\Theta_{(3)} \;:=\; \Theta_{21} \;=\; \Theta_{12} \;=\; \eta\left(\frac{\partial u_x}{\partial y} + \frac{\partial u_y}{\partial x}\right). \tag{3.9}$$

Consider a tiny cubical cell of fluid, with centre at O and square cross section $ABCD$ (side length δ) shown in Fig. 21. In the rest frame of the fluid at O, corner A has a velocity whose component along OA is

$$u_x(A)\cos\frac{\pi}{4} + u_y(A)\cos\frac{\pi}{4} \;=\; \frac{\delta}{2\sqrt{2}}\left(\frac{\partial u_x}{\partial x} + \frac{\partial u_x}{\partial y} + \frac{\partial u_y}{\partial x} + \frac{\partial u_y}{\partial y}\right).$$

Therefore in a reference frame such that the x-axis is rotated to x', which is parallel to OA, dividing by $\delta/\sqrt{2} = OA$ gives the velocity gradient along x' . Applying the same reasoning along OB, we find after using (3.9) that

$$2\frac{\partial u'_x}{\partial x'} \;=\; \frac{\partial u_x}{\partial x} + \frac{\partial u_y}{\partial y} - \frac{\Theta_{(3)}}{\eta} \qquad \text{and} \qquad 2\frac{\partial u'_y}{\partial y'} \;=\; \frac{\partial u_x}{\partial x} + \frac{\partial u_y}{\partial y} + \frac{\Theta_{(3)}}{\eta}. \tag{3.10}$$

Subtracting Eqs. (3.10) from one another, and solving for $\Theta_{(3)}$ indeed gives

$$\Theta_{(3)} \;=\; \eta\left(\frac{\partial u'_x}{\partial x'} - \frac{\partial u'_y}{\partial y'}\right).$$

In terms of the isotropic pressure, $\Theta_{(3)} = \frac{1}{2}(\Theta'_{22} - \Theta'_{11})$ which combines with the previous equation to provide a rotationally invariant object; (extending to three dimensional flow)

$$\Theta'_{11} + 2\eta\frac{\partial u'_x}{\partial x'} \;=\; \Theta'_{22} + 2\eta\frac{\partial u'_y}{\partial y'} \;=\; \Theta'_{33} + 2\eta\frac{\partial u'_z}{\partial z'}. \tag{3.11}$$

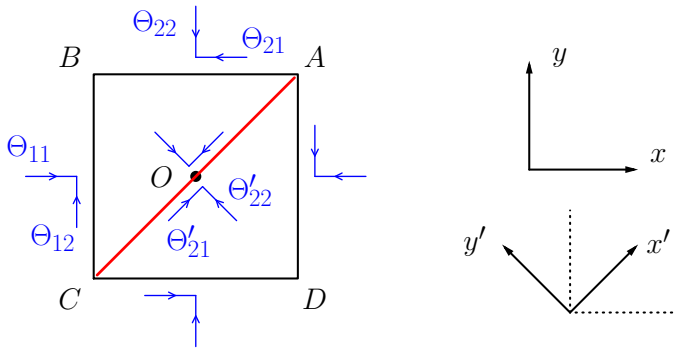

Figure 21: Shear forces on an infinitesimal cube; cross section $ABCD$ and centre O.

Eqs. (3.11) hold in any frame, and lead to the following expression for the normal stress.

$$\Theta_{11} \;=\; p - \eta\Big(2\frac{\partial u_x}{\partial y} - \frac{2}{3}\nabla\cdot\boldsymbol{u}\Big)\,,$$

where $p = \frac{1}{3}\left(\sum_i \Theta_{ii}\right)$ and similarly for Θ_{22} and Θ_{33}. This equation says that to draw out a fluid in a direction, say x, the normal pressure in that direction must be *less* than its average, i. e. $\Theta_{11} < p$. All that was needed to arrive at this conclusion was the assumption that shear flow was both rotationally symmetric and isotropic, and the balancing of Newtonian forces in Fig. 21.

All the above discussion may be compactly summarised by two coefficients, associated with the rank-2 basis $\nabla_i u_j$ and $\delta_{ij}\nabla\cdot\boldsymbol{u}$. In proportion to the latter, there is a second coefficient of *bulk flow*, characterised by ζ, the bulk viscosity [19]. To first order in the gradients,

$$\Theta_{ij} \;=\; p\cdot\delta_{ij} - \eta\cdot\Big(\nabla_i u_j + \nabla_j u_i - \frac{2}{3}\delta_{ij}\nabla\cdot\boldsymbol{u}\Big) - \zeta\cdot\delta_{ij}\nabla\cdot\boldsymbol{u}\,. \tag{3.12}$$

Linearised Boltzmann equation

Consider now small deviations from the *global equilibrium* in (3.4), by allowing for $\boldsymbol{u}$ to weakly depend on $\boldsymbol{x}$ and consider as an Ansatz to solving (3.3) the function $f(\boldsymbol{x},\boldsymbol{k}) = f_{\rm eq}\big(\boldsymbol{k}\,;\boldsymbol{u}(\boldsymbol{x})\big)$, the so called 'local' equilibrium [to be distinguished from the general off-equilibrium $f_\star$]. Small gradients in $\boldsymbol{u}$, in particular, are characterised by (3.12) and we may, by boosting into the local rest frame, assume $|\boldsymbol{u}| \ll 1$. This implicit dependence of $\boldsymbol{u}$ on $\boldsymbol{x}$ means that f no longer satisfies the Boltzmann equation (3.3), since[20]

$$\mathcal{D} f_{\rm eq}\big(\boldsymbol{k}\,;\boldsymbol{u}(\boldsymbol{x})\big) \;=\; S\Big(\hat{k}_i\hat{k}_j - \frac{1}{3}\delta_{ij}\Big)\cdot\nabla_i u_j\,, \quad \text{with} \quad S(k) := f\bar{f}\frac{k}{T}\,, \tag{3.13}$$

while $\mathcal{F}[f]$, which determines the collision operator in the Boltzmann equation (3.3), still vanishes. Thus, the solution to (3.3) should somewhat depart from local equilibrium,

$$f_\star(\boldsymbol{x},\boldsymbol{k}) \;=\; f\big(\boldsymbol{x},\boldsymbol{k}\big) + \delta f(\boldsymbol{k})\,,$$

[20] We consider a steady solution, i. e. $\partial_t\boldsymbol{u} \to 0$, implying $\nabla T = 0$. However a nonzero $\partial_t T$ is connected to any divergence in $\boldsymbol{u}$, and is necessary for the second term in (3.13).

with δf being proportional to the velocity gradients $\nabla_i u_j$, in order for the collision operator $\mathcal{C}[f_\star]$ to compensate (3.13). Let us parametrise δf in the form, similar to [53],

$$\delta f \quad = \quad f\bar{f}\,\frac{\chi^{ij}(\boldsymbol{k})}{T}\cdot\nabla_i u_j\,,$$

where the rank-2 traceless tensor χ^{ij} is

$$\chi^{ij} \quad = \quad \chi(k)\Big(\hat{k}_i\hat{k}_j-\frac{1}{3}\delta_{ij}\Big)\,, \tag{3.14}$$

in terms of a scalar function $\chi(k)$.

The deviation δf from local equilibrium (alternatively χ), leads to a modification of the stress tensor, cf. (3.12),

$$\Theta_{ij}\,[f+\delta f] \quad = \quad d_g\int_{\boldsymbol{k}}\frac{k_ik_j}{k}\big(f(\boldsymbol{k})+\delta f(\boldsymbol{k})\big)\,.$$

From (3.14), the tracelessness of χ_{ij} implies zero bulk viscosity, i. e. $\zeta=0$ in (3.12). Using (3.14) to complete the angular integrations, we find that

$$\int_{\boldsymbol{k}}\frac{k_ik_j}{k}\delta f(\boldsymbol{k}) \quad = \quad d_g\nabla_m u_l\Big[\int_{\boldsymbol{k}}S\chi\;\hat{k}_i\hat{k}_j\hat{k}_m\hat{k}_l\;-\frac{1}{3}\delta_{ml}\int_{\boldsymbol{k}}S\chi\;\hat{k}_i\hat{k}_j\Big]\,.$$

Evidently, the $\boldsymbol{k}$-integration is sensitive to angles only through the tensor combinations. Indeed, the result of the integration follows by replacing these angles by their average value, for which the tensors can only be a linear combination of δ-functions:

$$\begin{aligned}\hat{k}_i\hat{k}_j \quad &\xrightarrow{\mathrm{d}\Omega\ \text{ave}} \quad \frac{1}{3}\delta_{ij}\,,\\ \hat{k}_i\hat{k}_j\hat{k}_m\hat{k}_l \quad &\xrightarrow{\mathrm{d}\Omega\ \text{ave}} \quad \frac{1}{15}\big(\delta_{ij}\delta_{ml}+\delta_{ik}\delta_{jl}+\delta_{il}\delta_{mj}\big)\,,\end{aligned}$$

where the prefactor follows by normalisation. Now contracting with the generic laminar gradient and matching against Eq. (3.12), we arrive at a key formula [53],

$$\eta \quad = \quad \frac{d_g}{15}\int_{\boldsymbol{k}}\chi S\,. \tag{3.15}$$

Before formula (3.15) may be of any use, the unknown function χ needs to be determined – under the simplifying assumption of small gradients in velocity. The left hand side of the Boltzmann equation (3.3), which controls the effective particle rate, is (to first order in the gradients) $\mathcal{D}(f+\delta f)\simeq\mathcal{D}f$, i. e. the convective derivative is approximated by (3.13). On the other hand side, the Ansatz (3.14) gives $\mathcal{F}[f+\delta f]\simeq\frac{1}{T}ff_2\bar{f}_3\bar{f}_4\Delta^{ij}[\chi]\nabla_i u_j$ up to higher orders in $\nabla_i u_j$, where

$$\Delta^{ij}\,[\chi_1] \quad := \quad \big\{\;\chi_1^{ij}+\chi_2^{ij}-\chi_3^{ij}-\chi_4^{ij}\;\big\}\,.$$

This makes the collision term a linear functional of χ (and proportional to the gradient)

$$\mathcal{C}\,[f_1] \quad \simeq \quad \frac{\nabla_i u_j}{2TE_1}\int\mathrm{d}\Gamma|\mathcal{M}|^2 f_1f_2\bar{f}_3\bar{f}_4\cdot\Delta^{ij}\,[\chi_1]\,, \tag{3.16}$$

Since $\nabla_i u_j$ was arbitrary, we may use the Boltzmann equation to equate (3.13) with (3.16) and hence replace $\nabla_i k_j$ by $\hat{k}_i\hat{k}_j$ to find

$$S(k) \quad =: \quad \mathcal{C}_L\,[\chi]\,(k)\,. \tag{3.17}$$

This relation defines the *linearised* collisional operator,

$$\mathcal{C}_L\left[\psi_1\right] \;=\; \frac{3}{2}\cdot\frac{\hat{k}_1^i\hat{k}_1^j}{2E_1}\int \mathrm{d}\Gamma|\mathcal{M}|^2 f_1 f_2 \bar{f}_3\bar{f}_4\cdot\Delta^{ij}\left[\psi_1\right],$$

where $\psi_i = \psi(k_i)$ is an arbitrary scalar function [we reserve χ for the actual solution of (3.17)]. Note that $\Delta^{ij}[\psi]$ is traceless, inherited directly from (3.14), and therefore

$$\int_{\boldsymbol{k}}\psi\mathcal{C}_L\left[\psi\right] \;=\; \frac{3}{8}\int_1\frac{1}{2E_1}\int \mathrm{d}\Gamma|\mathcal{M}|^2 f_1 f_2 \bar{f}_3\bar{f}_4\cdot\Big(\Delta^{ij}\left[\psi_1\right]\Big)^2, \tag{3.18}$$

where symmetry of the integrand was used to complete the square for Δ^{ij}. Therefore $\mathcal{C}_L$ is a positive semidefinite operator, over the Hilbert space of ψ-functions, which vanishes for collisionally conserved quantities.

Eq. (3.17) then determines δf [via $\chi(k)$], enabling (3.15) to be used formally with $\chi = \mathcal{C}_L^{-1}[S]$. One approach to solving this symbolic equation is to represent χ by a linear combination over some complete set of functions. Since $\mathcal{C}_L$ is linear, this would produce an (algebraic) matrix equation which may be solved for the coefficients. Such a strategy, using a truncated basis, gives a *lower* estimate for η as we now explain.

Define the quadratic functional, following [54],

$$\mathcal{Q}\left[\psi\right] \;=\; \int_{\boldsymbol{k}}\Big(S\psi-\frac{1}{2}\psi\mathcal{C}_L\left[\psi\right]\Big). \tag{3.19}$$

At the solution to (3.17), $\mathcal{Q}$ not only takes the value η (up to a prefactor) but is also a stationary point since

$$\frac{\delta\mathcal{Q}}{\delta\psi} \;=\; 0,$$

gives $\psi = \chi$. Because $\mathcal{C}_L$ is positive definite, the extremum of (3.19) at $\psi = \chi$ is in fact a *maximum*, such that

$$\eta \;=\; \frac{2}{15}d_g\mathrm{Max}\big(\mathcal{Q}\big), \tag{3.20}$$

which sidesteps the task of actually inverting $\mathcal{C}_L$. For example, the optimal norm of any test function may be derived from $\partial_A\mathcal{Q}\left[A\psi\right] = 0$, which allows us to replace (3.19) by[21]

$$\mathcal{Q}[\psi] \;=\; d_g\Big(\int_{\boldsymbol{k}}S\psi\Big)^2\Big/\int_{\boldsymbol{k}}\psi\mathcal{C}_L\left[\psi\right]. \tag{3.21}$$

3.3 QCD transport

Nucleus-nucleus collisions at RHIC and LHC have given evidence of pronounced collective behaviour, warranting further investigation into many-body QCD. The hydrodynamic simulations of these experiments cannot reproduce findings without assuming $\eta/s \lesssim 0.5$ (see Fig. 22 summarising the findings of Refs. [55, 56, 57, 58, 59, 60, 61]), indicating that the system is 'strongly coupled' [9]. But there is yet some controversy over why the QGP seems to have this unique cohesive property, as it seems difficult to explain on the basis of the perturbative result. The pervasive opinion is that perturbation theory, as a weak-coupling approach, cannot explain the small viscosity. On the other hand, a universal lower bound

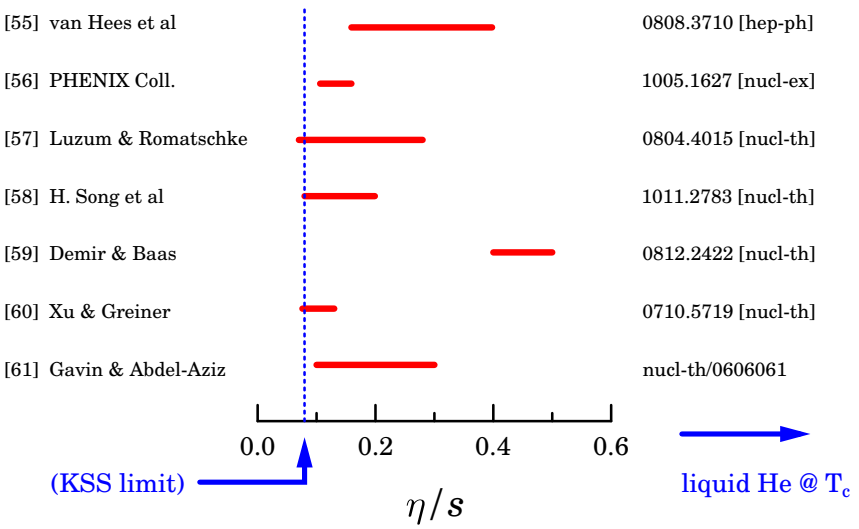

Figure 22: The dashed blue line (labelled KSS) is the conjectured lower bound of $1/(4\pi)$ [12].

$\eta/s \geq 1/(4\pi)$ has been conjectured from the AdS/CFT correspondence [12]. Although this approach gives a limit for certain supersymmetric theories, a rigorous connection to real-world QCD is still lacking.

For gauge theories it is important to distinguish between the total cross section and $\sigma_{\rm tr} = \int \mathrm{d}\Omega\,(1-\cos\theta)\,\mathrm{d}\sigma/\mathrm{d}\Omega$. Relevant for the viscosity is the latter, the so-called transport cross section, which takes into account that a single one of the prevailing small-angle scatterings is not sufficient to transfer the typical momentum $\bar{p} \sim T$ (for relativistic plasmas). To see this, we study transport in the quenched limit, i. e. $n_f = 0$. Fig. 23 shows the LO diagrams for gluon-gluon scattering, whose squared-matrix element reads (Ref. [62])

$$|\mathcal{M}|^2 = 72(4\pi\alpha)^2\left[3 - \frac{tu}{s^2} - \frac{su}{t^2} - \frac{ts}{u^2}\right]. \tag{3.22}$$

In light of (3.3), $|\mathcal{M}|^2$ was summed over colliding partners 2, 3 and 4, but averaged over particle 1. Soft scatterings are highly probable, as reflected by the terms with denominators t^2 and u^2. When t is small (much less than s), then $u \simeq -s$ and (3.22) is dominated by the term s^2/t^2. Similarly, when u is small the term s^2/u^2 dominates. However if s is 'small', both $-t, -u < s$, and therefore the term tu/s^2 is sub-leading. The differential cross section, for small t, is basically

$$\frac{\mathrm{d}\sigma}{\mathrm{d}t} = \frac{|\mathcal{M}|^2}{16\pi s^2} \overset{t\to 0}{\simeq} 72\pi\frac{\alpha^2}{t^2}, \tag{3.23}$$

yielding a $1/t$ divergence in the total cross section $\sigma = \int \mathrm{d}t\,\mathrm{d}\sigma/\mathrm{d}t$. Although the 'transport weight' $(1-\cos\theta)$, which is proportional[22] to the invariant momentum exchange t, does reduce the infrared sensitivity of relevant observables, the transport cross section is logarithmically divergent, taken at Born level. This is plainly unphysical, as it would imply

[21] This functional may also be obtained by a Cauchy-Schwarz inequality.

[22] In the notation of Fig. 17, the invariant transfer reads $t = -2E_1E_2(1-\cos\theta)$ implying that small θ is equivalent to small t for given incoming four momenta K_1 and K_2.

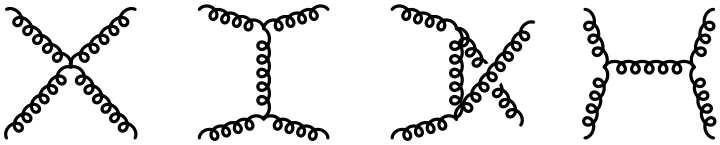

Figure 23: From left to right: the four gluon vertex, the t-, u- and s-channel diagrams.

zero viscosity for any value of the bare coupling α. Instead it is *mandatory* to also take into account loop corrections to tree level cross sections, in order to obtain non-trivial results. First steps in this direction (to calculate η) were based on (3.5) in place of the full collisional operator [63]. The essence is to use the transport mean free path $\lambda \sim (n\sigma_{\rm tr})^{-1}$ in Eq. (3.8), where $\sigma_{\rm tr}$ must be regulated in some way.

As discussed in Section 2.4, the mechanism for these loop corrections is that the exchanged boson acquires a self-energy, of the order $m_D \sim \sqrt{\alpha}T$, due to thermal fluctuations. This effect can be modeled by a mass-regulated cross section $d\sigma/dt \sim \alpha^2/(t - m_D^2)^2$. For small coupling α, the 'soft' scale m_D^2 is well separated from the typical invariant collision energy[23] $s \sim T^2$. Thus $\sigma_{\rm tr}$ can be 'mimicked' by the unscreened differential cross section integrated over an infrared restricted t-range, taking $-t^\star \sim m_D^2$ as a cutoff,

$$\sigma_{\rm tr}(s) \;=\; \frac{1}{s}\int_{-s}^{t^\star} \mathrm{d}t\,|t|\,\frac{\mathrm{d}\sigma}{\mathrm{d}t} \;\sim\; \frac{\alpha^2}{T^2}\log\left(\frac{s}{|t^\star|}\right). \tag{3.24}$$

The corresponding path length is $\lambda \sim (n\sigma_{\rm tr})^{-1} \sim 1/(T\alpha^2\log(\alpha^{-1}))$, where we used $n \sim T^3$ for the particle density. Since n is also proportional to the entropy density, (3.8) gives the generic α-dependence

$$\eta/s \sim \bar{p}\lambda \sim 1/\left(\alpha^2\log(\alpha^{-1})\right) \tag{3.25}$$

for hot gauge theories. Baym and collaborators determined the overall prefactor in (3.25), the so-called *leading logarithm* (LL) approximation, using the technique described in Section (3.2) to linearise the QCD Boltzmann equation [53, 64]. They also showed that the origin of $t^\star$, as an effective cutoff in (3.24), was dynamical screening of the matrix elements. We reproduce this result, with covariant integration variables, in Appendix E, by accounting for screening of soft scatterings due to loop corrections, to derive the logarithm of the hard and soft momentum transfers.

As it turned out, inelastic processes (naïvely of higher order in α) need also be included already at the LL level. This was recognized by Arnold, Moore and Yaffe [54], who subsequently also calculated the coefficient c in the *next-to leading log* (NLL) which gives the state-of-the-art result [65]

$$\eta_{\rm NLL} = \frac{bT^3}{\alpha^2\log(c/\alpha)}\,. \tag{3.26}$$

The constants b, c were computed numerically, for various number n_f of flavors, from the full leading order (LO) fixed-coupling result, $\eta_{\rm LO}(\alpha)$, obtained in the effective kinetic framework [66]. In the quenched limit ($n_f = 0$) $b \simeq 0.34$ and $c \simeq 0.61$. We note that b agrees with Baym's original result, without inelastic processes taken into account, within a few percents, i. e. inelastic processes are numerically less relevant.

[23] The context will make clear the distinction between Mandelstam s and the entropy.

Resuming 1-loop propagators only where necessary for screening [i. e. in the infrared sensitive terms of (3.22)] is the 'bare minimum' in order to calculate η. Striving for more loop insertions may not result in more reliable approximations for transport phenomena in heavy-ion physics, which are characterized by a 'fairly large' coupling[24]. Complemented by collinear $1 \to 2$ processes, this defines the framework of the effective kinetic theory developed in [65]. It enables one to calculate transport properties to LO at weak coupling, and may also (with the above motivation) make for a prudent compromise on which to base estimates at larger coupling. Regardless, it is the only feasible calculational scheme available at present.

Single function Ansatz

While a precise evaluation of (3.19) requires approximating χ by a suitably large basis of test functions, it has been found that the single function trial $\psi(k) = (k/T)^2$ is accurate already to 1-2%. Under this assumption, it is possible to find a good approximation to b in (3.26) analytically. Here we shall use it to confirm that our approach (formulated in a covariant way in terms of the Mandelstam variables s, t) gives the same LL prefactor for $n_f = 0$.

The numerator term in (3.21) is simple to evaluate,

$$\int_{\boldsymbol{k}} S\psi\Big|_{\psi=(k/T)^2} \;=\; \frac{\beta^3}{2\pi^2}\int \mathrm{d}k\, f\bar{f}\, k^5 \;=\; T^3\frac{60}{\pi^2}\zeta(5)\,.$$

We calculate the denominator in (3.21) for hard $|t| > |t^\star|$ (details are given in Appendix D), where the thermal corrections to the propagator can be dropped. In this kinetic region, keeping only the necessary transport weight up to $\mathcal{O}(t)$,

$$\int_k \psi\mathcal{C}_L[\psi]\Big|_{\psi=(k/T)^2}^{|t|>|t^\star|} \;\simeq\; \frac{d_g}{8(2\pi)^4}\int \mathrm{d}E_1\mathrm{d}E_2\; f_1 f_2 \bar{f}_1 \bar{f}_2 \big(E_1^2+E_2^2\big)\cdot \\ \cdot \int_0^{s_{\max}} \mathrm{d}s\,\big(8E_1E_2+s\big)\int_{-s}^{t^\star}\mathrm{d}t\,|t|\frac{\mathrm{d}\sigma}{\mathrm{d}t}\,,$$

where $s_{\max} = 4E_1E_2$. Note that the $\bar{f}_i$ of outgoing particles are evaluated with the corresponding incoming momenta (although t is hard). With the soft cut off, a tree-level cross section [i. e. (3.23)] is sufficient to evaluate the LL coefficient. Evidently the t-integration produces the usual Coulomb-log, cf. Eq. (3.24), which is to be folded together with a thermal weight. Using (3.24) with the normalisation (3.23), the s-integral reduces to

$$\frac{d_g}{8(2\pi)^4}\int \mathrm{d}s\, s(8E_1E_2+s)\cdot\sigma_{\mathrm{tr}}(s) \;=\; \alpha^2 d_g \frac{45}{2\pi^3}\,E_1^2E_2^2\Big[\,\log\left(\frac{s_{\max}}{|t^\star|}\right)+\mathcal{O}(|t^\star|^0)\,\Big]\,. \tag{3.27}$$

The terms in square brackets next to the logarithm are subdominant [they only contribute to the constant under the log, c in (3.26)] and to the same level of accuracy we can replace $\log\left(s_{\max}/|t^\star|\right) \to \log\left(T^2/|t^\star|\right)$, since the subsequent E_1 and E_2 integrals gives $E_i \sim T$ in the

[24] Assuming that perturbative expansions have similar properties to asymptotic series, the higher order contributions may improve this 'minimal' scheme, but the relative corrections are small for weak coupling.

upper bound $s_{\max} = 4E_1E_2$. With the aid of the definite integral, $\int \mathrm{d}x\, x^n f\bar{f} = n!\zeta(n)$, the outstanding E_1- and E_2-integration contribute

$$\int_p \psi \mathcal{C}_L[\psi]\Big|_{|t|>|t^\star|} \;=\; \alpha^2 d_g 4\pi^3 \log\left(\frac{T^2}{|t^\star|}\right). \tag{3.28}$$

The matrix element (3.22) is also infrared divergence in the region of $-t \simeq s$ (small u), which must be treated similarly. By crossing symmetry, i. e. $t \leftrightarrow u$, it is sufficient to multiply (3.28) by two. After replacing $|t^\star| \to \alpha T^2$, we recover the (approximate) LL result (3.26) with [53]

$$b \;=\; d_g \zeta(5)^2 \frac{60}{\pi^7} \;\simeq\; 0.34\,,$$

which is within 1% of the exact result, including inelastic contributions [65]. Moreover, the exact δf obtained as a variational maximum tends to $(k/T)^2$ for large arguments [64]. Working *beyond* logarithmic order, i. e. retaining the constant $\sim \mathcal{O}(1)$ in (3.27), it is necessary to properly consider also the kinematic region of soft transfers. Doing so prohibits an analytic evaluation of (3.21), and the five-dimensional integral for (3.18) must be evaluated numerically.

Fixed α-dependence

For weak coupling, $\eta(\alpha)$ should be a decreasing function as expected on physics grounds: velocity gradients should equilibrate more efficiently by stronger interactions. As mentioned before, η should decrease with increasing coupling (unless the quasiparticle structure of the system changes, like in phase transitions) – an expectation indeed met by the NLL result (3.26) for small α, where it is strictly justified. However, $\eta_{\mathrm{NLL}}(\alpha)$ has a minimum at $\alpha^\star = c/\sqrt{e}$ (e is Euler's number). Numerically, $\min[\eta_{\mathrm{NLL}}] = 2beT^3/c^2$ turns out to be close to the free entropy $s_0(T) = (16 + \frac{21}{2}n_f)\frac{4\pi^2}{90}T^3$, see (2.10), for all reasonable values of n_f, (note that s_0 overestimates the interacting entropy, in particular near the confinement transition). Thus it is plain that the NLL result (3.26) is incompatible with $\eta/s \lesssim 0.5$ – which may have led to the common view that perturbative QCD cannot explain the experimental findings. In order to scrutinize this view, we may see the minimum at $\alpha^\star$ as a precursor to the singularity of $\eta_{\mathrm{NLL}}(\alpha)$ at $\alpha = c$, which marks the ultimate break-down of the NLL approximation (see Fig. 24). However, as is obvious from the derivation of the parametric formula (3.25), this singularity is *unphysical* because it stems from a swapping of integration bounds in (3.24), where screening was pragmatically taken into account by modifying $t_{\max} = 0 \to t^\star$. This suggests that also the minimum of η_{NLL} is an artefact and will motivate us to withhold the expansion in powers of $\log 1/\alpha$ [25], focusing instead on the full (unexpanded in logarithms of α) LO result as depicted in Fig. 24.

As a monotonously decreasing function, $\eta_{\mathrm{LO}}(\alpha)$ could potentially explain $\eta/s \lesssim 0.5$ – depending on the value of α. A common prescription is to replace α, in the *fixed coupling* result $\eta_{\mathrm{LO}}(\alpha_{\mathrm{fix}})$, with the running coupling evaluated at a thermal scale, $\alpha_{\mathrm{fix}} \to \alpha(Q_T^2)$, usually with $Q_T = 2\pi T$. Although this recipe gives somewhat lower values than with η_{NLL}, normalising it to the *interacting* entropy (obtained from lattice QCD calculations) yields $\eta_{\mathrm{LO}}(\alpha(Q_T))/s \gtrsim 0.7$, which still does not explain the fairly conservative upper bound $\eta/s \lesssim 0.5$ from heavy-ion experiments.

[25] The situation may not improve by higher order terms in the log-expansion, because the latter seems not to be Borel summable [65].

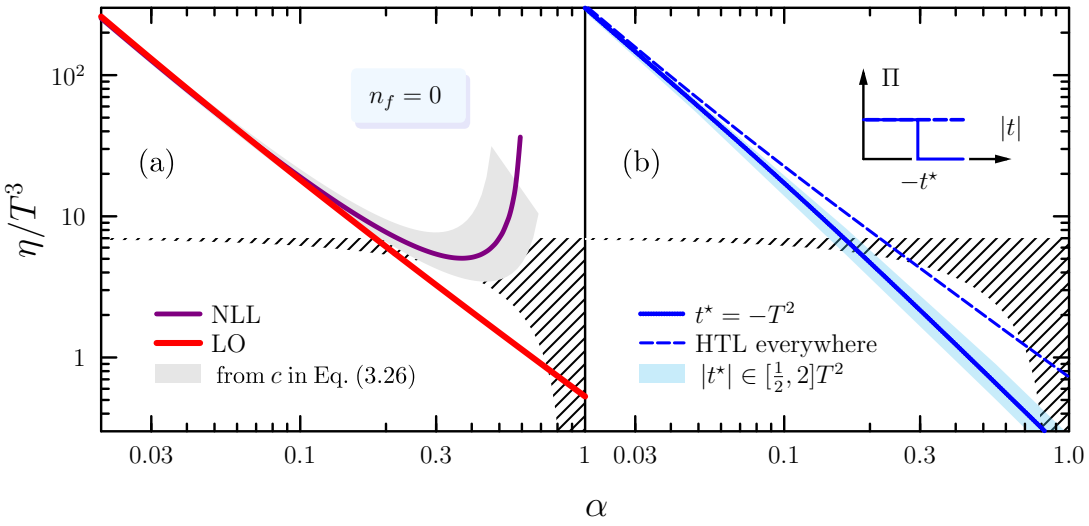

Figure 24: Dependence of the shear viscosity on the interaction strength, for various approximations in the quenched limit ($n_f = 0$). The hatched region demarcates the entropy, between the free limit and the LO correction, so that $\eta/s \lesssim 1$ is guaranteed if $\eta(\alpha)$ lies below this region. Left panel: the LO (red) and NLL (3.26), (the band arises from 10% variation in c). Right panel: The results of our calculation (in blue), dropping the inelastic processes and using a simplified functional basis. We estimate the HTL uncertainty via a hard cut-off $t^\star$ (see text for details) giving the band. The dashed line uses HTL functions for all t, and is the 'canonical' choice by the Authors of [65].

Setting the scale(s) for α

Evidently it may be possible to explain $\eta/s \lesssim 0.5$ on the basis of a leading order treatment (see Fig. 24), but to do so requires a proper understand of how 'the' value of α is specified by the temperature. So far in our parametric considerations, we have focused on screening described by the thermal parts of the quantum fluctuations, sidelining the vacuum contribution (which actually underpin the magnitude of α). Physics at $T = 0$ is relevant for any gauge theory, but in particular for QCD where there is no preferred value for α (such as $\alpha_{\rm em} = 1/137$ in QED for all practical purposes). Using hard momenta Q_T to determine the coupling is not at all obvious, especially given the importance of the soft sector below $|t^\star| \sim \alpha T^2$ throughout the previous section.

We explored this notion in § 2, for *static* observables which simplified the argument considerably. But because the ideas are general, based on the renormalisation group equations, Eq. (2.65) can be used to absorb the vacuum self-energy into an effective cross section $\mathrm{d}\sigma/\mathrm{d}t \sim \alpha^2(t)/t^2$. Although the processes here are dynamical, the renormalisation group equations hold in general. Therefore, refining our earlier formula (3.24) for the transport cross section leads to

$$\begin{aligned} \sigma_{\rm tr}(s) \sim \frac{1}{s}\int_{-s}^{t^\star} \mathrm{d}t\,|t|\,\frac{\alpha(t)^2}{t^2} &= \frac{1}{s}(4\pi/\beta_0)^2 \frac{1}{\log\left(|t|/\Lambda^2\right)}\Bigg|_{-s}^{t^\star} \\ &= \frac{1}{s}\alpha(-t^\star)\alpha(s)\log\left(\frac{s}{|t^\star|}\right). \end{aligned} \tag{3.29}$$

A similar setting of scales, balanced between hard and soft modes, was found for the QCD

collisional energy loss [67]. The overall structure is unchanged, cf. (3.25), but note the substitution $\alpha^2 \to \alpha(\text{hard})\alpha(\text{soft})$ in going from (3.26) to (3.29) reflects the relative importance of different scales. Since α increases for at smaller scales, a sensitivity to the soft sector enhances the transport cross section. Rather than α depending only on the hard scale $s \sim T^2$, the additional factor $\alpha(-t^\star)$ considerably reduces η.

We shall now explain some of the more technical aspects to our calculation. The functional form of $\widetilde{\pi}(\omega, \boldsymbol{q})$ is calculable analytically in the HTL approximation [see Eq. (2.50)], valid where $t = Q^2 \ll T^2$ and thus appropriate for the LO kinetic theory [66]. The screened amplitude takes the generic form, for a t-channel process,

$$\begin{aligned} \mathcal{M}(12 \to 34) &= C\alpha(Q^2) D_{\mu\nu}(Q)(K_1 + K_3)^\mu (K_2 + K_4)^\nu \\ &= (s-u)^2 \sum_{i=T,L} C_i \alpha(Q^2) \cdot D_i(Q)\,, \end{aligned} \tag{3.30}$$

where D_L and D_T are the longitudinal and transverse propagators respectively and C_i are constants. In our 1-loop resummed framework, the dressed propagators have HTL self-energies with a running coupling, i. e.

$$D_i^{-1} = t - \alpha(t) T^2 \cdot \widetilde{\pi}_i(\omega, \boldsymbol{q})\,, \qquad i = (T, L)\,.$$

With these functions, screening is suppressed by a factor α

In the denominator of the terms in Eq. (3.30), the Born term will always dominate for large enough $|t|$. However for soft momenta, where screening is crucial, the running coupling $\alpha(t)$ in the denominator enhances the effect. Based on (2.65), we may note that as t approaches the QCD scale, $|t| \to \Lambda^2$, the coupling in both the numerator and denominators of (3.30) become large and in this limit $\alpha(Q^2) D_i(Q) \to (-T^2 \bar{\pi})^{-1}$. Thus where pQCD becomes dubious, the matrix element saturates at some finite value, rather than giving an obviously unphysical result. At 'strong coupling' the totally screened cross section actually leads to a *minimum* bound on η. On these grounds, an extrapolation of σ_{tr} using Eq. (3.30) may actually yield reasonable estimates, e. g. for η, since screening protects $Q \to \Lambda$.

Along these lines, the relevant momentum scale, at which to evaluate $\alpha(Q^2)$, is that of the virtual intermediate state $Q^2 = \{s, t, u\}$. Depending on the channel, (time- or space-like), we make use of the continuation of (2.65), as advocated in [71],

$$\alpha_{\text{eff}}(Q^2) = \frac{4\pi}{\beta_0} \begin{cases} L^{-1} \\ \dfrac{1}{2} - \dfrac{1}{\pi} \tan^{-1}(L/\pi) \end{cases} \qquad \text{for } Q^2 \lessgtr 0\,, \tag{3.31}$$

where $L = \log |Q^2| / \Lambda^2$. Despite intrinsic difficulties with QCD in the far infrared, perturbation theory can give semiquantitative results [72]. Soft interactions are more probable (due to an overall factor of α^2 in $\mathrm{d}\sigma/\mathrm{d}t$) but are also more screened due to the running coupling; $\widetilde{\Pi}(Q) = \alpha(Q^2)\widetilde{\pi}(\omega, \boldsymbol{q})$ for the self energy (recall, for example, Fig. 14).

Our results for the shear viscosity to entropy ratio are displayed in Fig. 25, using a running coupling as described earlier. For $n_f = 0$ they are comparable with the expectation $\eta/s \sim 0.2$ at $T \gtrsim (1-3)T_c$. The interacting entropy is now quite well established according to lQCD numerical data [29], and we shall it to normalise the perturbative result for η. Adjusting the value of l 'dials in' the abscissa scale in Fig. 25; we put $l_{(n_f=0)} = l_{(n_f=3)} = 1$ (for simplicity and in light of the overbearing HTL uncertainties). This choice is based on fixing l from thermodynamics in § 2, ruling out the possibility of a misinterpreted fit (a more rigorous fitting may affect our results to the order 10%). Confronting our pure gauge analysis with recent lQCD values for η [68, 69, 70], we see agreement with $\eta_{\text{LO}}^{\text{renorm}}(T)$

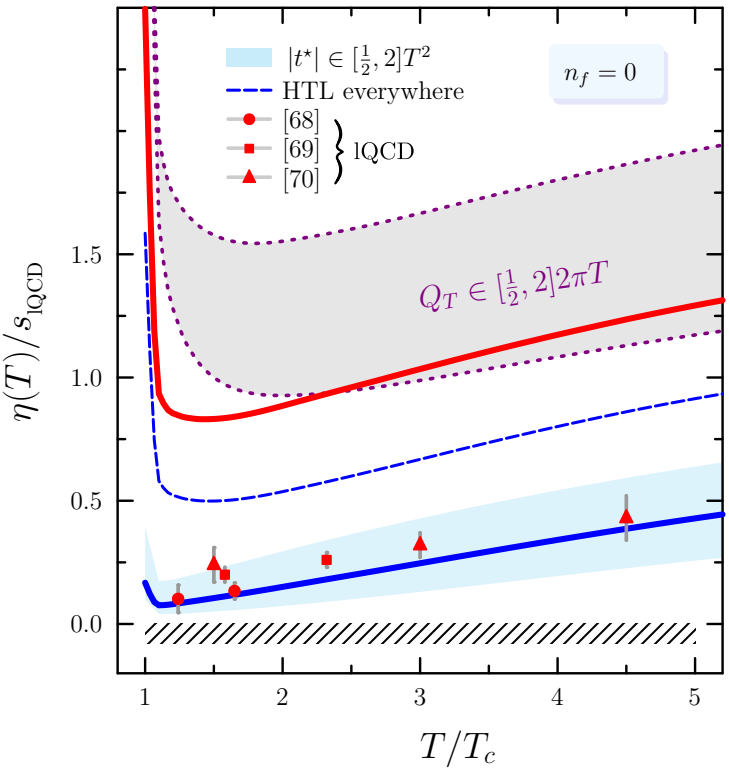

Figure 25: Temperature dependence of the viscosity to entropy density ratio in the quenched limit ($n_f = 0$). The (red) solid line represents the LO result for η (see Fig. 24), normalised by the interacting entropy [29], and with a coupling at the thermal scale $Q_T = 2\pi T$. The band enveloped by the dotted (purple) lines is the naïve NLL formula (3.26), with the running coupling evaluated at Q_T, which is varied by a factor of two. The data points summarise various lQCD attempts [68, 69, 70] to obtain the viscosity. The solid (blue) line, surrounded by a light band, is our 1-loop resummation scheme (see text for details) with a 'canonical' choice of screening only where $|t| < -t^\star = T^2$. Using an omnipresent HTL regulator (even for 'hard' t) gives the dashed line slightly above our canonical choice. A sharp rise in η/s very near to T_c is not unexpected, and is due to the sudden reduction of the interacting entropy as the quasiparticle structure changes.

almost down to T_c. These data are clearly overestimated by the naïve thermal scale Q_T in the running coupling (both with the LO and NLL approximation for η), even given the wide 'error' band from varying Q_T. Moreover, this approach will overestimate the correct η/s also for large temperatures, hinted in Fig. 25. Because the coupling varies (potentially) over the relevant soft scales, we may understand this reduction (by about a factor of four) as being principally due to 'strong' interactions near T_c. Within the present approach, the factor reduction in η/s could indicate less screening than accounted by HTL (which is difficult to read off Fig. 9).

Prediction for $n_f = 3$

Our preceding argument is basically unaffected by the addition of quarks, which does however introduce the necessity of screening a soft fermion exchange. The authors of [54] were

the first to correctly account for all binary scattering processes in modelling the QGP by the Boltzmann equation. Our discussion was based on a single-valued distribution function f, in Eq. 3.3. In order to also accommodate the quark population, $f = (f_g, f_q)$ generalises into a 'two-component' distribution which describes both quarks and gluons. The pure gauge sector basically remains unchanged, see Fig. 23, and the quark sector involves an QCD-like *Bhabha* scattering process shown in Fig. 26. Since a virtual gluon transfers momenta between quarks to LO, the dressed propagator is identical to the case with $n_f = 0$.

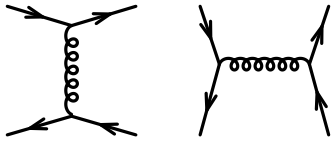

Figure 26: Binary scattering among the quarks and antiquarks, which also contribute to a QGP viscosity. All other permutations of the directions of the arrows are summed over. The exchanged space-like gluons give infrared divergent singularities in the tree level matrix elements that must be dressed, in an identical manner to the previous section ($n_f = 0$).

Gluons equilibrate faster than quarks alone, due to the availability of quantum numbers in scattering processes (i. e. the larger gauge group Casimir $C_A = 3$, from the sum over colours). Therefore processes which transfer momentum between the boson and fermion populations are important to consider, for example Compton scattering (Fig. 27). Here we encounter infrared sensitive diagrams with a soft fermion line, requiring the dressed quark propagator to account for screening. The HTL effective fermion mass was first calculated by Weldon [73].

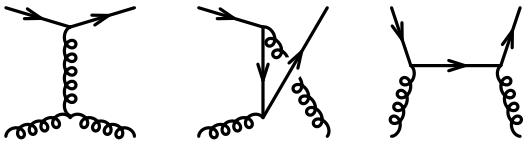

Figure 27: Compton scattering of gluons on quarks allows transfer of momentum between the boson and fermion species, but without changing the number in either distribution. The leftmost diagram includes a 3-gluon vertex, which is unique to QCD. Singularities in the tree level matrix elements require screening by gluon and fermion self-energies.

There are also interactions that serve to 'convert' quark-antiquark pairs into two gluons and vice versa. Fig. 28 illustrates the LO diagram for fermion annihilation into gluons, the reverse of which (gluon fusion) is also possible. Such processes, which not only transfer momentum, but also mix between particle species, will speed up equilibration. Although Baym *et al.* correctly analysed the gluonic viscosity [53], they dropped the diagrams in Figs. 27 and 28 with a soft fermion line in their treatment of $n_f > 0$ which was numerically off by about 3%.

The main result of this thesis is shown in Fig. 29, which depicts our prediction for the temperature dependence of η/s in a HTL resummed pQCD framework. Also for 3-flavour QCD, a LO treatment with running coupling is compatible with the small η/s needed for hydrodynamical fits to experiment [74]. Incidently, the conjectured lower bound is obtained (and even violated) for $T \approx 1.4T_c$, below which point η/s rises again because of

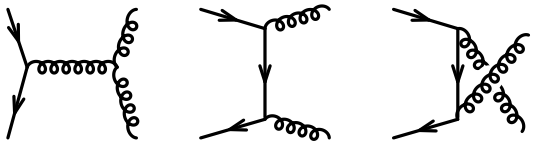

Figure 28: Quark-antiquark annihilation into two gluons (and the reverse; gluon fusion to a quark-antiquark pair) provides a means to mix the fermion and boson distributions. The leftmost diagram includes a 3-gluon vertex, which is unique to QCD.

the drastic reduction in entropy (which depends on the matching parameter l). Note that we find numerically very similar results for $n_f = 0$ and $n_f = 3$, so that the viscosity grows comparatively with the entropy density as more quark degrees of freedom are available. This, along with the fact that a QED plasma has a much higher η (due to the dearth of scattering possibilities), suggests that the consistently low value of η/s is intimately linked to the scale dependence of the strong interaction strength. The ambiguity that arises in parametrising $\alpha(Q^2)$ by a constant value *cannot* explain inferred transport coefficients.

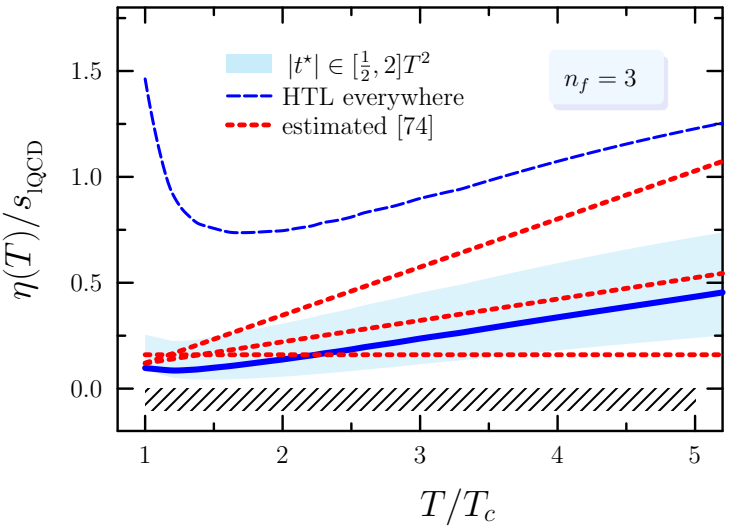

Figure 29: Temperature dependence of the viscosity to entropy ratio, in the physical case $n_f = 3$, along with several parametrisations extracted from hydrodynamics [74]. Our renormalised calculation for η is normalised by the lattice interacting entropy [31].

3.4 Range of applicability

To round off our discussion in § 3, let us make some comment on the scope of approximations. There are two principal concerns; 1) whether a kinetic description is valid, and 2) to what extent velocity gradients are small. As explained in the outline, the familiar skepticism based on 'convergence of perturbation theory' is only a secondary interest. We have already explained the shortcomings of using (3.24) where α is 'large', and are happy

to use the LO result, with parameters fixed in § 2 by the static limit of the same four-point function. However, this leaves open the question of whether the QGP is sufficiently 'dilute' for the Boltzmann equation to be used self-consistently. Shear viscosity was extracted as a coefficient in a gradient expansion, where the assumption was $\delta f \ll f$. Hence we may actually explore where this breaks down, i. e. what qualifies $\partial_y u_x$ to be small, which gives some insight into the value extracted by hydrodynamics.

Inter-particle distance

An important quantity in many-body physics, is the so-called 'mean inter-particle distance'. This length scale is intuitively related to the density of quanta, and should be smaller than the length between successive collisions (of a given particle) for kinetic theory to be valid. In this picture, excitations propagate ballistically over a mean free (transport) path λ [taking a time τ, cf. (3.1)] and have some chance to recoil instantaneously (at least to the resolution of the particle wavelength) off another particle in the medium.

To a first approximation, one may imagine that each particle occupies, on average, a volume $V/N = 1/\sqrt[3]{n}$. Then, denoting by $\bar{r}$ the mean inter-particle separation, we would expect $\bar{r}$ to be roughly given by the radius of this sphere, (R_d in d-dimensions)

$$R_d \;=\; (V_d \cdot n)^{-1/d} \,; \qquad V_d = \frac{2\pi^{d/2}}{\left[\frac{d}{2}-1\right]!} \,. \tag{3.32}$$

V_d is the volume of a unit d-ball. However, the choice of (hyper-)sphere was arbitrary, and an equally valid supposition might be a cube, which would give $\bar{r} \sim n^{-1/d}$. Although $\bar{r}$ is certainly proportional to $n^{-1/d}$, the definition (in particular, of the dimensionless prefactor) is somewhat ambiguous. To be more precise, we must regard the particles as being randomly arranged in space, and that the mutual distances fall into some probability distribution $\mathcal{P}$ which we now determine.

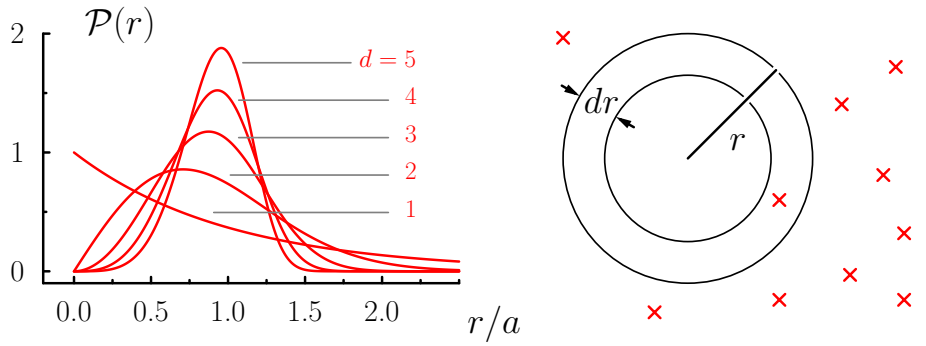

Figure 30: Right: We consider the closest particle to be in the ring $(r, r+\mathrm{d}r)$, and all other particles further away. Left: Probability distribution for the nearest neighbour distribution, $\mathcal{P}(r)$. Note that in higher dimensions, the peak is becomes narrower. For short distances (relative to R_d), the probability grows $\sim r^{d-1}$ (in proportion to the surface area. While for larger distances, the likelihood is suppressed exponentially.

For concreteness, take a hyper-cubical box of volume V in d-dimensions and fill it with point-like particles. If there are N particles, uniformly distributed, we would like to know the average distance from a single particle to its nearest neighbour. The probability for the

situation depicted in Fig. 30 is given by the product of the chance that there is one particle at a distance $(r, r + \mathrm{d}r)$ and all the remaining fall outside are further away. At a radius r, the shell of thickness $\mathrm{d}r$ has a volume $dV_d \cdot r^{d-1}\mathrm{d}r$. If the particles are independently located, then the nearest neighbour distribution $\mathcal{P}$ satisfies

$$\begin{aligned} \mathcal{P}(r)\mathrm{d}r &= n(dV_d \cdot r^{d-1}\mathrm{d}r)\left(1 - \frac{V_d}{V}r^d\right)^{N-1} \\ &\overset{N,V\to\infty}{=} d \cdot \frac{\mathrm{d}r}{R_d}\left(\frac{r}{R_d}\right)^{d-1} \exp\left[-\left(\frac{r}{R_d}\right)^d\right]. \end{aligned} \tag{3.33}$$

One may easily check that $\mathcal{P}$ is normalised, i. e. $\int \mathrm{d}r\mathcal{P}(r) = 1$. A plot of the distribution (3.33) is shown in Fig. 30.

The ℓ-th moments of this distribution function are

$$\int \mathrm{d}r \cdot r^\ell \mathcal{P}(r) = R_d^\ell \cdot \left[\frac{\ell}{d}\right]! \,.$$

We note that $\mathcal{P}$ (see Fig. 30) is a fairly broad function, except for higher dimensions. It has a peak near R_d, at the argument

$$r_{\mathrm{peak}} = R_d \cdot \left(1 - \frac{1}{d}\right)^{1/d},$$

which solves the condition for a vanishing derivative; $\partial_r \mathcal{P}(r) = 0$.

In three dimensions, the first moment is the mean inter-particle distance and is approximately equal to

$$\bar{r} = (0.893)R_d = (0.560)n^{-1/3}, \tag{3.34}$$

which is numerically quite close to the peak position

$$r_{\mathrm{peak}} \xrightarrow{d=3} (0.874)R_d \,.$$

Validity of Kinetic Theory

Using (3.3) requires that the mean-free path $\lambda \sim (gT)^{-1}$ is sufficiently large for collisions between particles to be isolated. Indeed the effective kinetic theory [66] has some limitations, and we attempt here to provide an *a posteriori* justification to apply it where $\alpha = g^2/(4\pi)$ is not asymptotically small. The self-consistency condition would demand that the mean free path is at least as large as $\bar{r}$, the mean inter-particle distance, as a very general condition on the Boltzmann equation.

The right hand side of Eq. (3.3) contains a difference between gain and loss rates forming the net transfer into a momentum state. There is nothing stopping us from regarding both rates separately, in order to discover how well attended collisions will be. Defining the rate per volume

$$J_{\gtrless} = \int_{\boldsymbol{k}} \frac{1}{2E} \int \mathrm{d}\Gamma |\mathcal{M}|^2 \begin{cases} \bar{f}_1 \bar{f}_2 f_3 f_4 \\ f_1 f_2 \bar{f}_3 \bar{f}_4 \end{cases}, \tag{3.35}$$

in which we count *all* scattering events, either into a momentum state $\boldsymbol{k}$, or out of it, and then sum over $\boldsymbol{k}$. In (local) equilibrium, collisions still occur even though $\mathcal{C}$ vanishes. Regardless of f, particle number is conserved, within our approximation, taking into account

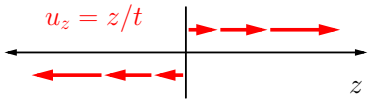

Figure 31: Bjorken expansion in one dimension. The gradient in velocity is parallel to the direction of propagation, thus serving to dampen sound modes travelling in the z-direction.

only binary processes, and thus the net current vanishes; $\partial_t n + \nabla \cdot (\boldsymbol{u} n) = J_> - J_< = 0$ [this may be seen by directly relabelling the integration variables in (3.35)].

It is possible to extract the leading behaviour of (3.35), for equilibrium distribution functions (where the two rates will be equal). Indeed the small momentum exchange $t \simeq 0$ dominates the integrand to the extent that it is permissible to replace $E_1 = E_4$ and $E_2 = E_3$. For definiteness let us consider only $n_f = 0$. Then, following the integration procedure of Appendix D,

$$J_{\gtrless} \;=\; \frac{\mathrm{d}_g}{16(2\pi)^5} \int \mathrm{d}E_1 \mathrm{d}E_2 \, f_1 \bar{f}_1 f_2 \bar{f}_2 \int_0^{s_{\max}} \mathrm{d}s \int_{-s}^{t^\star} \frac{\mathrm{d}t}{s} \cdot |\mathcal{M}|^2 \,. \tag{3.36}$$

The net rate is determined by the total cross section $\sigma(s)$, since $|\mathcal{M}|^2 = 16\pi s^2 \, \mathrm{d}\sigma/\mathrm{d}t$ is proportional to the differential cross section. In the Born approximation, and catering for the t- and u-channel together

$$\frac{\mathrm{d}\sigma}{\mathrm{d}t} \;=\; 144\pi \frac{\alpha^2}{t^2} \,,$$

we need to regulate the infrared divergence by an effective cut-off $t^\star$ in (3.36). The leading α-contribution[26] is therefore

$$J \;=\; 4\pi d_g \frac{\alpha^2}{|t^\star|} T^6 \,.$$

The result is dependent on $t^\star$, which only drops out of the leading-log approximation, and we shall use $|t^\star| = \nu \cdot \alpha T^2$, based on our calculation of η/s in the previous section. Using the Stefan-Boltzmann number density, $n = d_g \zeta(3) T^3/\pi^2$, we may relate (3.34) to the temperature: $\bar{r} = (0.448) T^{-1}$. On the other hand the mean free path $\lambda = \tau \simeq n/J$. The mean free path becomes equal to $\bar{r}$ at the value $\alpha \simeq \nu/(46.22)$, which at $\nu = 4\pi$ (i. e. the Debye mass) gives $\alpha \simeq 0.273$. Evidently we cannot make a clear-cut statement in this regard, since the absolute scale $\nu = 4\pi$ is not necessarily the 'correct' scale at which to determine $t^\star$. On a more optimistic note, this rather stringent test does not rule out kinetic theory.

Is δf small?

Although local equilibrium in a heavy-ion collision is suspected to be reached in about 1 fm/c, the QGP still shows large corrections to ideal isotropic behaviour even after this time. For a system undergoing Bjorken expansion [8], i.e. $\boldsymbol{u} = (0, 0, z/t)$ in only the z-direction (see Fig. 31), the shear tensor (3.12) is diagonal and the term proportional to η is

$$\nabla_i u_j + \nabla_j u_i - \frac{2}{3} \delta_{ij} \nabla \cdot \boldsymbol{u} \;=\; \frac{2}{3t} \, \mathrm{diag}\,(-1, -1, 2) \;.$$

[26] We ignore corrections with higher powers of α, which may in isolation give an infinite contribution.

We should note that the velocity is strictly only defined when $|z| < t$, in order to respect causality outside of the expanding tube, and it is zero for $|z| > t$ (there is a 'shock' front at the edge of the lightcone). Fluid in the ensuing wake rapidly expands from the central slice in the longitudinal direction and thus cools, as pressure in transverse direction is able to build up. Let us examine it more closely at midrapidity ($z = 0$), where $u_z = 0$ but there is still a non-zero flow gradient which modifies the energy momentum tensor, (3.12), in proportion to η. Viscous corrections lead to 'effective' pressures, namely

$$p_L = \Theta_{zz} = p + \frac{4\eta}{3t} , \quad \text{and} \quad p_T = \Theta_{xx} = \Theta_{yy} = p - \frac{2\eta}{3t} ,$$

in the longitudinal and transverse directions respectively. The energy density at all times is given by $\varepsilon = 2p_T + p_L$. Thus first order hydrodynamics predicts that the ratio [75]

$$\frac{p_T}{p_L} = \frac{3tT - 8\frac{\eta}{s}}{3tT + 16\frac{\eta}{s}} , \tag{3.37}$$

where we have used the equilibrium relation $(p + \varepsilon) = sT$ and the ideal equation of state $\varepsilon = 3p$. Eq. (3.37) demonstrates that for large t (compared to a timescale set by η/s, whose source we elucidate in the conclusion) $p_T/p_L \to 1$, reflecting that the momentum distribution becomes isotropic. At the beginning, a highly off-equilibrium state (CGC briefly mentioned in § 1), p_L exceeds p_T and viscous hydrodynamics is only able to aptly describe the final approach to equilibrium.

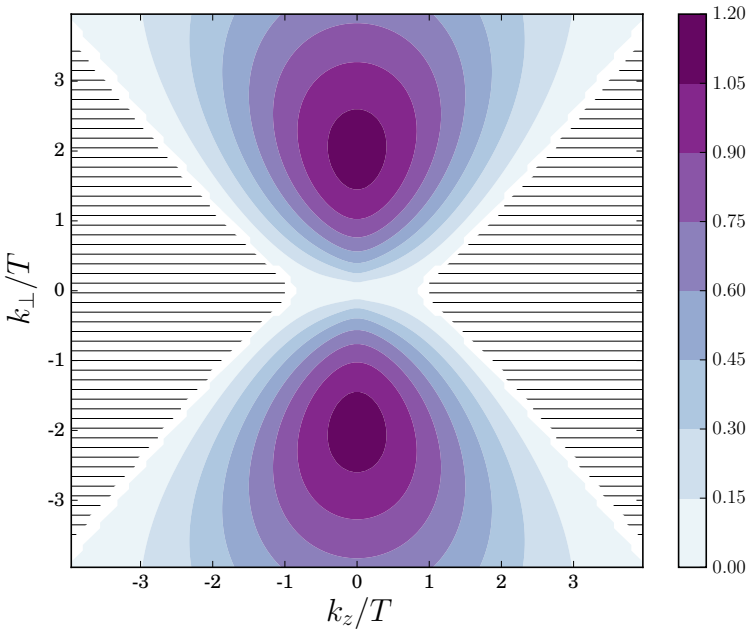

Figure 32: Contour plot of $f_\star = f_\star(k_\perp, k_z)$ as in Eq. (3.38) at $t = \tau$. The hatched region depicts where $f < 0$, an unphysical characteristic of the first order correction where $\partial \boldsymbol{u}$ is not sufficiently small. This does not affect the bulk of particles, since $f_\star$ is in any case small for large momenta.

We may estimate from (3.37) by how much the distribution function deviates from its equilibrium form, i. e. compare δf to f (where f is in equilibrium). The linearised Boltzmann

equation (3.13) readily determines, within the relaxation time approximation $\mathcal{C}[f] = -\delta f/\tau$, the functional form of the deviation from equilibrium, $\delta f(k) = f\bar{f}\chi(k)/T$ with $\chi(k) = k \cdot \tau$. The first order corrected solution to the Boltzmann equation is therefore [75]

$$f_\star(k_\perp, k_z) \;=\; f\,(k)\,\Big\{\,1\;+\;\frac{\tau}{t}\,\bar{f}\,(k)\Big[\;\frac{k_\perp^2 - 2k_z^2}{3Tk}\;\Big]\;+\;\ldots\;\Big\}; \qquad k \coloneqq \sqrt{k_\perp^2 + k_z^2}\;. \tag{3.38}$$

Note that the magnitude of the second term is $\sim 1/t$, and therefore δf is only small long after the initial collision (relative to τ), which is when the gradients in $\boldsymbol{u}$ are also small. Eq. (3.37) is thus a measure of the skew momentum distribution in (3.38). One drawback of expanding the off-equilibrium distribution according to (3.38), is that (even at late times) $f_\star$ is negative for some momentum regions. This is an artefact of the expansion, and affects the large momenta particles $k \gg T$ due to the functional dependence[27] of $\chi(k)$, see Fig. 32. Because the expansion evidently breaks down for large momenta $k \gg T$, the particles carrying a negative weight are in the minority.

The full scheme of linearising the Boltzmann equation, and solving for η by a variational approach, allows us make statements about δf. Thus, beyond just calculating the numerical value for the shear viscosity, it is also possible to self-consistently quantify where the approximation breaks down.

[27] The full solution for $\chi(k)$ tends to k^2 for large arguments, which would have an even more drastic effect on δf. By using a functional approach to calculating η, the fact that $f < 0$ is actually not relevant.

4. Conclusion

Following up on the emerging picture of a 'strongly coupled' QGP (sQGP), we shall put the viscosity into a broader context. Why the QGP thermalises so rapidly, explained from first principles, has remained an open question ever since the experimental indications were confirmed. The timescale for equilibrium to be reached is roughly given by the effective relaxation time in (3.5). The simplified collisional operator $\mathcal{C}[f] = -\delta f/\tau$ gives $\chi(k) = k \cdot \tau$. And thus by Eq. (3.15) the shear viscosity can be calculated in the relaxation time approximation, establishing a direct proportionality of τ and η,

$$\eta \quad = \quad \tau \cdot \frac{d_g}{15} \int_{\boldsymbol{k}} f \bar{f} \, \frac{k^2}{T} \quad = \quad \tau \cdot d_g T^4 \frac{2\pi^2}{225} \, .$$

Dividing by the Stefan-Boltzmann entropy (2.10), we find the useful 'pocket formula' for the viscosity to entropy density in terms of the relaxation time,

$$\eta/s \quad = \quad \frac{1}{5} \tau T \, . \tag{4.1}$$

Hence the robust phenomenological constraint, which we have here underpinned theoretically, of $\eta/s \simeq 0.2$ near the confinement temperature of $T = 200$ MeV yields $\tau \simeq 1$ fm/c. As alluded to in § 1, this estimate coincides with the typical timescale $\mathcal{O}(1 \text{ fm/c})$ as the starting point of hydrodynamical evolution in a heavy-ion collision [76].

Outlook

If we take our findings seriously, there are many natural courses to follow in the greater programme of understanding the interplay between renormalisation and screening in the sQGP. One obvious topic to pursue is the full one-loop gluon polarisation $\Pi_{\mu\nu}(Q)$, which must be calculated numerically (cf. Fig. 9). Since the primary source of uncertainty in our calculation for η/s is where to switch off the HTL insertions, which might be resolved by utilising the complete self-energy (valid for all Q). Another refinement would be to include inelastic processes and in particular, correctly identify the scale dependence in the coupling for such processes. Although this was not necessary for us to qualitatively obtain $\eta/s \lesssim 1$, it would certainly required for more than 10% accuracy and to test whether the calculational improvement is a robust approximation.

Summary

The purpose of this thesis was to revisit the viscosity to entropy ratio of the QGP and refute a widespread paradigm. Presuming that perturbation theory is incompatible with $\eta/s < 1$, in the context of heavy ion experiments, the (almost) ideal fluid nature of the 'strongly-coupled' plasma has been taken as an indicator for non-perturbative effects. In fact, the full numerical scheme put forward in [65] is capable of describing $\eta/s < 0.5$, (see our main result Figs. 25 and 25).

A central theme in our argument has been how to quantify the coupling strength α. For QCD it is important to take into account the running coupling, which is known to vary considerably over the potential range of interest. The increase in coupling strength at small momentum leads to an enhancement in the effectiveness of collisions in the plasma. In § 2 we elaborate on this scale setting for static quantities, such as pressure, entropy density and

energy density, and reflect on the approach to the asymptotically free limit of QCD. Having verified the consistency of various models, we speculate on the applicability of perturbation theory for 'moderately' large coupling.

The viscosity, as a measure of how effectively momentum can be transported across layers of a medium with a small gradient in collective velocity, is intimately connected to the strength of interactions. Previous kinetic theory approaches, which apply (3.26) at face value, are handicapped for two reasons:

1. Logarithmic accuracy is appropriate only in scenarios where the coupling may be regarded as (asymptotically) weak. The increase of $\eta_{\mathrm{NLL}}(\alpha)$ in (3.26) for $\alpha > \alpha^\star$ is *unphysical*: we expect that the viscosity to decrease with the coupling strength.

2. A common procedure is to *choose* the value of α as the running coupling $\alpha(Q^2)$ at, or near, the lowest Matsubara energy. Even the LO result (fixed-α)with this choice does not give $\eta/s \sim 0.5$, see Fig. 25.

In fact, a scale-dependent coupling and the calculation scheme of LO (as well as NLL and LL) approximations are closely related: both emerge from/take into account loop corrections to tree level-amplitudes. Together, these improvements enable us to hopefully estimate η even in a regime which is usually thought of as 'strongly coupled', near to the QGP phase transition, provided binary scatterings form the principal source of equilibration. It is natural to expect that the η/s makes a smooth approach towards the critical temperature, below which the basic excitations switch to massive hadronic degrees of freedom. To investigate the possibility that an effective running coupling may qualitatively describe scatterings just above T_c, we lay out a scheme to renormalise the collisional operator in Eq. (3.3). This indeed leads us to conclude that the low viscosity of the QGP can actually be explained by 'perturbative' means.

Acknowledgements

What I write here will not be enough to thank André Peshier, who has encouraged and supported me since I began to study physics (first as my lecturer in 2011, and now as my supervisor). His deep understanding and technical know-how have made it a privilege to collaborate together. We share a similar attitude to problem solving in physics, and I hope that one day I will be able to baffle him with some cryptic riddles!

Let me express my thanks to members of our working group; namely Brandon Viljoen, Dino Giovannoni and Sylvain Mogliacci, with whom I had some rich discussions (sometimes even physics-related). Sylvain was kind enough to read the draft of this thesis and provide very useful feedback. I am grateful to Andrey Grozin for explaining some of the details in the calculation of the gluon self-energy. I also wish to thank the examiners, who gave valuable advice on this report which undoubtedly went into improving its quality.

The National Institute for Theoretical Physics (NITheP) provided the financial support for this work, and very generously extended that support for travel purposes. NITheP enabled my participation in the Strangeness in Quark Matter conference (Russia) in 2015, and the 26^{th} Jyväskylä Summer School (Finland) in 2016. I would also like to convey my appreciation to the University of Cape Town (UCT), which has provided a wonderful academic environment for research and teaching. The Department of Physics at UCT is a special community, of which I am very grateful to be a part.

Thanks to my friends and family for everything else.

A. Coulomb gauge Feynman rules

Having at hand the partition function, Eq. (2.6), paves the way for a perturbative approach. In this addendum we summarise the diagrammatic rules in Coulomb gauge QCD, namely the gauge propagators and the interaction vertices. We shall also discuss some general aspects of the scalar propagator in d-dimensions, although it goes beyond what is needed in the main text.

Propagators

As we have found, each mode is an *independent* Gaussian random variable with zero mean. From (2.6), one may read off the two-point correlation[28] functions

$$\langle \varphi_{\boldsymbol{k}}\ \varphi_{\boldsymbol{k}'}\rangle \;=\; \frac{\delta_{\boldsymbol{k},-\boldsymbol{k}'}}{\boldsymbol{k}^2} \qquad \text{and} \qquad \left\langle A^i_{\boldsymbol{k}} A^j_{\boldsymbol{k}'}\right\rangle \;=\; \frac{\delta_{\boldsymbol{k},-\boldsymbol{k}'}}{\omega^2+\boldsymbol{k}^2}\left(\delta^{ij}-\frac{k^i k^j}{\boldsymbol{k}^2}\right).$$

The presence of a heat bath breaks the $O(d,1)$ symmetry to $O(d)$, putting the Coulomb gauge on an equal footing with covariant gauges. Returning now to the representation of the Greens' function in momentum space, we include the transverse field and the propagator,

$$D^{(0)}_{\mu\nu}(\omega,\boldsymbol{k}) = \begin{pmatrix} -1/\boldsymbol{k}^2 & \mathbf{0}^t \\ \mathbf{0} & \Delta_K\left(\delta_{ij}-\hat{k}_i\hat{k}_j\right)\end{pmatrix}; \qquad \Delta_K = \frac{-1}{\omega^2+\boldsymbol{k}^2}.$$

This basis naturally separates the gluon propagator, μ 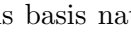 ν, into the two polarisations with external 4-momentum Q, which we draw as a dashed and wavy line for the longitudinal and transverse fields respectively;

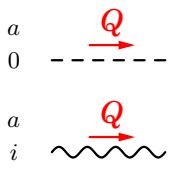

$$= -i\delta^{ab} D^{(0)}_{00}(Q)\,,$$

$$= -i\delta^{ab} D^{(0)}_{ij}(Q)\,.$$

For our concerns, the bookkeeping of colour indices is unaffected by the gauge choice. Here the convenience comes from treating the longitudinal and transverse fields as if they were *different* particles.

The 00-propagator represents an instantaneous interaction (it is a static potential), we call this mode the 'Coulomb gluon'. Although it appears that the instantaneous Coulomb field interaction violates causality, physically observable quantities are independent of the choice of gauge [77], The ij-components are dynamical, representing the propagator for a massless particle with indices transverse to $\boldsymbol{k}$, we call it 'transverse gluon' [38].

To return to coordinate space, one needs to take the inverse Fourier transform. Clearly the mean values vanish; $\langle\varphi(\boldsymbol{x})\rangle = \langle A^i(\boldsymbol{x})\rangle = 0$ by symmetry, while

$$\langle\varphi(\boldsymbol{x})\ \varphi(\boldsymbol{x}')\rangle \;=\; \frac{1}{V}\sum_{\boldsymbol{k}}\frac{e^{i\boldsymbol{k}\cdot(\boldsymbol{x}-\boldsymbol{x}')}}{k^2} \;=:\; -D^{(0)}_{00}(\boldsymbol{x}-\boldsymbol{x}'),$$

[28] In this appendix we denote the expectation value by angular brackets, $\langle O\rangle = \bar{O}$.

and similarly for the $\vec{A}$ fields (although the projector complicates this somewhat). In the continuum limit, $D^{(0)}_{00}$ is proportional to the Coulomb potential of a unit charge at the origin in $\mathbb{R}^d$, since it solves

$$\nabla^2 D^{(0)}_{00}(\boldsymbol{x}) \;=\; \int_{\boldsymbol{k}} \frac{k^2 e^{i\boldsymbol{k}\cdot\boldsymbol{x}}}{k^2} \;=\; \delta^{(d)}(\boldsymbol{x})\,.$$

According to Gauss' theorem,

$$1 \;=\; \int \mathrm{d}^d\boldsymbol{x}\nabla^2 D^{(0)}_{00} \;\stackrel{!}{=}\; \oint \mathrm{d}\boldsymbol{a}\cdot\nabla D^{(0)}_{00}\,.$$

Since the Green's function is spherically symmetric, we can simply integrate over a hypersphere of radius r, the solid angle being

$$\Omega_d \;=\; dV_d\,; \qquad V_d \;=\; \frac{2\pi^{d/2}}{\left[\frac{d}{2}-1\right]!}\,.$$

Then

$$\partial_r D^{00}_{(0)} = \frac{1}{\Omega_d r^{d-1}} \quad\Rightarrow\quad D^{00}_{(0)}(r) = \frac{r^{2-d}}{(2-d)\Omega_d} + \mathsf{b}\,, \tag{A.1}$$

where b is a constant of integration, which may be dropped. The long distance behaviour of $D^{(0)}_{00}$, which is a vital property for aspect of screening, depends on the value of d in three different ways

$$\lim_{r\to\infty} D^{(0)}_{00}(r) \;=\; \begin{cases} \mathsf{b} & \\ \dfrac{r^{2-d}}{(2-d)\Omega_d} & d \;<\; 2\,. \\ \dfrac{\log(r)}{2\pi} & \;=\; \end{cases}$$

The fluctuations in the φ fields extend asymptotically for $d \le 2$. Returning to examine the transverse correlation function, we can consider the coordinate-space Greens' function since

$$D^{ii}_{(0)}(\boldsymbol{r}) = \frac{-1}{V}\sum_{\boldsymbol{k}} \frac{e^{i\boldsymbol{k}\cdot\boldsymbol{r}}}{\omega^2+k^2} \underbrace{\left(\delta^{ii} - \frac{\boldsymbol{k}^i\boldsymbol{k}^i}{k^2}\right)}_{=(d-1)} \;=:\; (d-1)\Delta_d(\omega,\boldsymbol{r})\,, \tag{A.2}$$

where $\boldsymbol{r} = \boldsymbol{x} - \boldsymbol{x}'$. In the continuum limit, (this is the so-called "mixed" representation)

$$\Delta_d(\omega,\boldsymbol{r}) \;=\; -\int_{\boldsymbol{k}} \frac{e^{i\boldsymbol{k}\cdot\boldsymbol{r}}}{\omega^2+k^2} \;=\; \int_{\boldsymbol{k}} e^{i\boldsymbol{k}\cdot\boldsymbol{r}}\Delta_K\,.$$

Put another way, Δ_d satisfies the following differential equation[29]. Spherical symmetry [which we got by taking the trace in (A.2)] implies that the Laplacian can be written

$$\Delta_d'' + \frac{d-1}{r}\Delta_d' \;=\; \omega^2\Delta_d + \delta^{(d)}(\boldsymbol{r})\,, \tag{A.3}$$

where a prime flags the derivative with respect to r. Making the *Ansatz* that $\Delta_d \propto e^{-x\omega}/x^\xi$, where ξ is a subleading power growth and ω^{-1} characterises the screening length, one finds a consistency equation for ξ, viz.

$$\frac{1}{x^2}\xi\left(\xi+2-d\right) + \frac{\omega}{x}\left(2\xi+1-d\right) \;\stackrel{!}{=}\; 0\,. \tag{A.4}$$

[29] This solutions to (A.3) are in general *Bessel functions* of various pedigree.

The constant terms $\sim \omega^2$, in Eq. (A.4), cancel by our choice of exponential decay. The power ξ is related to the dimension d through (A.4), which simplifies in two special limits.

Close to the origin (where $r \ll \omega^{-1}$), the $1/r^2$ terms are the most important. For (A.4) to be true in this limit, we must set $\xi = d-2$. This coincides with what we found in (A.1), where $\omega \to 0$ for the longitudinal field. At small length scale, the Coulomb interactions override the screening effect.

Far away from the source, $r \gg \omega^{-1}$, the term ω/r in (A.4) is actually the most important. In order for these terms to cancel we require that $\xi = (d-1)/2$. We fix the overall constant of proportionality by requiring that (A.2) agrees with this expression at an intermediate distance $r \simeq \omega^{-1}$. The result is

$$\Delta_d(\omega, \boldsymbol{r}) \quad = \quad \frac{\omega^{(d-2)} \cdot e^{-r\omega}}{(2-d)\Omega_d} (r\omega)^{(1-d)/2} \qquad \text{for} \qquad r \gg \omega^{-1} \,.$$

Vertices

In a covariant gauge, the three gluon vertex is a combination of the metric tensor g and permitted 4-momentum exchanges [37]. In Coulomb gauge, we choose to unpack the vertices in terms of the possible polarisation states [contract with $v^\mu = (1, \mathbf{0})$ to set an index to 0]. Thus, the vertices where at least one Coulomb gluon is involved are (Colour factors are as in covariant gauges):

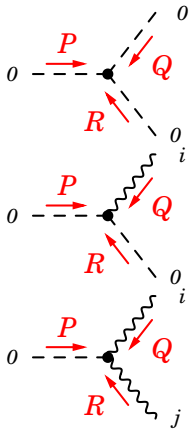

$$= \quad (q_0 - p_0) + (p_0 - r_0) - (q_0 - r_0) = 0$$

$$= \quad g^{00}(p-r)_i = \boldsymbol{p} - \boldsymbol{r} \tag{A.5}$$

$$= \quad g_{ij}(r-q)_0 = \delta_{ij}(q_0 - r_0)$$

The coupling to the quarks is as usual, with the simplification that for an infinitely heavy quark (which always has an on-shell energy of 0), the transverse gluon does not couple. The reason being that ∞-mass quarks only exchange $K = (0, \boldsymbol{k})$ which is orthogonal to the transverse propagator D_{ij}.

The vertex with all bosons static vanishes trivially. Further, because of the Lorentz-pairing of indices, there must be an even number of transverse attachments, with the *all*-transverse being very similar to the most general form. All that remains is a vertex with two transverse and two longitudinal bosons:

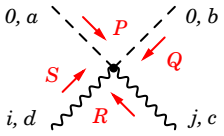

$$= \quad ig^2\delta_{ij}\left[f^{ace} f^{ebd} + f^{ade} f^{ebc} \right] . \tag{A.6}$$

The colour contractions follow lines along dissimilarly polarised gluons.

B. Frequency Sums

The partition sum, Eq. (2.5), was calculated with the help of a formal analogy between quantum field theory and statistical mechanics. This 'imaginary time formalism' enables the energy direction to be compactified in Euclidean space, giving a discrete frequency spectrum. Thus in the thermodynamic limit $V \to \infty$, but $T \neq 0$, the aggregate of momentum modes is

$$\not{\int}_L := T \sum_{\ell_0} \int_{\boldsymbol{\ell}} , \qquad \ell_0 \in i\pi T \begin{cases} 2n \\ 2n+1 \end{cases} \text{for} \begin{matrix} \text{Bosons} \\ \text{Fermions} \end{matrix} , \qquad n \in \mathbb{Z} . \tag{B.1}$$

The even frequencies for bosons are a consequence of periodic boundary conditions on the fundamental fields; the odd frequencies for fermions are due to anti-periodic boundary conditions [14]. Define the general scalar propagator, with energy-momentum relation, to be $\epsilon_{\boldsymbol{\ell}} = \sqrt{\ell^2 + m^2}$.

$$\Delta_L \;=\; \frac{1}{L^2 - m^2} \;=\; \left(\ell_0^2 - \epsilon_{\boldsymbol{\ell}}^2 \right)^{-1} .$$

The frequency sums can be evaluated with help from Cauchy's residue theorem. Before carrying out the sum, it is convenient to express Δ_L by its *Saclay* representation [15], namely

$$\Delta_L \;=\; -\int_0^\beta \mathrm{d}\tau e^{\ell_0 \tau} \Delta(\tau, \boldsymbol{\ell}) .$$

The discrete ℓ_0-frequencies are traded for an imaginary time $\tau \in [0, \beta]$ to give a 'mixed' function $\Delta(\tau, \boldsymbol{\ell})$. It may be obtained by a discrete Fourier transformation,

$$\Delta(\tau, \boldsymbol{\ell}) \;=\; -T \sum_{\ell_0} e^{-\ell_0 \tau} \Delta_L . \tag{B.2}$$

To carry out the sum over ℓ_0 in this definition, we shall use an elegant trick based on complex integration. For the statistical factors I introduce the functions

$$\phi_{\boldsymbol{\ell}} \;=\; s f_s(\epsilon_{\boldsymbol{\ell}}) , \qquad \bar{\phi}_{\boldsymbol{\ell}} \;=\; 1 + s f_s(\epsilon_{\boldsymbol{\ell}}) \;=\; -s f_s(-\epsilon_{\boldsymbol{\ell}}) .$$

Here the subscript $s = \pm 1$ on the distribution functions is such that

$$f_s(\epsilon_{\boldsymbol{\ell}}) \;=\; \left(e^{\epsilon_{\boldsymbol{\ell}}/T} + s \right)^{-1} ,$$

which augments the definition of the Boson ($s = +1$) and Fermion ($s = -1$) distribution functions (1.2). Note that the $\phi_{\boldsymbol{\ell}}$ have unit residues for the energy argument $\epsilon_{\boldsymbol{\ell}}$ at the respective Matsubara frequencies. Therefore, to evaluate the sum (B.2), consider a contour $\mathcal{C}$ in the complex ℓ_0-plane with arbitrarily large radius and note that

$$\oint_{\mathcal{C}} \frac{\mathrm{d}\ell_0}{2\pi i} \Big(s f_s(\ell_0) \cdot e^{-\ell_0 \tau} \Delta_L \Big) \;=\; T \sum_{\ell_0} e^{-\ell_0 \tau} \Delta_L \;+ \tag{B.3}$$
$$T \sum_{\pm} s f_s(\pm \epsilon_{\boldsymbol{\ell}}) \cdot \exp(\pm \epsilon_{\boldsymbol{\ell}} \tau) \mathrm{Res}\left[\Delta_L\right]\big|_{\ell_0 = \pm \epsilon_{\boldsymbol{\ell}}} .$$

The integrand has poles at the Matsubara frequencies and at the poles of Δ_L, i. e. $\ell_0 = \pm \epsilon_{\boldsymbol{\ell}}$. Evidently in (B.3) we may isolate the frequency sum (B.2), thus expressing $\Delta(\tau, \boldsymbol{\ell})$ in terms of the two real energy poles, minus a contour integral. While $f_s(z)$ decreases explicitly only

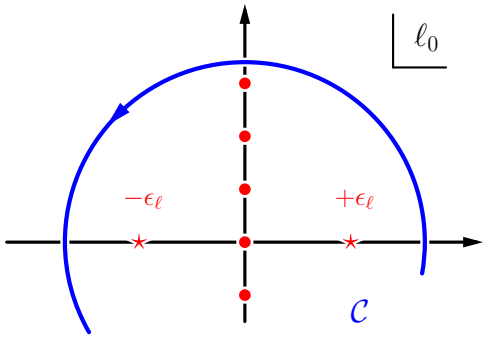

Figure 33: The locations of poles in the complex frequency plane for various functions.

for positive real z, the second function Δ_L drops sufficiently fast as $\mathcal{C}$ is enlarged. Hence the integral in (B.3) satisfies Jordan's lemma so that the contour does not contribute. This gives the explicit form

$$\begin{aligned}\Delta(\tau,\boldsymbol{\ell}) &= T\sum_{\pm} s f_s(\pm\epsilon_{\boldsymbol{\ell}})\exp(\pm\epsilon_{\boldsymbol{\ell}}\tau)\mathrm{Res}\left[\Delta_L\right]\big|_{\ell_0=\pm\epsilon_{\boldsymbol{\ell}}} \\ &= \frac{1}{2\epsilon_{\boldsymbol{\ell}}}\left[\ \phi_{\boldsymbol{\ell}}\,\exp\left(\epsilon_{\boldsymbol{\ell}}\tau\right) + \bar{\phi}_{\boldsymbol{\ell}}\,\exp\left(-\epsilon_{\boldsymbol{\ell}}\tau\right)\ \right].\end{aligned}$$

An important special case is $\tau = 0$, which gives the 'tadpole' loop diagram, (a) in Fig. 34,

$$\sum_{\ell_0}\Delta_L \;=\; \Delta(0,\boldsymbol{\ell}) \;=\; \frac{1}{2\epsilon_{\boldsymbol{\ell}}}\Big[\,\boxed{1} + 2\phi_{\boldsymbol{\ell}}\,\Big]. \tag{B.4}$$

The red boxed term is the vacuum contribution, which diverges after integration over the loop 3-momentum. Thermal distribution functions shield the divergent region, and give a finite result, for the tadpole (dropping the vacuum piece)

$$\not{\int}_L \Delta_L \;=\; \int_{\boldsymbol{\ell}}\Delta(0,\boldsymbol{\ell}) \;=\; \frac{T^2}{24}\begin{cases} 2 \\ -1 \end{cases} \quad \text{for} \quad \begin{matrix}\text{Bosons}\\ \text{Fermions}\end{matrix}\ .$$

The 'fish' topology, Fig. 34, is somewhat more complicated, by the allowed kinematics for propagating intermediate states. Frequency sums can still be taken by using the Saclay representation (B.2), and identifying the (discrete) Fourier transformed δ-function [15].

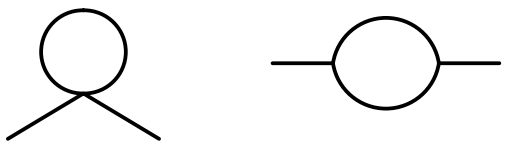

(a) tadpole (b) fish

Figure 34: The two topologies needed in 1-loop calculations. The 'tadpole' (left) is local in momentum space and thus independent of the momentum in the external line. The 'fish' (right) topology, due to separated vertices, has momentum dependence, with loop kinematics detailed in § 2.3.

The same strategy may be used to evaluate more complicated frequency sums, such as those that arise in loop diagrams. For our purposes, three sums are of importance and we shall state them below; see Ref. [36] for a general analysis.

$$T\sum_{\ell_0}\Delta_L\Delta_{\underline{K}} = \frac{1}{4\epsilon_{\boldsymbol{\ell}}\epsilon_{\boldsymbol{k}}}\Big\{\Big(\boxed{1}+\phi_{\boldsymbol{\ell}}+\phi_{\boldsymbol{k}}\Big)\Big[\frac{1}{\omega+\epsilon_{\boldsymbol{\ell}}+\epsilon_{\boldsymbol{k}}}-\frac{1}{\omega-\epsilon_{\boldsymbol{\ell}}-\epsilon_{\boldsymbol{k}}}\Big] + \Big(\phi_{\boldsymbol{\ell}}-\phi_{\boldsymbol{k}}\Big)\Big[\frac{1}{\omega-\epsilon_{\boldsymbol{\ell}}+\epsilon_{\boldsymbol{k}}}-\frac{1}{\omega+\epsilon_{\boldsymbol{\ell}}-\epsilon_{\boldsymbol{k}}}\Big]\Big\}, \tag{B.5}$$

$$T\sum_{\ell_0}\ell_0\Delta_L\Delta_{\underline{K}} = \frac{-1}{4\epsilon_{\boldsymbol{k}}}\Big\{\Big(\boxed{1}+\phi_{\boldsymbol{\ell}}+\phi_{\boldsymbol{k}}\Big)\Big[\frac{1}{\omega+\epsilon_{\boldsymbol{\ell}}+\epsilon_{\boldsymbol{k}}}+\frac{1}{\omega-\epsilon_{\boldsymbol{\ell}}-\epsilon_{\boldsymbol{k}}}\Big] - \Big(\phi_{\boldsymbol{\ell}}-\phi_{\boldsymbol{k}}\Big)\Big[\frac{1}{\omega-\epsilon_{\boldsymbol{\ell}}+\epsilon_{\boldsymbol{k}}}+\frac{1}{\omega+\epsilon_{\boldsymbol{\ell}}-\epsilon_{\boldsymbol{k}}}\Big]\Big\}, \tag{B.6}$$

$$T\sum_{\ell_0}\ell_0\underline{k}_0\Delta_L\Delta_{\underline{K}} = -\frac{1}{4}\Big\{\Big(\boxed{1}+\phi_{\boldsymbol{\ell}}+\phi_{\boldsymbol{k}}\Big)\Big[\frac{1}{\omega+\epsilon_{\boldsymbol{\ell}}+\epsilon_{\boldsymbol{k}}}-\frac{1}{\omega-\epsilon_{\boldsymbol{\ell}}-\epsilon_{\boldsymbol{k}}}\Big] - \Big(\phi_{\boldsymbol{\ell}}-\phi_{\boldsymbol{k}}\Big)\Big[\frac{1}{\omega-\epsilon_{\boldsymbol{\ell}}+\epsilon_{\boldsymbol{k}}}-\frac{1}{\omega+\epsilon_{\boldsymbol{\ell}}-\epsilon_{\boldsymbol{k}}}\Big]\Big\}. \tag{B.7}$$

The energy is $\epsilon_{\boldsymbol{\ell}} = \sqrt{\boldsymbol{\ell}^2+m^2}$ and $\phi_{\boldsymbol{k}} = sf_s(\epsilon_{\boldsymbol{\ell}})$ defined earlier. Outlined by a (red) box are the divergent vacuum contributions, which are usually derived at $T=0$ by an integration over the energy $\int \mathrm{d}\ell_0$.

C. Vacuum spectral density

To handle the $T = 0$ contribution to the gluon self-energy in § 2.3, we use dimensional regularisation which isolates the ultraviolet (UV) divergent terms; a powerful technique originally conceived by 't Hooft and Veltman [4] where the number of dimensions d is analytically extended to $\mathbb{C}$. In order to retain the overall correct dimension, an auxiliary scale μ must be introduced into the sum over momenta $L = (\ell_0, \boldsymbol{\ell})$,

$$\oint\!\!\!\!\!\!\diagup_L \xrightarrow{T=0} \frac{\mu^{2\varepsilon}}{h^1} \int \mathrm{d}\ell_0 \int_{\boldsymbol{\ell}} \quad ; \quad d = 3 - 2\varepsilon\,. \tag{C.1}$$

The divergence of 1-loop diagrams, after expanding the dimension $d = 3 - 2\varepsilon$, in small ε, is closely related to the (finite) imaginary part of these diagrams.

In our case, for the 1-loop gluon self energy, the function $\bar{\pi}$ [see for example Eq. (2.28)] is dimensionless and turns out to be of the form

$$\bar{\pi}(Q^2) \;=\; \bar{c}\cdot\mathcal{X}\left(Q^2/\mu^2\right) + \;\mathcal{O}(\varepsilon)\,,$$

where $\bar{c}$ is a constant and

$$\mathcal{X}(x) \;:=\; \frac{1}{\varepsilon}(x)^{-\varepsilon} \;\simeq\; \frac{1}{\varepsilon} - \log(x) + \mathcal{O}(\varepsilon)\,. \tag{C.2}$$

Thus in the limit $\varepsilon \to 0$, the UV divergence emerges as a pole which has the same prefactor as the logarithm in (C.2) yielding an imaginary part for negative arguments. The constant $\bar{c}$ is of physical relevance, and usually the objective of a calculation. We may extend the divergent part of $\bar{\pi}$ to take values at $s = Q^2$ in the complex plane, where $\bar{\pi}$ is analytic in s everywhere except on the positive real axis (see Fig. 35).

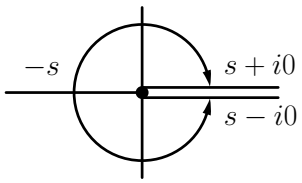

Figure 35: We show the domain of $\bar{\pi}(s)$ in the complex s-plane. The function is regular except on the positive real axis, where it has a discontinuity [7].

Starting at $s = 0$, the threshold for pair production of massless particles, there is a branch cut for real $s > 0$. The discontinuity, which is finite by a cancellation of the $1/\varepsilon$ in (C.2), is also μ^2 independent;

$$\mathrm{disc}\;\bar{\pi} \;=\; \bar{\pi}(s + i0) - \bar{\pi}(s - i0) \;\xrightarrow{\varepsilon=0}\; 2i\;\mathrm{Im}[\bar{\pi}(s + i0)]\,.$$

This forms the basic motivation for introducing the so-called *spectral representation*,

$$\varrho(s) \;=\; \frac{1}{\pi}\mathrm{Im}[\bar{\pi}(s + i0)]\,. \tag{C.3}$$

The spectral density has zero support, i. e. $\varrho = 0$, where $\bar{\pi}$ is regular because there is no discontinuity. For positive reals, the function ϱ is non-negative and in fact, using (C.2), one finds that it is constant in our example; $\lim_{\varepsilon\to 0}\varrho(s) = \bar{c}$.

Knowing the discontinuity $\varrho(s)$, it is possible to reconstruct the original function $\bar{\pi}$ under certain conditions. Since $\bar{\pi}(s)$ is analytic [except on the cut $s \in (0, \infty)$], the residue theorem gives

$$2\pi i\;\bar{\pi}(Q^2) \;=\; \int_{\mathcal{C}} \mathrm{d}s \frac{\bar{\pi}(s)}{s - Q^2}\,,$$

where the contour $\mathcal{C}$ runs just above and below the cut, closed by a large-radius circle in the counterclockwise direction. Provided $\bar{\pi}$ decreases sufficiently fast with $|s| \to \infty$, the integral over the circle is zero. The line segments above and below the cut indeed give

$$\bar{\pi}(Q^2) \;=\; \frac{1}{2\pi i}\int_0^\infty \mathrm{d}s\;\frac{\mathrm{disc}\;\bar{\pi}}{s-Q^2} \;=\; \int \mathrm{d}s\,\frac{\varrho(s)}{s-Q^2}\;, \tag{C.4}$$

which inverts Eq. (C.3).

The argument fails if $\bar{\pi}$ does not decrease sufficiently fast, so that the circular part of $\mathcal{C}$ gives a non-zero contribution to the integral. This is the case, e. g. for $\bar{\pi}(s) = \text{const}$. It has $\varrho = 0$, but $\bar{\pi} \neq 0$ contradicting (C.4). If $\bar{\pi}(s) \to \bar{c}_0$ at $|s| \to \infty$, then a subtracted dispersion relation may be written

$$\bar{\pi}(Q^2) \;=\; \bar{c}_0 + \int_0^\infty \mathrm{d}s\,\frac{\varrho(s)}{s-Q^2}\,,$$

where $\varrho(s)$ is given by the discontinuity of $\bar{\pi}(s) - \bar{c}_0$ on the cut (which is, of course, the same as $\mathrm{disc}\;\bar{\pi}$). If $\bar{\pi}(s)$ behaves as a polynomial $\sum_i \bar{c}_i s^i$ at $|s| \to \infty$, we need to do several subtractions. These changes only modify (C.4), all such functions have the same ϱ because the polynomial gives not contribution to the cut.

What is important for *renormalisation* is the UV term in $\bar{\pi}$. In calculating (C.3) it was not necessary to resort to dimensional regularisation because imaginary part, and thus the spectral function was finite. To connect back to $\bar{\pi}$ we shall have to make use of the auxiliary scale μ so that ϱ retains the correct dimension as $d \to 3$. The divergent piece of (C.4) is extracted from the spectral function where the argument s becomes large relative to Q^2. We may thus replace the lower bound on the integration of (C.4) by $0 \to Q^2$ and take $s \gg Q^2$, so that

$$\lim_{\varepsilon\to 0}\;\bar{\pi}(Q^2) \;=\; \bar{c}\cdot\mu^{2\varepsilon}\int_{Q^2}^\infty \mathrm{d}s\;s^{-1-\varepsilon} \;=\; \bar{c}\cdot\mathcal{Y}\left(Q^2/\mu^2\right)\,,$$

leading back to Eq. (C.2).

The fact that the gluon spectral functions is positive, $\varrho \geq 0$, has considerable implication for the quantum corrections to scattering process. Take, for the sake of illustration, the static quark potential (§ 2.4). The exchanged longitudinal gluon has a (dressed) propagator (2.59) which becomes [38]

$$D_{00}\,(0,\boldsymbol{q}) \;\simeq\; \frac{-1}{\boldsymbol{q}^2}\Big(1-\int \mathrm{d}s\frac{\varrho(s)}{s}\Big) - \int \mathrm{d}s\frac{\varrho(s)}{s}\cdot\frac{1}{\boldsymbol{q}^2+s} + \ldots\,, \tag{C.5}$$

after using a partial fractions trick to rewrite the spectral representation for Π. Since the static quark potential is (in momentum space) $\mathcal{V}_{\boldsymbol{q}} = -g^2 C_F D_{00}(0,\boldsymbol{q})$, this leads more or less directly to [38]

$$\mathcal{V}(r) \;=\; -C_F\frac{\alpha}{r}\left[1-\int \mathrm{d}s\frac{\varrho(s)}{s}+\int \mathrm{d}s\frac{\varrho(s)}{s}\exp\left(-r\sqrt{s}\right)+\ldots\right]. \tag{C.6}$$

The second term in the bracket above is $\lim_{\boldsymbol{q}\to 0}\Pi(0,\boldsymbol{q})$, the static limit of the self energy at $\omega = 0$. As one gets further away from the source, the remaining 'screened' terms are exponentially suppressed. These Yukawa-type interaction terms are superimposed with the Coulomb potential – coming with positive weights and varying radii.

Useful 1-loop cut

In order to take the imaginary part, it is convenient to make use of the Cutkotsky rules as was done in § 2.3. We therefore consider the subsequent 3-momentum integration of the fish-topology diagram in Fig. 34, with both internal loop momenta put on shell.

Consider a function $f(\ell_0, \boldsymbol{\ell})$, depending on the loop momentum L for a fixed external momentum $Q = (\omega, \boldsymbol{q})$. In order to calculate the cut diagrams of i. e. Fig. 36, it is useful to study a generic integral with two on-shell lines

$$\mathcal{J}(Q) \;:=\; \frac{1}{h}\int \mathrm{d}\ell_0 \int_{\boldsymbol{\ell}} \delta(L^2)\delta(\underline{K}^2) f(\ell_0, \boldsymbol{\ell})\,, \tag{C.7}$$

where $\underline{K} = L + Q$ is fixed by energy and momentum conservation. The condition that $L^2 = K^2 = 0$ allows us to easily perform two integration and restricts the allowed values of ℓ and k, shown in Fig. 7. Based on the orientation of L in the loop diagram (Fig. 36), the on-shell condition gives $\ell_0 = -\ell$ (the 'backward' energy is negative). This fixes $\underline{k} = k_0 = \omega - \ell$ by energy conservation, so that using Eq. (2.32) yields

$$\mathcal{J}(Q) \;=\; \frac{1}{h^3}\int \mathrm{d}\ell \int_{k_{\min}}^{k_{\max}} \mathrm{d}k \frac{1}{4q}\delta\big(k - \underline{k}\big) f(-\ell, \boldsymbol{\ell})\,.$$

On the other hand, 3-momentum conservation gives $\boldsymbol{q} = \boldsymbol{k} - \boldsymbol{\ell}$. Hence the magnitude of the vector $\boldsymbol{q}$ satisfies a triangle inequality,

$$q \;<\; \ell + k \;=\; \omega \quad\Rightarrow\quad Q^2 = \omega^2 - \boldsymbol{q}^2 > 0\,.$$

In other words, the δ-function to fix k only has a solution for timelike Q, otherwise $\mathcal{J} = 0$. The kinematically permitted region is illustrated in Fig. 7. For a given ω and $\boldsymbol{q}$, the on-shell condition restricts ℓ to an interval $[\ell_{\min}, \ell_{\min}]$ where

$$\ell_{\min}^{\max} \;=\; \frac{1}{2}\big(\omega \pm q\big)\,; \qquad \omega > q\,.$$

Thus we have fully specified the integration domain, which is in fact one-dimensional. With k, ℓ and q given, the pairwise angles are similarly determined and functions f depending only on ℓ,

$$\mathcal{J}(Q) \;=\; \frac{1}{4h^3 q}\theta(Q^2)\int_{\ell_{\min}}^{\ell_{\max}} \mathrm{d}\ell f(-\ell, \boldsymbol{\ell})\,. \tag{C.8}$$

The dependence of f on the direction of $\boldsymbol{\ell}$ may be entirely expressed in terms of the other quantities, namely through the relations (2.33).

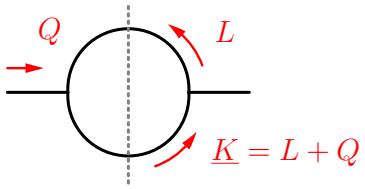

Figure 36: Labelling convention for the fish-type topology. The cut indicates that internal lines are put on-shell, i. e. $L^2 = K^2 = 0$.

D. Two-body phase space

The collisional operator (3.3) expresses the rate of binary encounters, integrated over partner momenta $\boldsymbol{k}_2$, $\boldsymbol{k}_3$ and $\boldsymbol{k}_4$. For a given function $g\big(\{\boldsymbol{k}_i\}\big)$ which depends on the participant momenta, we evaluate

$$\mathcal{I}\,[g]\,(\boldsymbol{k}_1) \quad := \quad \int \mathrm{d}\Gamma \cdot g\,.$$

One of the integrals may be completed using energy-momentum conservation; we choose the k_4-integral,

$$\int_4 \frac{g}{2E_4} \;=\; 2\pi\delta(\underline{K}_4^2)\theta(\underline{E}_4)\;\underline{g}\,. \tag{D.1}$$

Here the underline indicates a dependence on the fixed 4-momentum $\underline{K}_4 = K_1 + K_2 - K_3$. For instance, $\underline{f}_4$ depends on the energy $\underline{E}_4 = E_1 + E_2 - E_3$. It will turn out that the on-shell constraint $\underline{K}_4^2 = 0$, expressed by the δ-function in (D.1), implies already $\underline{E}_4 \geq 0$, making the factor of $\theta(\underline{E}_4)$ redundant in (D.1). The remaining fivefold integral is further reduced as follows [78]. We align the z-axis with $\boldsymbol{k}_1$ and orient the zy-plane to contain $\boldsymbol{k}_3$ viz.

$$\begin{aligned}
\boldsymbol{k}_1 &= E_1(0,0,1)\,,\\
\boldsymbol{k}_2 &= E_2(\sin\phi\sin\theta_2, \cos\phi\sin\theta_2, \cos\theta_2)\,,\\
\boldsymbol{k}_3 &= E_3(0, \sin\theta_3, \cos\theta_3)\,.
\end{aligned} \tag{D.2}$$

The argument of the δ-function in (D.1) depends on ϕ through

$$\begin{aligned}
\underline{K}_4^2 &= 2(K_1K_2 - K_1K_3 - K_2K_3)\\
&= s + t - 2K_2K_3\,.
\end{aligned}$$

Thus, using (D.2) to simplify the outstanding 4-product, we have $\underline{K}_4^2 = A + B\cos\phi$ where

$$\begin{aligned}
A &= s + t - 2E_2E_3(1 - \cos\theta_2\cos\theta_3)\,,\\
B &= 2E_2E_3\sin\theta_1\sin\theta_3\,.
\end{aligned} \tag{D.3}$$

Emphasising the azimuthal dependence in $g = g(\phi)$, the ϕ-integral is elementary

$$\int_0^{2\pi} \mathrm{d}\phi\;\delta\left(\underline{K}_4^2\right)\;g(\phi) \;=\; E_1\frac{\theta(h)}{\sqrt{h}}\sum_{\pm} g(\phi_\pm)\,,$$

where $\phi_\pm = \pi \pm \arccos(A/B)$ and $h = E_1^2(B^2 - A^2)$ (E_1 is factored out for convenience). Next, we reformulate the remaining integration over $\cos\theta_{2,3}$ in terms s and t, whose values are specified by $\boldsymbol{k}_1, \boldsymbol{k}_2$ and $\boldsymbol{k}_3$:

$$\begin{aligned}
s &= 2E_1E_2(1 - \cos\theta_2)\,,\\
t &= -2E_1E_3(1 - \cos\theta_3)\,,
\end{aligned} \tag{D.4}$$

with Jacobian $4E_2E_4 \cdot E_1^2$. Using this, and (D.1), we arrive at

$$\mathcal{I}\,[g] \;=\; \frac{1}{16(2\pi)^4E_1}\int \mathrm{d}s\mathrm{d}t \int \mathrm{d}E_2\mathrm{d}E_3\frac{\theta(h)}{\sqrt{h}}\sum_{\pm}\underline{g}(\phi_\pm)\,. \tag{D.5}$$

The function h is quadratic in E_3, written as $h(E_3) = aE_3^2 + bE_3 + c$ the coefficients are found from (D.3) and (D.5) to be

$$\begin{aligned} a &= -s^2\,, \\ b &= -2s(uE_1 + tE_2)\,, \\ c &= -(uE_1 - tE_2)^2 - stu\,. \end{aligned}$$

Since $a < 0$, $\theta(h)$ constrains the E_3-integration to the interval $[E_3^-, E_3^+]$, where

$$E_3^\pm = \frac{-b \pm \sqrt{\Delta}}{2a}\,.$$

Positivity of the discriminant $\Delta = 4s^2tu(4E_1E_2 - s)$ summarises the 2-body phase space: $0 \le s \le s_{\max} = 4E_1E_2$ and $-s \le t \le 0$.

With the kinematic bounds fully specified, the factor $\theta(h)$ can indeed (as anticipated) be dropped in (D.5) to give

$$\int \mathrm{d}\Gamma \cdot g = \frac{1}{16(2\pi)^4 E_1} \int \mathrm{d}E_2 \int_0^{s_{\max}} \mathrm{d}s \int_{-s}^{0} \mathrm{d}t \int_{E_3^-}^{E_3^+} \frac{\mathrm{d}E_3}{\sqrt{h(E_3)}} \sum_\pm g(\cdots)\,. \tag{D.6}$$

Up to this point, there have been no simplifying approximations. Phase space in (D.6) is furnished as a four dimensional integration, after reducing from nine by means of energy and momentum conservation as well as symmetry in one of the azimuths.

Small-t approximation

Of interest to § 3.3, is the behaviour of (D.6) assuming dominance of small angle scatterings. For small $\omega = E_1 - E_3$, it is reasonable to replace in $g(E_3)$ the energy $E_3 \to E_1$. However, for $-t \ll T^2$ the possibility for both $|\omega|$ and q to become separately large withholds this simplification. We now discuss in some more detail how to complete the E_3-integral of (D.6), keeping terms of relevant powers in t. The integrand has nonzero support for $h(E_3) > 0$, which as $|t| \to 0$ becomes restricted to $\left(E_1 - \sqrt{\frac{t}{s}(s - 4E_1E_2)}, E_1 + \sqrt{\frac{t}{s}(s - 4E_1E_2)}\right)$.

Let us, with regard to (D.6), define

$$\mathcal{K}[g] := \frac{s^2}{\pi} \int \frac{\mathrm{d}E_3}{\sqrt{h}} g(E_3)\,.$$

Expanding in $(E_2 - E_1)$ and keeping the terms at most linear in t,

ℓ	0	1	2	$\ell \ge 3$
$\mathcal{K}\left[(E_3 - E_1)^\ell\right]$	s	$\lvert t\rvert(E_2 - E_1)$	$+\frac{1}{4}\lvert t\rvert(4E_1E_2 - s)$	$\mathcal{O}(t^2)$

By elementary integration, we obtain for the inner integral in (D.6), letting $g' = \mathrm{d}g/\mathrm{d}E_3$, the series

$$\mathcal{K}[g] \simeq sg(E_1) + |t|(E_2 - E_1)g'(E_1) + \frac{1}{2}|t|(4E_1E_2 - s)g''(E_1) + \mathcal{O}(t^2)\,. \tag{D.7}$$

Of special relevance for the viscosity calculation, is the symmetric form of the linearised collisional operator (3.18). In the covariant formulation (D.6), we find

$$\mathcal{K}[\left(\Delta^{ij}\left[\psi_1\right]\right)^2] \simeq \frac{2}{3}|t|(E_1^2 + E_2^2)(8E_1E_2 + s) + \mathcal{O}(t^2)\,,$$

which was used to arrive at the small-$|t|$ expansion in Eq. (3.27).

E. Soft & hard contributions

Here we give some details on calculating analytically, in the framework of HTL perturbation theory, a number which seems to be known only numerically for the viscosity, and is also relevant for other observables. Particle production rates and transport coefficients require kinematic integral convolutions with matrix elements. In a thermal setting, particle propagators are modified by their interaction with the medium, a feature already stressed in § 2.3. The general form of this screening is a T^2 multiplied by a dimensionless function of (separately) the momentum and frequency. The HTL approximation [36] affords an analytic representation depending only on $z = \omega/q$. While usually derived under the assumption that both $\omega, q \ll T$, the approximation is in fact valid for $|\omega^2 - q^2| \lesssim T^2$ [39].

As explained in § 3.3, we opt for a covariant separation of phase space with $t^\star$ as the cut-off parameter. Using the Born cross section for hard interactions where $-s < t < t^\star$, for the t-channel contribution of the scattering cross section gives a 'trivial' result. The essential contribution is

$$\mathcal{Y}(t^\star)\Big|_{\text{hard}} = \int_{-s}^{t^\star} \mathrm{d}t\,|t|\frac{1}{t^2} = \log\left(\frac{s}{|t^\star|}\right), \tag{E.1}$$

identical to (3.24) as it should be.

Screening is necessary to characterise the complementary soft region, where $t^\star < t < 0$. The 1-loop self energies depend separately on ω and q via the ratio $x = \omega/q$ which for timelike exchanges, $x \in [-1, 1]$.

$$\mathcal{Y}(t^\star)\Big|_{\text{soft}} = \int_{-1}^{+1} \mathrm{d}x \int_{t^\star}^{0} \mathrm{d}t \frac{t}{|t + \Pi|^2}, \tag{E.2}$$

where $\Pi = \Pi_{L,T}(x)$ is the self energy. Adding the soft and hard contributions (E.1) and (E.2), the separation scale $t^\star$ basically drops out (up to subleading terms). In other words, it tells us at which point the HTL dressing could to be replaced by tree level functions in order to omit the soft contribution altogether. The expression in Eq. (E.2) has only been determined numerically, or in specific limiting cases [64]. However it is possible to find the dominant contribution analytically in general. Keeping only relevant terms,

$$\int \mathrm{d}t \frac{t}{|t + \Pi|^2} = \int \frac{\mathrm{d}t}{\Pi - \Pi^*}\left(\frac{\Pi}{\Pi + t} - \frac{\Pi^*}{\Pi^* + t}\right) \simeq \log|t^\star| + \mathrm{Im}\left[\frac{\Pi \log(\Pi)}{\mathrm{Im}\,[\Pi]}\right] + \mathcal{O}\left(\frac{1}{|t^\star|}\right).$$

A familiar log-structure emerges when $|t^\star| \to \infty$. What remains is the x-integration which traces out a contour in the complex Π-plane, see Fig. 37. One has the freedom to deform this contour to a simple one (just above the real axis), say $\Pi = \zeta + i\delta$ and examine the limit $\delta \to 0$. Observing

$$\int \mathrm{d}x\ \mathrm{Im}\left[\frac{\Pi \log(\Pi)}{\mathrm{Im}\,[\Pi]}\right] \overset{\delta\to 0}{\simeq} \int_{\zeta_1}^{\zeta_2} \mathrm{d}\zeta(1 + \log\zeta) = \frac{\zeta_2 \log|\zeta_2| - \zeta_1 \log|\zeta_1|}{\frac{1}{2}(\zeta_2 - \zeta_1)},$$

completes the calculation for $\mathcal{Y}(t^\star)$. Here we have left the ζ-bounds unspecified. By construction, they are equal to the value of the self-energy evaluated on the lightcone.

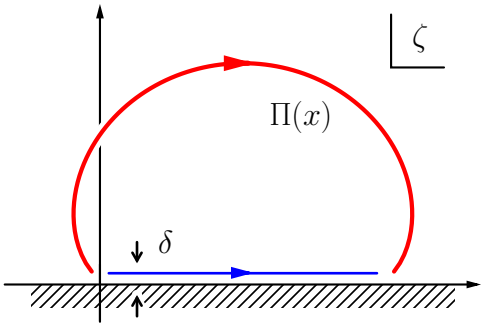

Figure 37: The transport cross section takes into account screening via the self energy Π (which has real and complex parts), thus tracing a curve (red) in the complex plane with $-1 < x < +1$ as the parameter. We deform this contour to a simpler one (blue), still starting at $\Pi(-1)$ and ending at $\Pi(+1)$ and running just above the axis.

The result for Eq. (E.2) is directly applicable to, e. g. the calculation for the transport cross section. In the quenched case, one needs the screened matrix element from $gg \to gg$ interactions. The essential contribution is

$$\begin{aligned} \mathcal{Y}(t^\star)\Big|_{\text{soft}} &= \frac{1}{3}\int_{-1}^{+1}\mathrm{d}x\int_{t^\star}^{0}\mathrm{d}t\,|t|\left[\,\frac{1}{|t+(1-x^2)\Pi_L(x)|^2}+\frac{1/2}{|t+\Pi_T(x)|^2}\,\right] \\ &= \log\left(\frac{|t^\star|}{2^{1/3}m_D^2}\right). \end{aligned} \tag{E.3}$$

We have used our technique with explicit forms for the HTL gluon self energies, viz.

$$\begin{aligned} \Pi_L(x) &= m_D^2\left[1-\frac{x}{2}\log\left(\frac{x+1}{x-1}\right)\right], \\ \Pi_T(x) &= m_D^2\left[\frac{x^2}{2}+\frac{x(1-x^2)}{4}\log\left(\frac{x+1}{x-1}\right)\right]. \end{aligned}$$

Since Π is symmetric in x which means we can simply integrate from $x = 0$ to $x = 1$ and multiply by 2 in the application of our result.

Combining the contribution from hard and soft regions given by (E.1) and (E.3) produces

$$\mathcal{Y}(t^\star) = \log\left(\frac{s}{2^{1/3}m_D^2}\right).$$

This LL result matches the expectation of (3.24) and confirms the numerical result of Heiselberg in Eq. (B7) [64]. Incidently, our technique is applicable in the calculation of the photon rate and proves a result in [79] previously known only numerically. Formally, $\mathcal{Y}$ is then independent of $t^\star$ in the Braaten-Yuan scheme resting on the assumption that $m_D^2 \ll -t \ll s \sim T^2$ [80]. Since the infrared cutoff is $\sim \alpha T^2$, we must have $-t^\star \in [\alpha, 1]T^2$ (parametrically). For example, taking the geometric mean $-t^\star = \sqrt{\alpha}\,T^2$ implies that the residual dependence on $t^\star$ is small for weak coupling; since in (E.3) the subleading terms are $\sim \Pi/|t^\star|$ and in (E.1) they are $\sim |t^\star|/s$.

References

[1] F. Halzen and A. D. Martin, *Quarks and Leptons: An Introductory Course in Modern Particle Physics*. Wiley, 1984.

[2] V. E. Barnes *et al.* *Phys. Rev. Lett.* **12** (1964) 204–206.

[3] C.-N. Yang and R. L. Mills *Phys. Rev.* **96** (1954) 191–195.

[4] G. 't Hooft and M. J. G. Veltman *Nucl. Phys.* **B44** (1972) 189–213.

[5] K. G. Wilson *Phys. Rev.* **D10** (1974) 2445–2459.

[6] D. J. Gross and F. Wilczek *Phys. Rev. Lett.* **30** (1973) 1343–1346.

[7] A. Grozin, *Lectures on QED and QCD: Practical calculation and renormalization of one- and multi-loop Feynman diagrams*. 2007.

[8] J. Bjorken *Phys.Rev.* **D27** (1983) 140–151.

[9] D. Teaney *Phys. Rev.* **C68** (2003) 034913, arXiv:nucl-th/0301099 [nucl-th].

[10] L. P. Csernai, J. Kapusta, and L. D. McLerran *Phys. Rev. Lett.* **97** (2006) 152303, arXiv:nucl-th/0604032 [nucl-th].

[11] P. Danielewicz and M. Gyulassy *Phys.Rev.* **D31** (1985) 53–62.

[12] P. Kovtun, D. T. Son, and A. O. Starinets *Phys. Rev. Lett.* **94** (2005) 111601, arXiv:hep-th/0405231 [hep-th].

[13] L. D. Landau and E. M. Lifshitz, *Statistical Physics*. Pergamom Press, 1959.

[14] J. I. Kapusta and C. Gale, *Finite-Temperature Field Theory: Principles and Applications*. Cambridge University Press, 2011.

[15] M. L. Bellac, *Thermal Field Theory*. Cambridge University Press, 1996.

[16] M. Kardar, *Statistical Physics of Fields*. Cambridge University Press, 2007.

[17] J. C. Collins, *Renormalization*. Cambridge University Press, 1986.

[18] O. Kalashnikov *Fortsch. Phys.* **32** (1984) 525.

[19] L. D. Landau and E. Lifshitz, *Fluid Mechanics*. Butterworth-Heinemann, 1987.

[20] M. Kardar, *Statistical Physics of Particles*. Cambridge University Press, 2007.

[21] J. M. Luttinger and J. C. Ward *Phys. Rev.* **118** (Jun, 1960) 1417–1427.

[22] P. B. Arnold and C.-X. Zhai *Phys.Rev.* **D50** (1994) 7603–7623, arXiv:hep-ph/9408276 [hep-ph].

[23] A. D. Linde *Phys. Lett.* **B96** (1980) 289–292.

[24] K. Kajantie, M. Laine, K. Rummukainen, and Y. Schroder *Phys. Rev.* **D67** (2003) 105008, arXiv:hep-ph/0211321 [hep-ph].

[25] K. Symanzik *Nucl. Phys.* **B226** (1983) 205–227.

[26] A. Peshier, B. Kampfer, O. P. Pavlenko, and G. Soff *Phys. Rev.* **D54** (1996) 2399–2402.

[27] S. Borsanyi, G. Endrodi, Z. Fodor, S. D. Katz, and K. K. Szabo *JHEP* **07** (2012) 056, arXiv:1204.6184 [hep-lat].

[28] G. Endrodi, Z. Fodor, S. D. Katz, and K. K. Szabo *PoS* **LAT2007** (2007) 228, arXiv:0710.4197 [hep-lat].

[29] G. Boyd, J. Engels, F. Karsch, E. Laermann, C. Legeland, M. Lutgemeier, and B. Petersson *Nucl. Phys.* **B469** (1996) 419–444, arXiv:hep-lat/9602007 [hep-lat].

[30] **HotQCD** Collaboration, A. Bazavov *et al.* *Phys. Rev.* **D90** no. 9, (2014) 094503, arXiv:1407.6387 [hep-lat].

[31] S. Borsanyi, Z. Fodor, C. Hoelbling, S. D. Katz, S. Krieg, and K. K. Szabo *Phys. Lett.* **B730** (2014) 99–104, arXiv:1309.5258 [hep-lat].

[32] J. Engels, J. Fingberg, F. Karsch, D. Miller, and M. Weber *Phys. Lett.* **B252** (1990) 625–630.

[33] J. O. Andersen, M. Strickland, and N. Su *Phys. Rev. Lett.* **104** (2010) 122003, arXiv:0911.0676 [hep-ph].

[34] H. A. Weldon *Phys.Rev.* **D26** (1982) 1394.

[35] U. W. Heinz, K. Kajantie, and T. Toimela *Annals Phys.* **176** (1987) 218.

[36] E. Braaten and R. D. Pisarski *Nucl.Phys.* **B337** (1990) 569.

[37] C. Itzykson and J.-B. Zuber, *Quantum Field Theory*. Dover Publications, 2006.

[38] A. Grozin arXiv:0803.2589 [physics.hist-ph].

[39] A. Peshier, K. Schertler, and M. H. Thoma *Annals Phys.* **266** (1998) 162–177, arXiv:hep-ph/9708434 [hep-ph].

[40] O. Kaczmarek and F. Zantow *Phys.Rev.* **D71** (2005) 114510, arXiv:hep-lat/0503017 [hep-lat].

[41] M. E. Peskin and D. V. Schroeder, *An Introduction To Quantum Field Theory*. Westview Press, 1995.

[42] R. Kobes, G. Kunstatter, and A. Rebhan *Phys.Rev.Lett.* **64** (1990) 2992–2995.

[43] I. B. Khriplovich *Sov. J. Nucl. Phys.* **10** (1969) 235–242. [Yad. Fiz.10,409(1969)].

[44] H. D. Politzer *Phys. Rev. Lett.* **30** (1973) 1346–1349.

[45] A. Peshier arXiv:hep-ph/0601119 [hep-ph].

[46] O. Kaczmarek, F. Karsch, F. Zantow, and P. Petreczky *Phys.Rev.* **D70** (2004) 074505, arXiv:hep-lat/0406036 [hep-lat].

[47] A. Nakamura, T. Saito, and S. Sakai *Phys. Rev.* **D69** (2004) 014506, arXiv:hep-lat/0311024 [hep-lat].

[48] E. M. Lifshitz and L. P. Pitaevskii, *Physical Kinetics*. Pergamon Press, 1981.

[49] G. Baym *Phys. Lett.* **B138** (1984) 18–22.

[50] F. Reif, *Fundamentals of Statistical and Thermal Physics*. McGraw Hill, 1964.

[51] G. D. Moore, "Transport coefficients in hot QCD," in *6th International Conference on Strong and Electroweak Matter (SEWM 2004) Helsinki, Finland, June 16-19, 2004*. 2004. arXiv:hep-ph/0408347 [hep-ph].

[52] T. E. Faber, *Fluid Dynamics for Physicists*. Cambridge University Press, 1995.

[53] G. Baym, H. Monien, C. Pethick, and D. Ravenhall *Phys.Rev.Lett.* **64** (1990) 1867–1870.

[54] P. B. Arnold, G. D. Moore, and L. G. Yaffe *JHEP* **0011** (2000) 001, arXiv:hep-ph/0010177 [hep-ph].

[55] H. van Hees, M. Mannarelli, V. Greco, and R. Rapp *Eur. Phys. J.* **C61** (2009) 799–806, arXiv:0808.3710 [hep-ph].

[56] **PHENIX** Collaboration, A. Adare *et al.* *Phys. Rev.* **C84** (2011) 044905, arXiv:1005.1627 [nucl-ex].

[57] M. Luzum and P. Romatschke *Phys. Rev.* **C78** (2008) 034915, arXiv:0804.4015 [nucl-th]. [Erratum: Phys. Rev.C79,039903(2009)].

[58] H. Song, S. A. Bass, U. Heinz, T. Hirano, and C. Shen *Phys. Rev. Lett.* **106** (2011) 192301, arXiv:1011.2783 [nucl-th]. [Erratum: Phys. Rev. Lett.109,139904(2012)].

[59] N. Demir and S. A. Bass *Phys. Rev. Lett.* **102** (2009) 172302, arXiv:0812.2422 [nucl-th].

[60] Z. Xu and C. Greiner *Phys. Rev. Lett.* **100** (2008) 172301, arXiv:0710.5719 [nucl-th].

[61] S. Gavin and M. Abdel-Aziz *Phys. Rev. Lett.* **97** (2006) 162302, arXiv:nucl-th/0606061 [nucl-th].

[62] R. Cutler and D. W. Sivers *Phys. Rev.* **D17** (1978) 196.

[63] A. Hosoya and K. Kajantie *Nucl.Phys.* **B250** (1985) 666.

[64] H. Heiselberg *Phys.Rev.* **D49** (1994) 4739–4750, arXiv:hep-ph/9401309 [hep-ph].

[65] P. B. Arnold, G. D. Moore, and L. G. Yaffe *JHEP* **0305** (2003) 051, arXiv:hep-ph/0302165 [hep-ph].

[66] P. B. Arnold, G. D. Moore, and L. G. Yaffe *JHEP* **01** (2003) 030, arXiv:hep-ph/0209353 [hep-ph].

[67] A. Peshier *Phys.Rev.Lett.* **97** (2006) 212301, arXiv:hep-ph/0605294 [hep-ph].

[68] H. B. Meyer *Phys. Rev.* **D76** (2007) 101701, arXiv:0704.1801 [hep-lat].

[69] H. B. Meyer *Nucl. Phys.* **A830** (2009) 641C–648C, arXiv:0907.4095 [hep-lat].

[70] S. W. Mages, S. Borsányi, Z. Fodor, A. Schäfer, and K. Szabó *PoS* **LATTICE2014** (2015) 232.

[71] Y. L. Dokshitzer, G. Marchesini, and B. R. Webber *Nucl. Phys.* **B469** (1996) 93–142, arXiv:hep-ph/9512336 [hep-ph].

[72] Y. Dokshitzer *Nucl. Phys.* **A711** (2002) 11–18, arXiv:hep-ph/0510199 [hep-ph].

[73] H. A. Weldon *Phys.Rev.* **D26** (1982) 2789.

[74] H. Niemi, K. J. Eskola, and R. Paatelainen arXiv:1505.02677 [hep-ph].

[75] M. Strickland *Acta Phys. Polon.* **B45** no. 12, (2014) 2355–2394, arXiv:1410.5786 [nucl-th].

[76] D. A. Teaney arXiv:0905.2433 [nucl-th].

[77] O. Brill and B. Goodman *Am. J. Phys* **35** no. 9, (1967) 832–837.

[78] S. Peigne and A. Peshier *Phys.Rev.* **D77** (2008) 014015, arXiv:0710.1266 [hep-ph].

[79] J. I. Kapusta, P. Lichard, and D. Seibert *Phys.Rev.* **D44** (1991) 2774–2788.

[80] E. Braaten and T. C. Yuan *Phys. Rev. Lett.* **66** (1991) 2183–2186.